RADC-TR-82-286, Vol V (of six)
Final Technical Report
October 1984

BASIC EMC TECHNOLOGY ADVANCEMENT FOR C³ SYSTEMS - Model Revision for IEMCAP

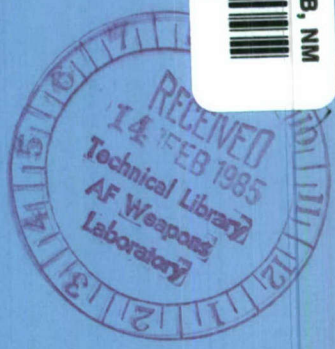

Southeastern Center for Electrical Engineering Education

Clayton R. Paul

ROME AIR DEVELOPMENT CENTER
Air Force Systems Command
Griffiss Air Force Base, NY 13441-5700

This report has been reviewed by the RADC Public Affairs Office (PA) and is releasable to the National Technical Information Service (NTIS). At NTIS it will be releasable to the general public, including foreign nations.

RADC-TR-82-286, Volume V (of six) has been reviewed and is approved for publication.

APPROVED: By F. Stratton

ROY F. STRATTON
Project Engineer

APPROVED: W. S. Tuthill

W. S. TUTHILL, Colonel, USAF
Chief, Reliability & Compatibility Division

FOR THE COMMANDER: John A. Ritz

JOHN A. RITZ
Acting Chief, Plans Office

If your address has changed or if you wish to be removed from the RADC mailing list, or if the addressee is no longer employed by your organization, please notify RADC (RBCT) Griffiss AFB NY 13441. This will assist us in maintaining a current mailing list.

Do not return copies of this report unless contractual obligations or notices on a specific document requires that it be returned.

UNCLASSIFIED
SECURITY CLASSIFICATION OF THIS PAGE

REPORT DOCUMENTATION PAGE

1a. REPORT SECURITY CLASSIFICATION UNCLASSIFIED	1b. RESTRICTIVE MARKINGS N/A
2a. SECURITY CLASSIFICATION AUTHORITY N/A	3. DISTRIBUTION/AVAILABILITY OF REPORT Approved for public release; distribution unlimited.
2b. DECLASSIFICATION/DOWNGRADING SCHEDULE N/A	
4. PERFORMING ORGANIZATION REPORT NUMBER(S) N/A	5. MONITORING ORGANIZATION REPORT NUMBER(S) RADC-TR-82-286, Vol V (of six)
6a. NAME OF PERFORMING ORGANIZATION Southeastern Center for Electrical Engineering Education 6b. OFFICE SYMBOL (If applicable)	7a. NAME OF MONITORING ORGANIZATION Rome Air Development Center (RBCT)
6c. ADDRESS (City, State and ZIP Code) 1101 Massachusetts Avenue St. Cloud FL 37206	7b. ADDRESS (City, State and ZIP Code) Griffiss AFB NY 13441
8a. NAME OF FUNDING/SPONSORING ORGANIZATION Rome Air Development Center 8b. OFFICE SYMBOL (If applicable) (RBCT)	9. PROCUREMENT INSTRUMENT IDENTIFICATION NUMBER F30602-81-C-0062
8c. ADDRESS (City, State and ZIP Code) Griffiss AFB NY 13441-5700	10. SOURCE OF FUNDING NOS. PROGRAM ELEMENT NO. 62702F; PROJECT NO. 2338; TASK NO. 03; WORK UNIT NO. 35

11. TITLE (Include Security Classification)
BASIC EMC TECHNOLOGY ADVANCEMENT FOR C^3 SYSTEMS - Model Revision for IEMCAP

12. PERSONAL AUTHOR(S)
Clayton R. Paul

13a. TYPE OF REPORT	13b. TIME COVERED	14. DATE OF REPORT (Yr., Mo., Day)	15. PAGE COUNT
Final	FROM Sep 82 TO Dec 83	October 1984	176

16. SUPPLEMENTARY NOTATION
Work was performed at University of Kentucky, Lexington KY 40506
Project Engineers - Gerald Capraro and Roy F. Stratton

17. COSATI CODES		
FIELD	GROUP	SUB. GR.
09	03	
09	02	

18. SUBJECT TERMS (Continue on reverse if necessary and identify by block number)
IEMCAP, wire-to-wire, field-to-wire, crosstalk, electromagnetic compatibility, EMC modeling

19. ABSTRACT (Continue on reverse if necessary and identify by block number)

This report documents suggested model and code revisions for the wire-to-wire and field-to-wire coupling subroutines in the Intrasystem Electromagnetic Compatibility Analysis Program (IEMCAP). The suggested revisions are to improve model predictions, remove unnecessary code, and modularize the subroutines. An assessment of the advisability of including models for system perturbations (cable clamps, ribs, bulkheads, etc.) is also given.

20. DISTRIBUTION/AVAILABILITY OF ABSTRACT	21. ABSTRACT SECURITY CLASSIFICATION
UNCLASSIFIED/UNLIMITED ☒ SAME AS RPT. ☐ DTIC USERS ☐	UNCLASSIFIED

22a. NAME OF RESPONSIBLE INDIVIDUAL	22b. TELEPHONE NUMBER (Include Area Code)	22c. OFFICE SYMBOL
Roy F. Stratton	(315) 330-2563	RADC (RBCT)

DD FORM 1473, 83 APR EDITION OF 1 JAN 73 IS OBSOLETE.

UNCLASSIFIED
SECURITY CLASSIFICATION OF THIS PAGE

TABLE OF CONTENTS

I. INTRODUCTION

In 1974, the McDonnel Aircraft Corporation delivered to the U.S. Air Force a digital computer program IEMCAP (Intrasystem ElectroMagnetic Compatibility Analysis Program) [1]. This code was designed for and intended to be used to model all electronic systems in the U.S. Air Force inventory for the purpose of assisting in the analysis and prediction of electromagnetic interference in those systems. The types of systems which were intended to be modeled by this code range from ground systems to aircraft as well as space-missle systems.

There are essentially three major categories of models used in the analysis/prediction process employed by this code - emitters, coupling paths, and receptors. The process is illustrated in Fig. 1-1. Presently the code performs all analyses in the frequency domain. The emission spectrum, E(f), of an emitter (intended or unintended) is determined from its time-domain characteristics via Fourier techniques. Similarly, the frequency-domain transfer function of the coupling path, T(f), is determined from the physical properties of the transmission medium. The spectrum of the signal received at the receptor is obtained as

$$R(f) = E(f) \cdot T(f) \qquad (1\text{-}1)$$

It should be pointed out that some portion(s) of the received spectrum may be a desired signal (e.g., a carrier frequency) whereas the remaining portion of the spectrum will be an undesired signal (e.g., harmonics). The received spectrum is compared to some susceptibility spectrum of the receptor, S(f), and if it exceeds, by some measure, that spectrum, interference is said to exist. Of course, this occurrence of interference is not, in reality, a binary decision; there are degrees of measure of the "severity" of this interference. Also

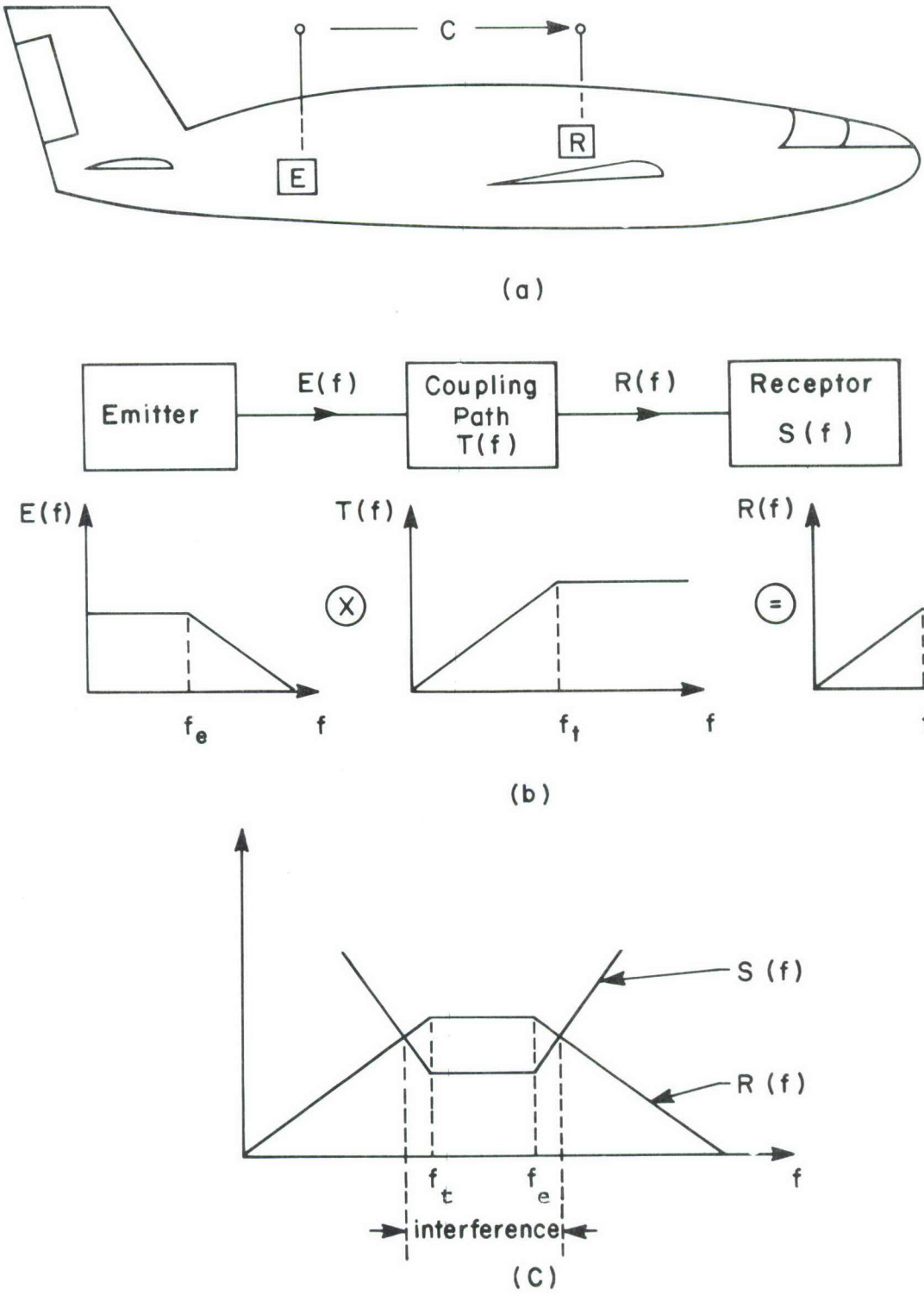

Fig. 1-1. Illustration of the analysis model of IEMCAP.

signals of other emitters may impinge upon this receptor. The effects of these combined spectra affect the receptor in a manner depending on how the receptor processes signals, e.g., analog or digital.

IEMCAP performs the analysis and prediction of interference in the above manner via frequency-domain methods. It is appropriate to note that these calculations could, theoretically, be performed in the time domain. A possible method would be to compute the time-domain received signal R(t) as

$$R(t) = E(t) * T(t) \tag{1-2}$$

where * denotes convolution. Alternatively, one could obtain R(t) from R(f) using the inverse Fourier Transform. Both of these methods require that the coupling path be linear since they inherently rely on superposition. One (perhaps major) difficulty with this time-domain approach is that to obtain even the maximum value of R(t) one must preserve the phase of E(f) and T(f), whereas to compute the maximum value of $|R(f)|$ one does not need to preserve phase information.

These concepts were outlined previously [2] and are included here for the purpose of clarifying the rationale and impact of suggested revisions of the code. In this report we will focus only on characterizing the coupling path, T(f). We will concentrate on the frequency-domain characterization.

The coupling paths assumed in IEMCAP fall into six distinct categories:

(1) wire-to-wire

(2) field-to-wire

(3) antenna-to-wire

(4) field-to-antenna

(5) antenna-to-antenna

(6) case-to-case

In this report we will concentrate only on (1) and (2), namely, wire-to-wire coupling contained in the WTWTFR subroutine and field-to-wire coupling contained in the FTWTFR subroutine. The report will be divided into three major areas: (1) revision of the WTWTFR subroutine, (2) revision of the FTWTFR subroutine and (3) the effect of system perturbations not presently included in the coupling path models. We will suggest revision of the above two subroutines for the purposes of (1) improving their prediction and modeling capabilities, (2) correcting deficiencies and errors presently in those subroutines, (3) providing a more modular structure for these subroutines, (4) providing a more sound theoretical basis for the models and (5) streamlining those subroutines to reduce code execution time.

Chapter 2 considers the WTWTFR subroutine. Exact models for predicting wire-to-wire coupling in transmission lines are reviewed to illustrate the reasons supporting the recommended revisions. Chapter 3 considers the FTWTFR subroutine. Exact models for predicting field-to-wire coupling in transmission lines are also considered here for the important purpose of justifying and supporting the recommended revisions.

A consideration of the effects of typical system perturbations which cause the system to deviate from the ideal physical model assumed by the above subroutine mathematical models will be given in Chapter 4. First, the effects of selected perturbations (ribs, cable clamps, hydraulic lines, bulkheads, junction boxes, cable trays, etc.) will be considered to ascertain whether these parameters in fact affect the coupling; that is, if the system perturbations were not present on a system would the coupling be altered significantly for practical system configurations, dimensions and frequencies of interest? Exact methods of characterizing these line perturbations and their incorporation

into conventional transmission line models will be reviewed.

Next, the effects of including models of these perturbations in the suggested WTWTFR and FTWTFR models will be examined. This latter consideration is very important. Even though a system perturbation affects the coupling in a physical system, inclusion of models for this perturbation into IEMCAP may not significantly affect the prediction accuracy of the wire-to-wire and field-to-wire coupling models. The proposed (and presently included) coupling models are simple models representing only first-order effects. The IEMCAP is a large code intended to handle large systems. Fine-grained, precide modeling of the coupling mechanisms would require complex, mathematical models which could cause the code execution times to be prohibitive. Consequently these simple prediction models may not predict certain second order effects such as high-frequency resonances. Certain perturbations such as periodically-spaced cable clamps can cause high frequency resonances in the coupling which would not appear if the clamps were removed. If the wire-to-wire models are not capable of predicting these resonances when models of the cable clamps are included, there is no need to include models of the cable clamps.

The results presented in Chapters 2 and 3 concerning the wire-to-wire and field-to-wire coupling models represent a distillation of some 10 years of research into these problems by the author.. Over that period of time it has become clear that these two very common (and very important) coupling mechanisms are much more complex than they may appear. Characterizing the lines with mathematical models is not the problem; these models are rather straightforward to develop (one exception is the twisted pair). Gaining a qualitative understanding of the behavior of a particular configuration without computing

the response at an enormous number of frequencies is very difficult. In some cases, traditional intuition as outlined in numerous handbooks proves to be valid; in other cases, this intuition proves to be drastically in error. (Some examples of this will be given in the course of the development.) The values and configurations of the line's terminations can drastically affect the behavior of the coupling. Thus one cannot make many general statements about a line's behavior unless the terminal configuration is precisely described.

Another and more difficult problem is devising simple mathematical models for a complex problem. The code presently considers frequencies from 30 Hz to 18 GHz. It is unrealistic to expect to be able to provide accurate predictive models over this range which are also simple.

In the course of suggesting models for this coupling for inclusion in IEMCAP we will make some rather general conclusions regardless of the line terminations knowing full well that they will not be correct for all situations which the code may be called on to model. We do so because the only other course would be to implement "exact" models of the coupling which include all effects no matter how remote the possibility of their being encountered. Such a course of action would no doubt cause the size and execution times for even small systems to be exhorbitant.

Another important area of tradeoffs in selecting the models is that of electrical size of the system. We know that for frequencies of excitation where the system dimensions, e.g., transmission line length, are much less than a wavelength or electrically small, distributed effects are not generally significant and lumped models of the line suffice for accurate predictions. For higher frequencies the problem (and associated models) become considerably

more complex. We will take the attitude that it is important to primarily model the coupling from low frequencies (30 Hz) up to some frequency where the line dimensions become electrically large. Then we will attempt to bound this inherently complex, high-frequency behavior.

II. REVISION OF THE WIRE-TO-WIRE COUPLING SUBROUTINE (WTWTFR)

The wire-to-wire coupling subroutine in IEMCAP (WTWTFR) is intended to model the electromagnetic coupling between wires in cable harnesses. The types of interconnect wires include (1) unshielded wires above ground, (2) shielded wires above ground, (3) twisted pairs above ground, and (4) shielded, twisted pairs above ground. In all cases the cable is assumed to be parallel to some ground plane which is the reference conductor for all wire voltages. This ground plane may be representative of an aircraft fuselage, missle frame or metallic walls of cabinets. Cable harnesses are most likely routed in close proximity to such metallic planes and their effect should be accounted for.

The modeling of transmission lines for the purposes of predicting electromagnetic coupling within those lines (crosstalk) can be a formidable problem [3]. "Exact" techniques for modeling transmission lines for the purposes of predicting crosstalk have existed for some time [3]. We use the term exact in the following sense. If the dimensions of the line (line length and cross-sectional dimensions such as conductor spacings) are electrically small at the frequency of excitation, then lumped models characterize the line with sufficient accuracy to predict experimental results [3]. As the frequency of excitation is increased to a point where the line length is no longer electrically small but the cross-sectional dimensions remain electrically small then the distributed parameter, transmission line models characterize the line with sufficient accuracy to predict experimental results [2]. If the frequency of excitation is increased further to the point where both the line length and the cross-sectional dimensions of the line are no longer electrically small neither the lumped models nor the transmission line model have sufficient accuracy to predict experimental results [4]. Thus the use of the term "exact"

is with regard to the prediction ability of the model for the frequency range of interest and not its inclusion of all effects no matter how insignificant. A general review of modeling of transmission lines is given in [5].

As one increases the frequency of excitation, the required "exact" prediction model not only changes in philosophy but also complexity. Certain simple lumped models which we will consider are suitable for hand calculation and yield considerable insight into the general behavior of the line which the distributed parameter, transmission line models do not. Where possible we will attempt to extend those simple, low-frequency models to higher frequencies where, although they do not apply, they are intended to either bound the exact results or indicate mean values of those results.

2.1 Untwisted, Unshielded Wires

The simplest configuration for which crosstalk can occur is the uniform, lossless three-conductor line immersed in a homogeneous medium shown in Fig. 2-1 [6]. The line consists of a generator (or emitter) conductor (wire) and a receptor conductor (wire) along with a reference conductor. The line is said to be uniform if the cross-sectional dimensions of the conductors and the properties of the surrounding medium do not change along with line axis (the x axis). The line is said to be lossless if the conductors are perfect conductors and the surrounding medium is lossless. The surrounding medium is said to be homogeneous if its constitutive parameters are independent of the cross-sectional coordinates. Suffice it to say that if we relax any of these requirements, the analysis of the line for its crosstalk properties becomes a formidable task. Only numerical solutions of the resulting transmission line equations have been obtained for lines in which any of the above properties are

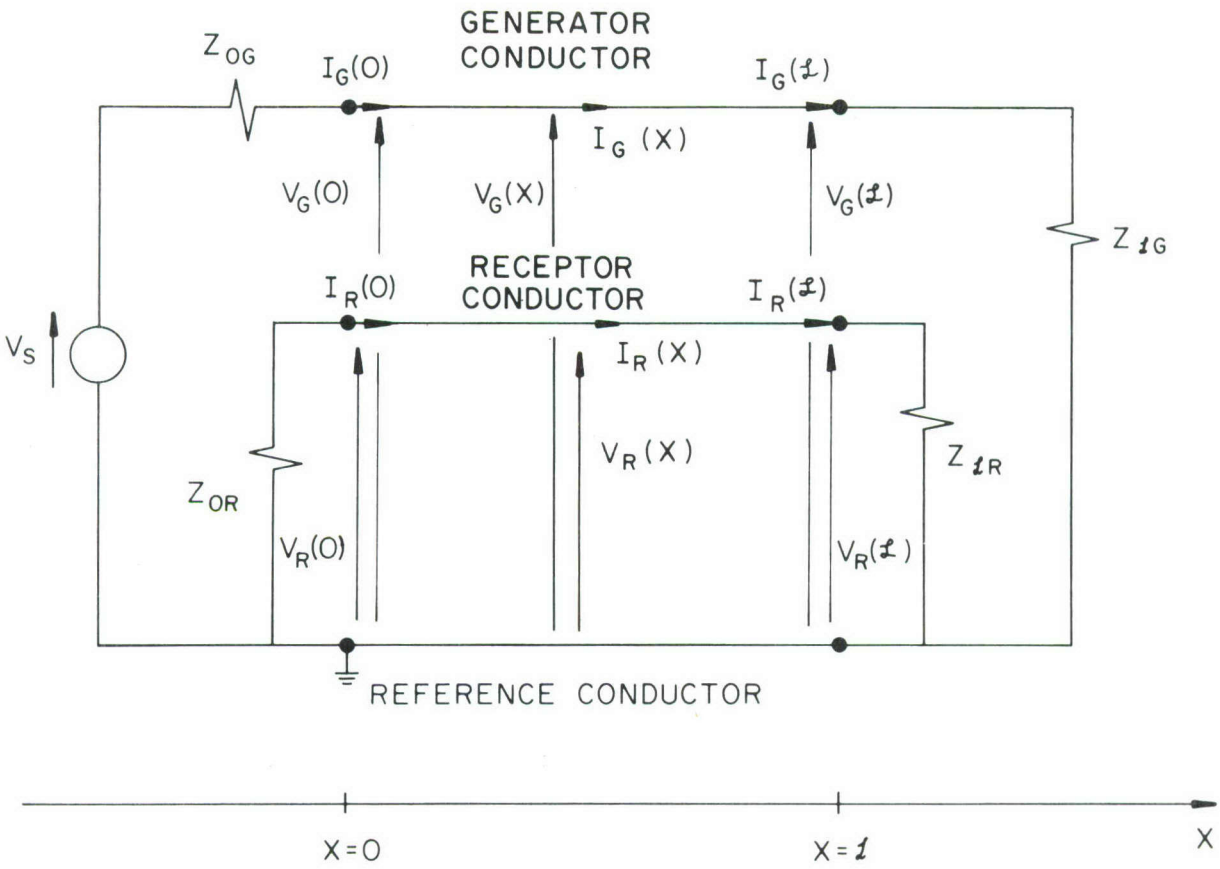

Fig. 2-1. The three-conductor transmission line.

relaxed. Some examples of line configurations represented by this class of line are shown in Fig. 2-2.

For this special class of line, however, one may solve the transmission line equations and incorporate the terminal constraints to yield literal (as opposed to numerical) solutions for the terminal currents induced in the receptor wire [6]. It is important to note that this is the simplest possible case of transmission lines which admits crosstalk. (Crosstalk is not meaningful for two-conductor lines.) Yet it is the only case for which closed form, literal solutions of the transmission line equations for the induced currents have been obtained. If we relax any of the above restrictions, add additional conductors (such as shields), twist the wires, etc., then the solution of the resulting "exact" transmission line equations with the terminal conditions incorporated have not been obtained in literal form. Only numerical solutions are available. Lumped circuit approximations of the transmission lines have been used in the past to avoid solution of the transmission line equations [3, 7]. However, these lumped circuit models are only valid for frequencies such that the line length is electrically small.

We now investigate this literal solution of the "exact" transmission line model of the above three-conductor line to (1) obtain some general conclusions as to the qualitative behavior of the crosstalk and (2) to illustrate the complexity of the problem.

The three-conductor line shown in Fig. 2-1 can be modeled as shown in Fig. 2-3. An electrically small, Δx section of the line is modeled with the per-unit-length line parameters of self inductance, l_G and l_R, mutual inductance, l_m, self capacitance, c_G and c_R, and mutual capacitance, c_m. The

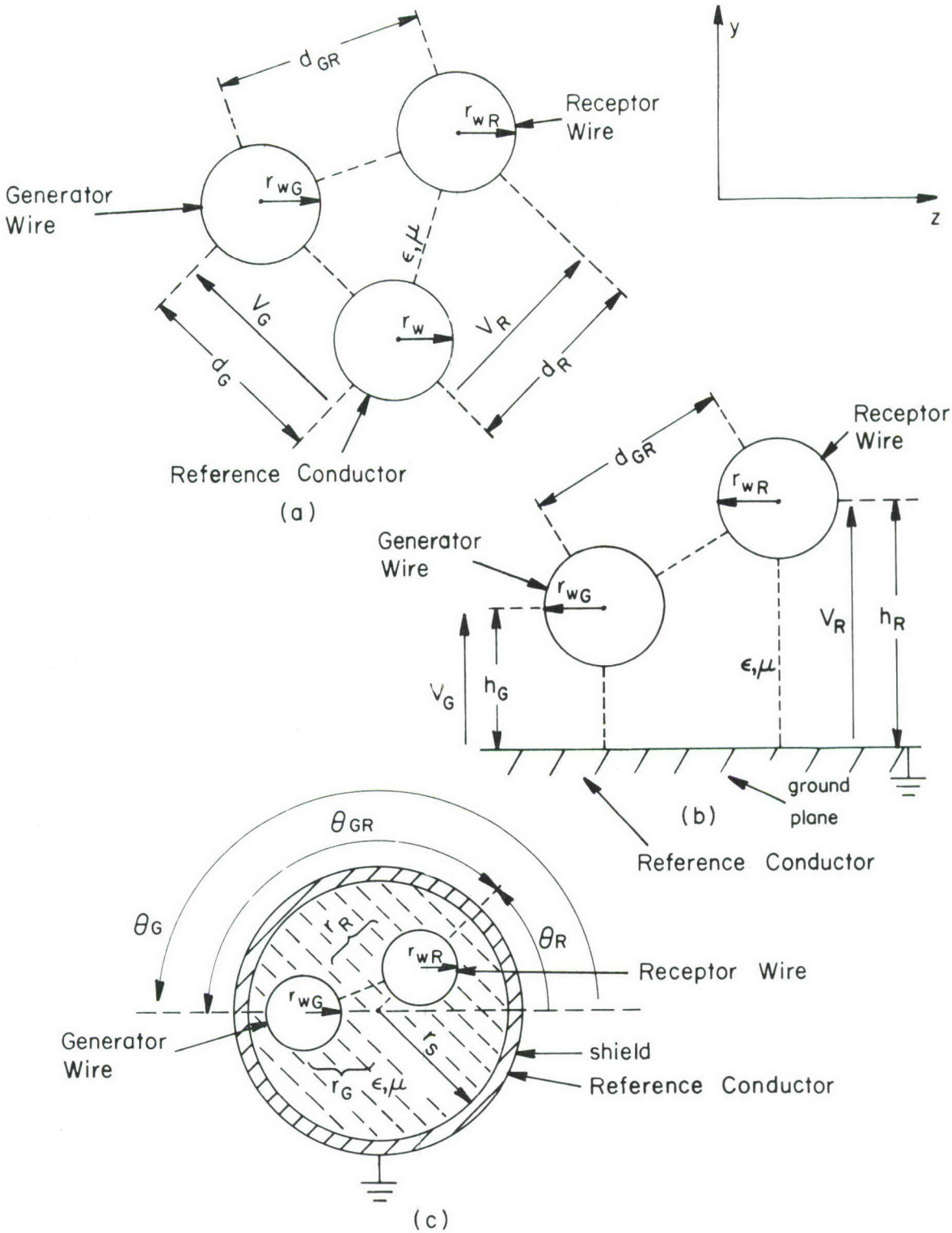

Fig. 2-2. Typical cross-sectional geometries.

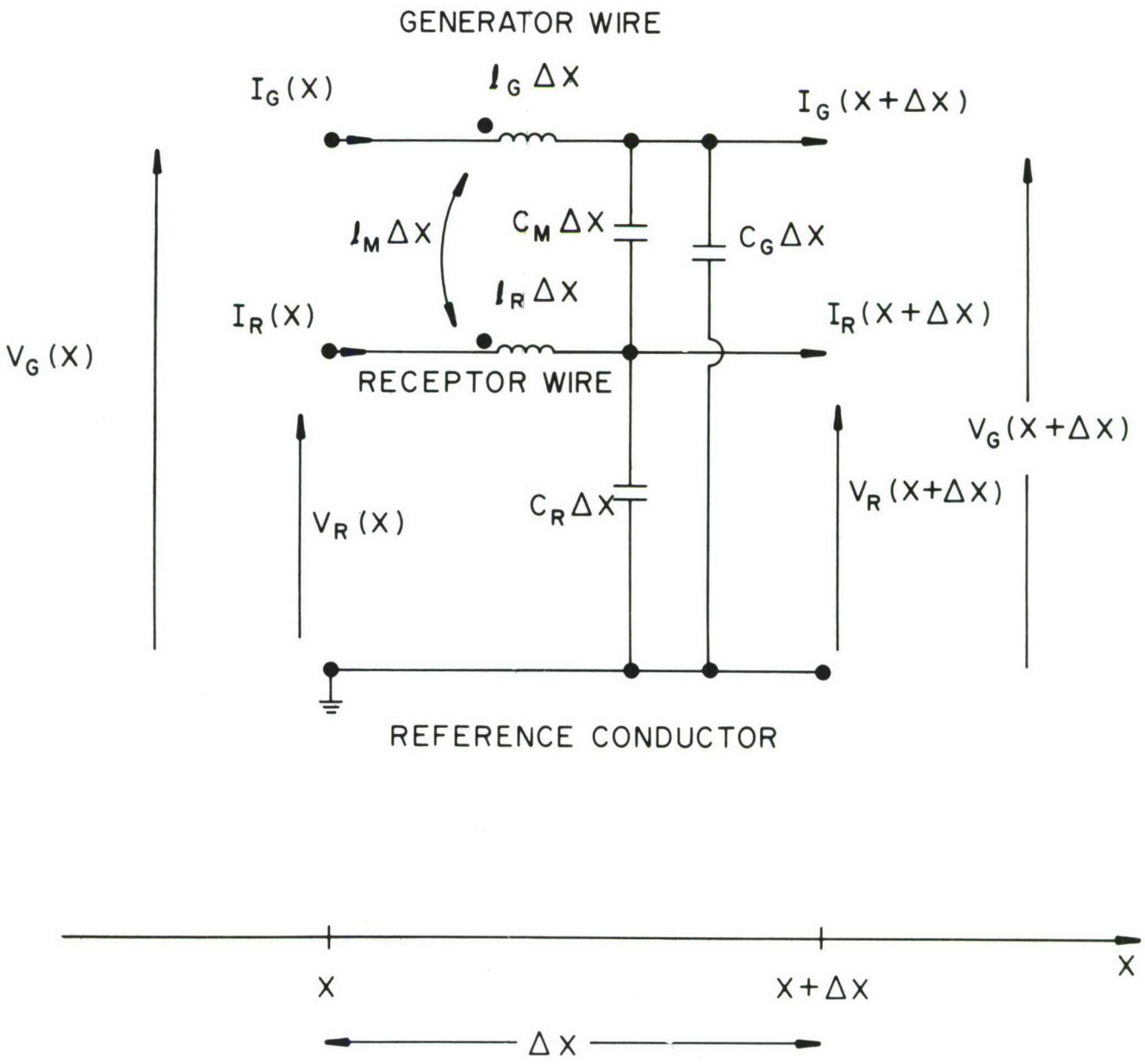

Fig. 2-3. The per-unit-length model.

transmission line equations are derived from this circuit in the limit as $\Delta x \to 0$ and become, in phasor form,

$$\begin{aligned}
\frac{dV_G(x)}{dx} &= -j\omega l_G\, I_G(x) - j\omega l_m\, I_R(x) \\
\frac{dV_R(x)}{dx} &= -j\omega l_m\, I_G(x) - j\omega l_R\, I_R(x) \\
\frac{dI_G(x)}{dx} &= -j\omega(c_G + c_m)\, V_G(x) + j\omega c_m\, V_R(x) \\
\frac{dI_R(x)}{dx} &= j\omega c_m\, V_G(x) - j\omega(c_R + c_m)\, V_R(x)
\end{aligned} \tag{2-1}$$

where $\omega = 2\pi f$ and f is the frequency of excitation of the line. The terminal constraints are

$$\begin{aligned}
V_G(0) &= V_s - Z_{0G}\, I_G(0) \\
V_G(\mathscr{L}) &= Z_{\mathscr{L}G}\, I_G(\mathscr{L}) \\
V_R(0) &= -Z_{0R}\, I_R(0) \\
V_R(\mathscr{L}) &= Z_{\mathscr{L}R}\, I_R(\mathscr{L})
\end{aligned} \tag{2-2}$$

The transmission line equations in (2-1) are solved and the terminal constraints in (2-2) are incorporated to yield equations for the induced voltages at the ends of the receptor wire:

$$V_R(\mathscr{L}) = \frac{S}{Den}\left[-\left(\frac{Z_{\mathscr{L}R}}{Z_{0R} + Z_{\mathscr{L}R}}\right)(j\omega l_m \mathscr{L})\, I_{GDC} + \left(\frac{Z_{0R}\, Z_{\mathscr{L}R}}{Z_{0R} + Z_{\mathscr{L}R}}\right) j\omega c_m \mathscr{L}\, V_{GDC}\right] \tag{2-3a}$$

$$V_R(0) = \frac{S}{Den}\left[\left(\frac{Z_{0R}}{Z_{0R} + Z_{\mathscr{L}R}}\right)(j\omega l_m \mathscr{L})\left\{C + \frac{j2\pi(\mathscr{L}/\lambda)}{\sqrt{1 - k^2}}\, \alpha_{\mathscr{L}G}\, S\right\} I_{GDC}\right. \tag{2-3b}$$

$$+ \left(\frac{Z_{0R} Z_{\ell R}}{Z_{0R} + Z_{\ell R}} \right) (j\omega c_m \ell) \left\{ C + \frac{j2\pi(\ell/\lambda)}{\sqrt{1 - k^2}} \frac{1}{\alpha_{\ell G}} S \right\} V_{GDC} \Bigg]$$

where

$$\text{Den} = C^2 - S^2 \omega^2 \tau_R \tau_G \left\{ 1 - k^2 \frac{(1 - \alpha_{0G}\alpha_{\ell R})(1 - \alpha_{0R}\alpha_{\ell G})}{(1 + \alpha_{0R}\alpha_{\ell R})(1 + \alpha_{0G}\alpha_{\ell G})} \right\} + j\omega CS (\tau_R + \tau_G) \tag{2-3c}$$

The various quantities in (2-3) are defined as follows. The terms C and S are

$$C = \cos(\beta\ell) = \cos\left(2\pi \frac{\ell}{\lambda}\right) \tag{2-4a}$$

$$S = \frac{\sin(\beta\ell)}{\beta\ell} = \frac{\sin\left(2\pi \frac{\ell}{\lambda}\right)}{(2\pi\ell/\lambda)} \tag{2-4b}$$

where λ is a wavelength at the frequency of excitation and is defined as $\lambda = v/f$ where v is the velocity of wave propagation. If the surrounding, homogeneous medium is described by permittivity ε and permeability μ, then $v = 1/\sqrt{\mu\varepsilon}$. The characteristic impedance of the generator (receptor) circuit is Z_{CG} (Z_{CR}) where

$$Z_{CG} = v l_G \sqrt{1 - k^2} \tag{2-5a}$$

$$Z_{CR} = v l_R \sqrt{1 - k^2} \tag{2-5b}$$

and the coupling coefficient between the two circuits is

$$k = \frac{l_m}{\sqrt{l_G l_R}} \quad 0<k<1 \tag{2-6}$$

The ratios of the terminating impedances to the appropriate characteristic im-

pedance are

$$\alpha_{0G} = \frac{Z_{0G}}{Z_{CG}} \qquad \alpha_{\ell G} = \frac{Z_{\ell G}}{Z_{CG}}$$
$$\alpha_{0R} = \frac{Z_{0R}}{Z_{CR}} \qquad \alpha_{\ell R} = \frac{Z_{\ell R}}{Z_{CR}} \tag{2-7}$$

and the time constants of the circuits are

$$\tau_G = \frac{l_G \ell}{Z_{0G} + Z_{\ell G}} + (c_G + c_m)\ell \quad \frac{Z_{0G} Z_{\ell G}}{Z_{0G} + Z_{\ell G}} \tag{2-8a}$$

$$\tau_R = \frac{l_R \ell}{Z_{0G} + Z_{\ell G}} + (c_G + c_m)\ell \quad \frac{Z_{0R} Z_{\ell R}}{Z_{0R} + Z_{\ell R}} \tag{2-8b}$$

The DC values of the generator line voltage and current are

$$V_{GDC} = \frac{Z_{\ell G}}{Z_{0G} + Z_{\ell G}} \quad V_s \tag{2-9a}$$

$$I_{GDC} = \frac{V_s}{Z_{0G} + Z_{\ell G}} \tag{2-9b}$$

Although the solutions in (2-3) are still quite involved, one can obtain considerable insight into the line behavior. An important example is the "low-frequency" behavior. Suppose the frequency of excitation is such that the line is electrically short ($\ell << \lambda$). Then $C \doteq 1$ and $S \doteq 1$. In the limit as the frequency is reduced, (2-3) become

$$V_R(\ell) \doteq -\left(\frac{Z_{\ell R}}{Z_{0R} + Z_{\ell R}}\right)(j\omega l_m \ell) \quad I_{GDC}$$
$$+ \left(\frac{Z_{0R} Z_{\ell R}}{Z_{0R} + Z_{\ell R}}\right)(j\omega c_m \ell) \quad V_{GDC} \tag{2-10a}$$

$$V_R(0) \doteq \left(\frac{Z_{0R}}{Z_{0R} + Z_{\ell R}}\right) (j\omega l_m \ell) \; I_{GDC} + \left(\frac{Z_{0R} Z_{\ell R}}{Z_{0R} + Z_{\ell R}}\right) (j\omega c_m \ell) \; V_{GDC} \qquad (2\text{-}10b)$$

These results can be obtained from the "low-frequency" equivalent circuit shown in Fig. 2-4. Note that (2-10) are the sum of two terms. One term depends on the mutual inductance between the two circuits, $l_m \ell$, and the other depends on the mutual capacitance between the two circuits, $c_m \ell$. These terms are referred to as inductive coupling and capacitive coupling contributions to the terminal voltages for obvious reasons. It can be shown that for "high impedance" loads, Z_{0G}, $Z_{\ell G} >> Z_{CG}$ and Z_{0R}, $Z_{\ell R} >> Z_{CR}$, that capacitive coupling dominates inductive coupling and vice-versa. This provides justification for an intuitive concept which has been used for many years without being formally justified. Clearly there is a frequency at which high order effects come into play and invalidate this simple "low-frequency" model. The precise frequency at which this occurs cannot be stated as an absolute quantity and depends very strongly on the values of the terminal impedances [7].

The behavior of the crosstalk for a "sufficiently small frequency" is clear from this low-frequency model - it increases linearly with frequency or 20 dB/decade. It would be advantageous to sketch the frequency response for higher frequencies without the need for computing the response at a large number of frequencies. This ability was provided in [8].

We will be interested in the voltage transfer ratios:

$$T_0 = \frac{V_R(0)}{V_S} \qquad (2\text{-}11a)$$

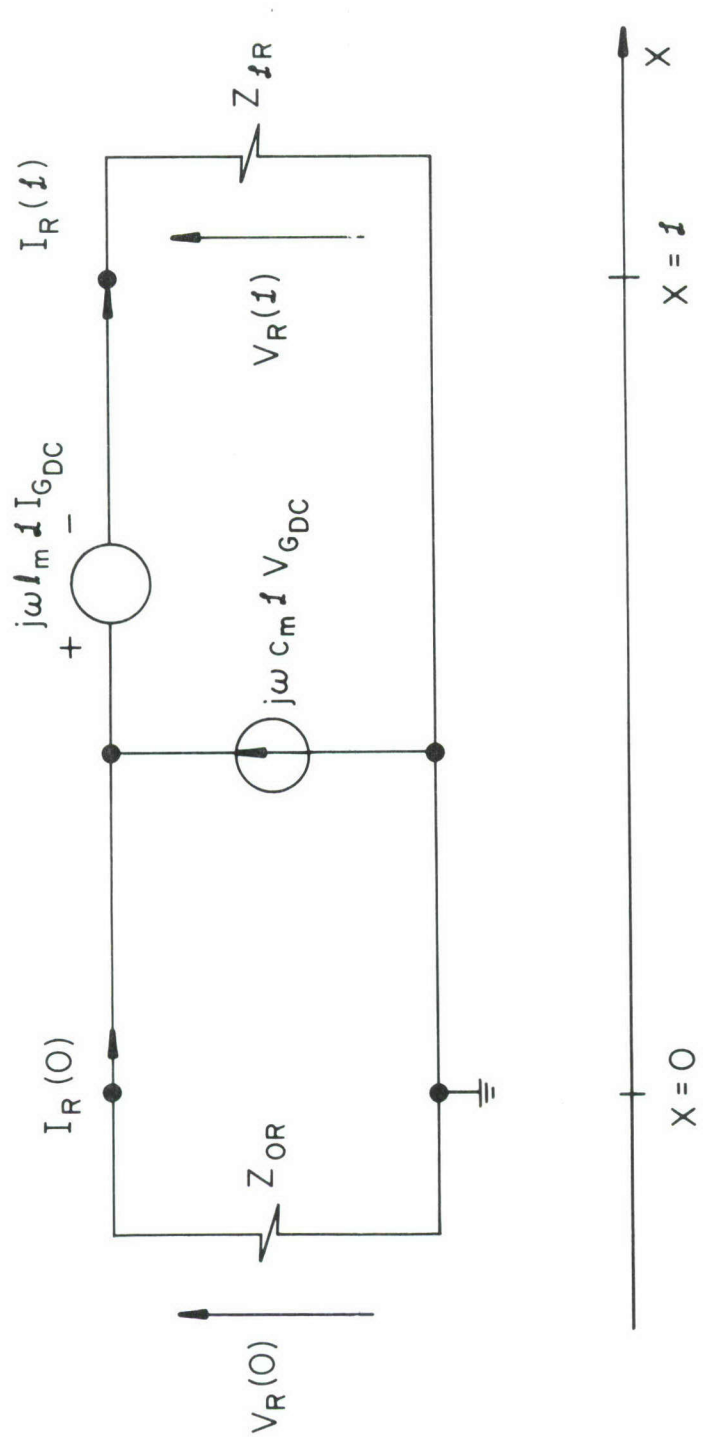

Fig. 2-4. The low-frequency approximation.

$$T_{\mathcal{L}} = \frac{V_R(\mathcal{L})}{V_S} \tag{2-11b}$$

The literal solution of the transmission line equations for this structure with the terminal conditions incorporated given in (2-3) can be placed in the following form:

$$T_0 = \frac{j \frac{\sin}{2\pi}(2\pi \frac{\mathcal{L}}{\lambda}) \left[\cos(2\pi \frac{\mathcal{L}}{\lambda}) + jT \frac{\sin}{2\pi}(2\pi \frac{\mathcal{L}}{\lambda})\right]}{\cos^2(2\pi \frac{\mathcal{L}}{\lambda}) + jA \frac{\sin}{2\pi}(2\pi \frac{\mathcal{L}}{\lambda})\cos(2\pi \frac{\mathcal{L}}{\lambda}) - B \frac{\sin^2}{(2\pi)^2}(2\pi \frac{\mathcal{L}}{\lambda})} M_0 \tag{2-12a}$$

$$T_{\mathcal{L}} = \frac{j \frac{\sin}{2\pi}(2\pi \frac{\mathcal{L}}{\lambda})}{\cos^2(2\pi \frac{\mathcal{L}}{\lambda}) + jA \frac{\sin}{2\pi}(2\pi \frac{\mathcal{L}}{\lambda})\cos(2\pi \frac{\mathcal{L}}{\lambda}) - B \frac{\sin^2}{(2\pi)^2}(2\pi \frac{\mathcal{L}}{\lambda})} M_{\mathcal{L}} \tag{2-12b}$$

Six parameters in these equations, A, B, T, M_0, $M_{\mathcal{L}}$ and λ, are defined as follows and are obtained by manipulating the results in [6].

In terms of the above basic parameters we may now obtain the parameters in (2-12) by manipulating the above solution to yield

$$A = T_G + T_R \tag{2-13a}$$

$$B = T_G T_R (1-\psi) \tag{2-13b}$$

$$T = \frac{2\pi}{\sqrt{1 - k^2}} \left[\frac{\alpha_{\mathcal{L}G} + \alpha_{\mathcal{L}R}}{1 + \alpha_{\mathcal{L}G}\alpha_{\mathcal{L}R}}\right] \tag{2-13c}$$

$$M_0 = 2\pi \frac{k}{\sqrt{1 - k^2}} \frac{Z_{0R}}{\sqrt{Z_{CG}Z_{CR}}} \left[\frac{(1 + \alpha_{\mathcal{L}R}\alpha_{\mathcal{L}G})}{(\alpha_{0G} + \alpha_{\mathcal{L}G})\ (\alpha_{0R} + \alpha_{\mathcal{L}R})}\right] \tag{2-13d}$$

$$M_{\mathcal{L}} = -2\pi \frac{k}{\sqrt{1 - k^2}} \frac{Z_{\mathcal{L}R}}{\sqrt{Z_{CG}Z_{CR}}} \left[\frac{(1 - \alpha_{0R}\alpha_{\mathcal{L}G})}{(\alpha_{0G} + \alpha_{\mathcal{L}G})\ (\alpha_{0R} + \alpha_{\mathcal{L}R})}\right] \tag{2-13e}$$

where the normalized time constants are

$$T_G = 2\pi \left(\frac{v}{\mathcal{L}}\right) \tau_G \tag{2-14a}$$

$$= \frac{2\pi}{\sqrt{1 - k^2}} \left[\frac{(1 + \alpha_{0G}\alpha_{\mathcal{L}G})}{(\alpha_{0G} + \alpha_{\mathcal{L}G})}\right]$$

$$T_R = 2\pi \left(\frac{v}{\mathcal{L}}\right) \tau_R \tag{2-14b}$$

$$= \frac{2\pi}{\sqrt{1 - k^2}} \left[\frac{(1 + \alpha_{0R}\alpha_{\mathcal{L}R})}{(\alpha_{0R} + \alpha_{\mathcal{L}R})}\right]$$

and

$$\psi = k^2 \frac{(1 - \alpha_{0G}\alpha_{\mathcal{L}R})(1 - \alpha_{\mathcal{L}G}\alpha_{0R})}{(1 + \alpha_{0G}\alpha_{\mathcal{L}R})(1 + \alpha_{0R}\alpha_{\mathcal{L}R})} \tag{2-15}$$

For the following results to be valid, we assume that the load impedances, Z_{0G}, $Z_{\mathcal{L}G}$, Z_{0R} and $Z_{\mathcal{L}R}$, are purely resistive, i.e., real.

From the solutions given in (2-12) it is clear that the frequency response is a function of frequency only in the ratio of the line length to the wavelength at that frequency:

$$\sigma = \frac{\mathcal{L}}{\lambda} \tag{2-16}$$

Also it is clear that this frequency dependence is manifested only in variations of the terms $\cos(2\pi\frac{\mathcal{L}}{\lambda})$ and $\sin(2\pi\frac{\mathcal{L}}{\lambda})$. From these observations we only need to plot the magnitudes of the transfer functions, T_0 and $T_{\mathcal{L}}$, for $0 \leq \frac{\mathcal{L}}{\lambda} \leq \frac{1}{4}$; that is, only the response for frequencies such that the line length is less than or equal to one quarter wavelength need be determined.

It is a simple matter to show this by showing that the magnitudes of the transfer functions, $|T_0|$ and $|T_{\mathcal{L}}|$, are periodic with period $\lambda/2$ and possess even symmetry about $\lambda/4$; that is

$$\left|T_0(\tfrac{\sigma}{2})\right| = \left|T_0(\tfrac{\sigma}{2} + \tfrac{n}{2})\right| \tag{2-17a}$$

$$\left|T_{\mathcal{L}}(\tfrac{\sigma}{2})\right| = \left|T_{\mathcal{L}}(\tfrac{\sigma}{2} + \tfrac{n}{2})\right| \tag{2-17b}$$

and

$$\left|T_0(\tfrac{\sigma}{4})\right| = \left|T_0(\tfrac{1}{2} - \tfrac{\sigma}{4})\right| \tag{2-18a}$$

$$\left|T_{\mathcal{L}}(\tfrac{\sigma}{4})\right| = \left|T_{\mathcal{L}}(\tfrac{1}{2} - \tfrac{\sigma}{4})\right| \tag{2-18b}$$

for $0 \leq \sigma \leq 1$ and $n = 1,2,3,\ldots$. Similar results apply to the phase angles of the transfer functions but are more difficult to describe. We will concentrate on plotting the magnitudes of the transfer functions. A typical plot is shown in Fig. 2-5 to illustrate these properties. Note in (2-12) that both transfer functions exhibit nulls at multiples of $\lambda/2$.

The basic idea of the method is to include the variable $\mathcal{L}/\lambda$, into a new variable, sketch the response as a function of that variable, and then transform or map that variable into the $\mathcal{L}/\lambda$ axis. To this end we define

$$\Theta = \frac{1}{2\pi} \tan(2\pi \frac{\mathcal{L}}{\lambda}) \tag{2-19}$$

In terms of this variable we may rewrite (2-12) as

$$T_0 = \frac{j\Theta(1 + j\Theta T)}{1 + j\Theta A + (j\Theta)^2 B} M_0 \tag{2-20a}$$

$$T_{\mathcal{L}} = \frac{1}{\cos(2\pi\frac{\mathcal{L}}{\lambda})} \frac{j\Theta}{1 + j\Theta A + (j\Theta)^2 B} M_{\mathcal{L}} \tag{2-20b}$$

Note that these forms are very similar to those encountered in automatic control and electric circuit theory where Θ here is analogous to radian frequency, ω, in those formulations. The common method of sketching those frequency responses is the logarithmic, asymptote plot commonly known as the Bode plot.

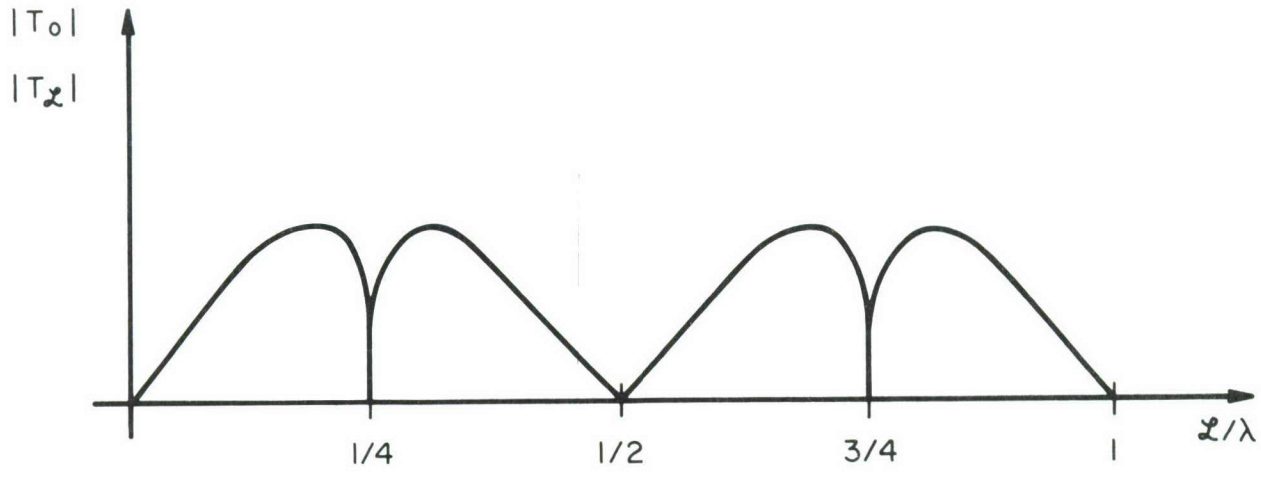

(a)

Fig. 2-5. Replication of the magnitudes of the transfer functions.

Separate Bode plots of magnitude and phase as a function of Θ can be easily generated from the results in (2-20). Then the Θ axis can be mapped into the $\frac{\ell}{\lambda}$ axis. Note that for electrically short lines, $\frac{\ell}{\lambda} << 1$,

$$\Theta \doteq \frac{\ell}{\lambda} \tag{2-21}$$

and the plots transform directly. Note that Θ is virtually identical to $\frac{\ell}{\lambda}$ for frequencies such that the line length is less than $\frac{1}{20}$ of a wavelength ($\frac{\ell}{\lambda} = 0.05$).

The reader will note that T_ℓ in (2-20b) is not free of the $\frac{\ell}{\lambda}$ variable since $\cos(2\pi\frac{\ell}{\lambda})$ remains in the denominator. With regard to plotting this transfer function via a Bode plot, the following theorem removes this difficulty.

Theorem:

$$\left|1 + j2\pi\Theta\right| = \left|\frac{1}{\cos(2\pi\frac{\ell}{\lambda})}\right| \tag{2-22}$$

Proof:

$$\left|1 + j2\pi\Theta\right| = \sqrt{1 + (2\pi\Theta)^2}$$

$$= \sqrt{1 + \tan^2(2\pi\frac{\ell}{\lambda})}$$

$$= \sqrt{\frac{\cos^2(2\pi\frac{\ell}{\lambda}) + \sin^2(2\pi\frac{\ell}{\lambda})}{\cos^2(2\pi\frac{\ell}{\lambda})}}$$

$$= \left|\frac{1}{\cos(2\pi\frac{\ell}{\lambda})}\right|$$

Thus to plot the magnitudes of the transfer ratios we may equivalently plot

$$\left|T_0\right| = \left|\frac{j\Theta(1 + j\Theta T)}{1 + j\Theta A + (j\Theta)^2 B} M_0\right| \tag{2-23a}$$

$$\left|T_{\mathcal{L}}\right| = \left| \frac{j\Theta(1 + j\Theta 2\pi)}{1 + j\Theta A + (j\Theta)^2 B} \; M_{\mathcal{L}} \right| \qquad (2\text{-}23b)$$

Of course the term $\cos(2\pi\frac{\mathcal{L}}{\lambda})$ in the denominator of (2-20b) can be removed when plotting the phase of $T_{\mathcal{L}}$.

If $|\psi| << 1$ then $A = T_G + T_R$ and $B \doteq T_G T_R$. In this case the denominator of the transfer functions factor as

$$1 + j\Theta A + (j\Theta)^2 B \doteq (1 + j\Theta T_G)\ (1 + j\Theta T_R), \quad |\psi| << 1 \qquad (2\text{-}24)$$

For this case, preparation of the Bode plots is quite simple. If $|\psi|$ is not much less than unity such that the denominators of the transfer functions do not factor as in (2-24) their contributions to the magnitude and phase plots can also be plotted in the usual fashion since A and B can be shown to be nonnegative. For this case the reader is referred to the numerous textbooks detailing this situation. In the following illustrations we will assume $|\psi| << 1$ so that the denominator of the transfer functions factors as in (2-24).

Assuming the denominator to factor as in (2-24), i.e., $|\psi| << 1$, the magnitudes become

$$\left|T_0\right| = \left| \frac{j\Theta(1 + j\Theta T)}{(1 + j\Theta T_G)\ (1 + j\Theta T_R)} \; M_0 \right| \qquad (2\text{-}25a)$$

$$\left|T_{\mathcal{L}}\right| = \left| \frac{j\Theta(1 + j\Theta 2\pi)}{(1 + j\Theta T_G)\ (1 + j\Theta T_R)} \; M_{\mathcal{L}} \right| \qquad (2\text{-}25b)$$

In decibels these become

$$\left|T_0\right| = 20 \log_{10}\left|T_0\right|$$

$$= \left|M_0\right|_{dB} + \left|j\Theta\right|_{dB} + \left|1 + j\Theta T\right|_{dB} - \left|1 + j\Theta T_G\right|_{dB} \qquad (2\text{-}26a)$$

$$- \left|1 + j\Theta T_R\right|_{dB}$$

$$\left|T_{\ell}\right|_{dB} = 20 \log_{10} \left|T_{\ell}\right|$$

$$= \left|M_{\ell}\right|_{dB} + \left|j\Theta\right|_{dB} + \left|1 + j\Theta 2\pi\right|_{dB} - \left|1 + j\Theta T_G\right|_{dB} \qquad (2\text{-}26b)$$

$$- \left|1 + j\Theta T_R\right|_{dB}$$

The terms M_0, M_{ℓ} and $j\Theta$ contribute a 20 dB/decade asymptote with levels $\left|M_0\right|_{dB}$ and $\left|M_{\ell}\right|_{dB}$ at $\Theta = 1$. The terms $\left|1 + j\Theta T\right|_{dB}$ and $\left|1 + j\Theta 2\pi\right|_{dB}$ in the numerators contribute 20 dB/decade asymptotes beginning at $\Theta = \frac{1}{T}$ and $\Theta = \frac{1}{2\pi}$, respectively. Similarly the denominator terms $\left|1 + j\Theta T_G\right|_{dB}$ and $\left|1 + j\Theta T_R\right|_{dB}$ contribute asymptotes of -20 dB/decade beginning at $\Theta = \frac{1}{T_G}$ and $\Theta = \frac{1}{T_R}$, respectively.

We will consider an example to illustrate the method. The cross-sectional structure of the line will consist of two #20 gauge wires (radius of 16 mils) located a height of 2 cm above a ground plane and separated a distance of 2 cm. One may compute [3]

$$\ell_G = \ell_R$$

$$= 9.18 \times 10^{-7} \text{ H/m}$$

$$\ell_m = 1.61 \times 10^{-7} \text{ H/m}$$

From this one may compute

$$k = \frac{\ell_m}{\sqrt{\ell_G \ell_R}}$$

$$= .1753$$

and

$$Z_{CG} = Z_{CR} = 271.1\ \Omega$$

Suppose

$$Z_{0G} = Z_{\mathcal{L}G} = Z_{0R} = Z_{\mathcal{L}R} = 1\ \Omega$$

We then compute

$$\alpha_{0G} = \alpha_{\mathcal{L}G} = \alpha_{0R} = \alpha_{\mathcal{L}R} = 3.6886 \times 10^{-3}$$

and

$$T_G = T_R = 865.1$$

Also

$$\psi = 3.073 \times 10^{-2}$$

and therefore $|\psi| << 1$. Also

$$T = 4.708 \times 10^{-2}$$

Similarly

$$M_0 = 75.83$$

$$M_{\mathcal{L}} = -75.83$$

Thus

$$\left|M_0\right|_{dB} = \left|M_{\mathcal{L}}\right|_{dB} = 37.6\ dB$$

The Bode plots for the magnitudes of the transfer ratios are shown in Fig. 2-6. The break points occur at $\frac{1}{T_G} = \frac{1}{T_R} = 1.156 \times 10^{-3}$, $\frac{1}{T} = 21.24$ and $\frac{1}{2\pi} = .16$. The terms $\left|M_0\right|_{dB} + \left|j\Theta\right|_{dB}$ and $\left|M\right|_{dB} + \left|j\Theta\right|_{dB}$ give a 20 dB/decade asymptote with a level of $\left|M_0\right|_{dB} = 37.6$ at $\Theta = 1$. To translate this level to $\Theta = 10^{-5}$ we simply add -100 dB to 37.6 dB to obtain the level of -62.4 dB at $\Theta = 10^{-5}$. The corresponding values of $\frac{\mathcal{L}}{\lambda}$ are labeled along the top of the plots. For this example it is quite easy to visualize the frequency response as a function of $\frac{\mathcal{L}}{\lambda}$. Note that the magnitudes of the transfer ratios achieve a maximum

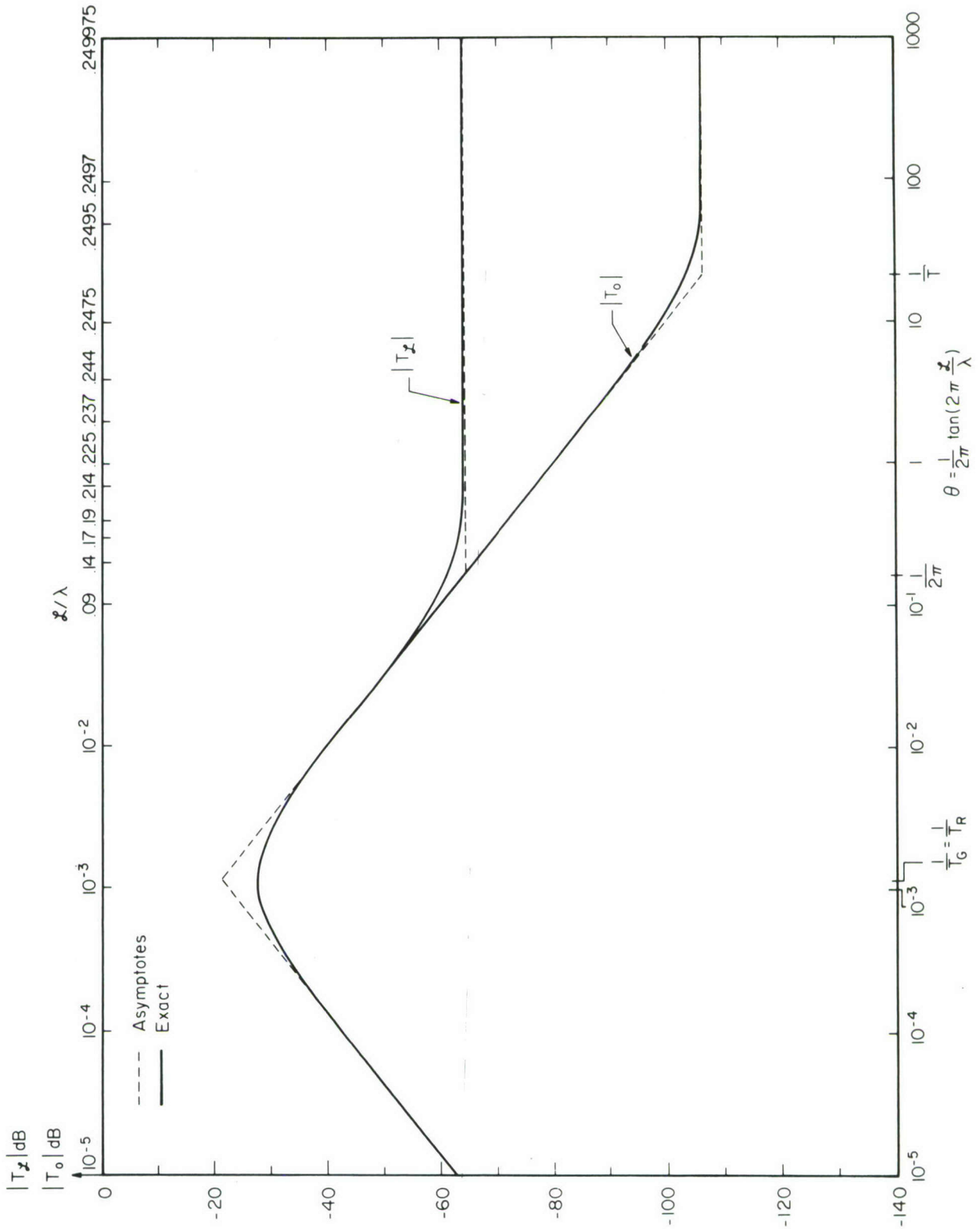

Fig. 2-6. Bode plots for the example.

of -23 dB at $\theta \doteq 1.25 \times 10^{-3} \doteq \frac{\ell}{\lambda}$. Thus the maximum response occurs at a frequency such that the line is very short, electrically. The plots of the magnitude of the transfer functions as a function of $\frac{\ell}{\lambda}$ for $10^{-5} \leq \frac{\ell}{\lambda} \leq 1$ are shown in Fig. 2-7.

The above example has shown that the maximum value of the crosstalk may occur at a frequency for which the line is electrically short. The maximum value of that crosstalk can be easily estimated from the asymptote plots.

To determine whether the maximum crosstalk occurs for frequencies where the line is less than one quarter of a wavelength now becomes a simple matter. Three possibilities occur as shown in Fig. 2-8. From these it is clear that the maximum crosstalk will occur when the line length is one quarter of a wavelength unless case (a) occurs that is, both normalized time constants, T_G and T_R, are greater than T or 2π as appropriate. From (2-13c), (2-14a) and (2-14b) this requires that the line time constants satisfy the following conditions for T_0:

$$\tau_R, \tau_G > \frac{\ell}{v} \frac{1}{\sqrt{1 - k^2}} \left[\frac{\alpha_{\ell G} + \alpha_{\ell R}}{1 + \alpha_{\ell G} \alpha_{\ell R}} \right] \tag{2-27}$$

For T_ℓ this requires that

$$\tau_R, \tau_G > \frac{\ell}{v} \tag{2-28}$$

i.e., the time constants of both circuits must be greater than the one-way transit time of the line.

The above example has illustrated that it is not a simple matter to bound the crosstalk in a transmission line. We have considered the simplest possible class of line and found that one cannot determine the maximum crosstalk without some effort. Certainly other classes of lines will be no less difficult to analyze.

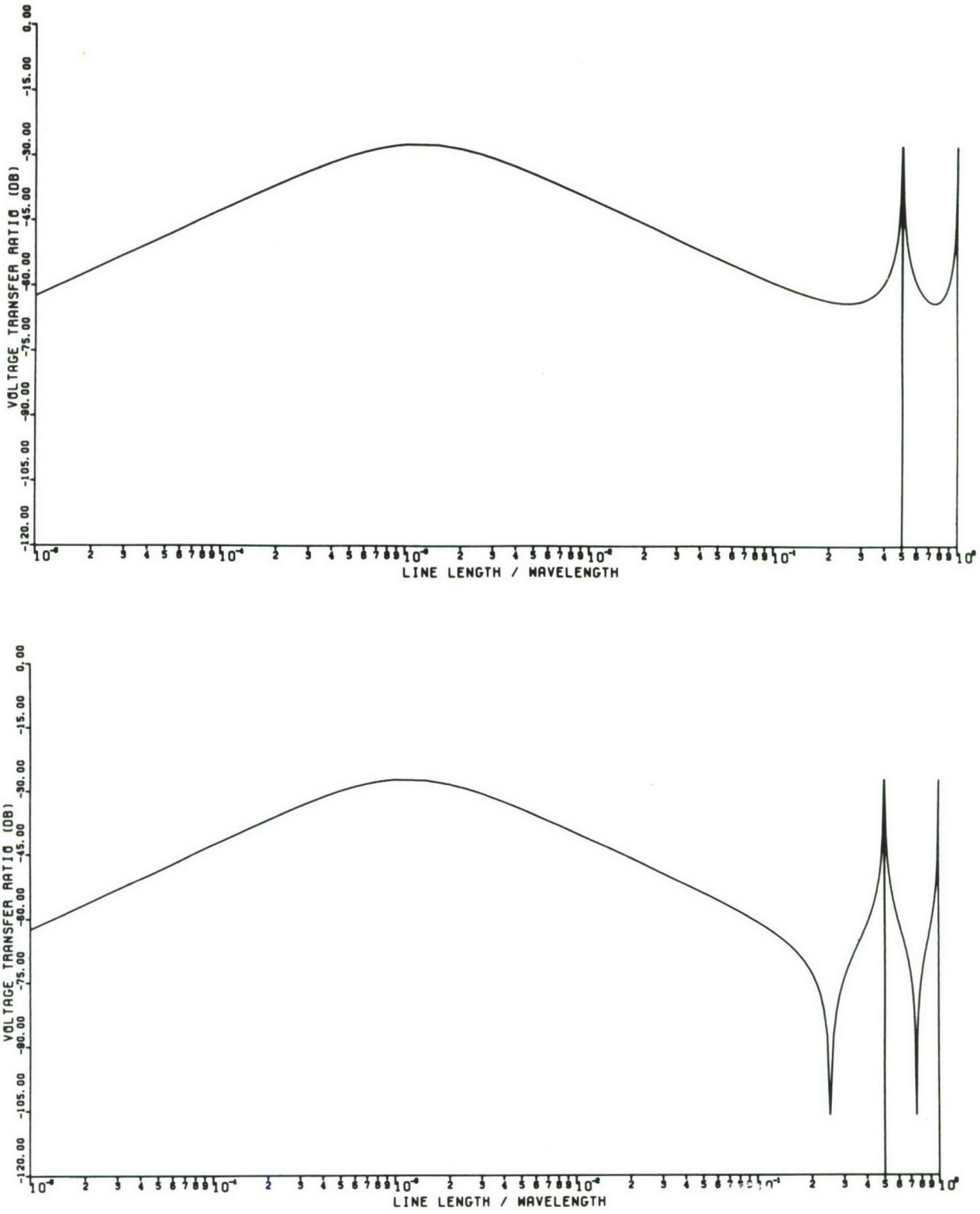

Fig. 2-7. Frequency response plots for the example.

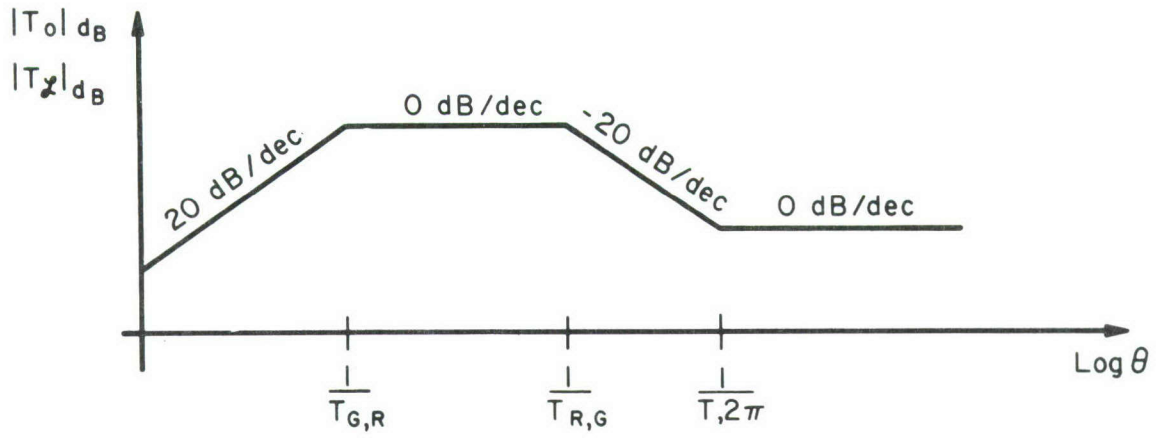

(a) $T_{G,R} > T, 2\pi$, $T_{R,G} > T, 2\pi$

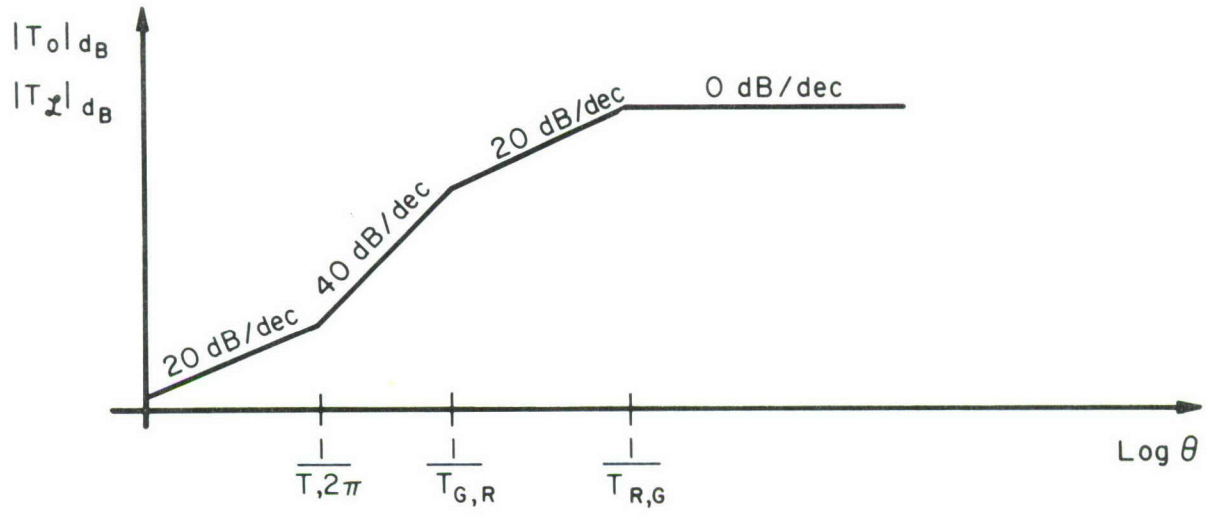

(b) $T, 2\pi > T_{G,R}, T, 2\pi > T_{R,G}$

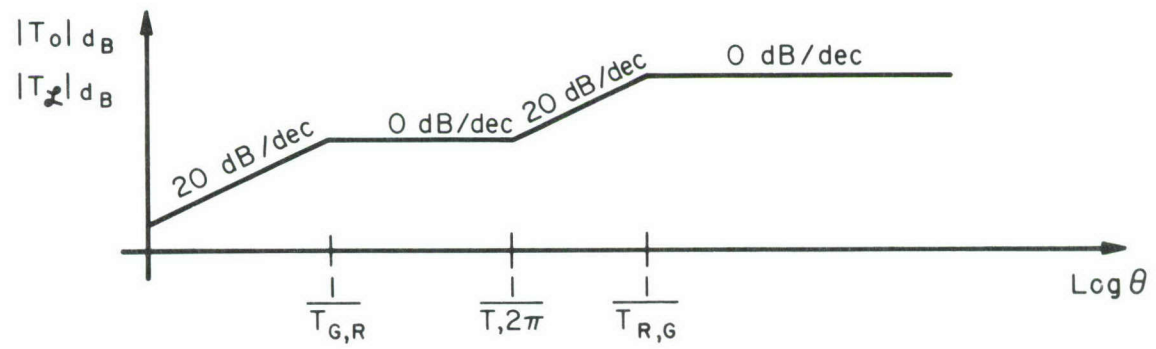

(c) $T_{G,R} > T_{R,G}$, $T, 2\pi > T_{R,G}$

Fig. 2-8. Three possibilities for the Bode plots. The maximum response occurs at $\mathcal{L} = \lambda/4$ except in case (a).

Before we proceed to those other classes of lines which IEMCAP considers let us consider the feasibility of extending the simple model in Fig. 2-4 to higher frequencies. The simple, low-frequency model in Fig. 2-4 applies for an electrically short line and a frequency of excitation which is "sufficiently small". We place the words sufficiently small, in quotes since there is no precise criterion for this which applies to all lines and termination impedances. Clearly the crosstalk increases at low frequencies linearly with frequency. Above a frequency where it no longer increases linearly with frequency, the low-frequency model in Fig. 2-4 is no longer valid. But this frequency is strongly dependent on the termination impedances. We showed an example where the low-frequency model of Fig. 2-4 applied only up to a frequency where the line length was equal to $\frac{1}{1000}$ of a wavelength; the line was very short, electrically. Other examples are given in [7] to illustrate this strong dependence on termination impedances.

We may extend this low-frequency model to higher frequencies so long as the line is electrically short. To do so let us assume that the line is electrically short such that $C \doteq 1$ and $S \doteq 1$. If we also assume weak coupling, $k << 1$, then (2-3) can be written as [7, 9]

$$V_R(\ell) = V_R^{IND}(\ell) + V_R^{CAP}(\ell) \tag{2-29a}$$

$$V_R(0) = V_R^{IND}(0) + V_R^{CAP}(0) \tag{2-29b}$$

where

$$V_R^{IND}(\ell) = -\left(\frac{Z_{\ell R}}{Z_{0R} + Z_{\ell R}}\right) \frac{j\omega l_m \ell I_{GDC}}{(1 + j\omega\tau_G)(1 + j\omega\tau_R)} \tag{2-30a}$$

$$V_R^{IND}(0) = \left(\frac{Z_{0R}}{Z_{0R} + Z_{\ell R}}\right) \frac{j\omega l_m \ell I_{GDC}}{(1 + j\omega\tau_G)(1 + j\omega\tau_R)} F_L \tag{2-30b}$$

$$V_R^{CAP}(\ell) = \frac{Z_{OR} Z_{\ell R}}{Z_{OR} + Z_{\ell R}} \quad \frac{j\, c_m \ell\, V_{GDC}}{(1 + j\omega\tau_G)\,(1 + j\omega\tau_R)} \tag{2-30c}$$

$$V_R^{CAP}(0) = F_C\, V_R^{CAP}(\ell) \tag{2-30d}$$

and

$$F_L = [1 + j\, 2\pi(\ell/\lambda)\, \alpha_{\ell G}] \tag{2-31a}$$

$$F_C = \left[1 + j\, \frac{2\pi(\ell/\lambda)}{\alpha_{\ell G}}\right] \tag{2-31b}$$

Note that the solutions for $V_R(\ell)$ are the low-frequency model solutions in (2-10) and obtained from Fig. 2-4 but divided by the terms

$$\text{Den} = (1 + j\omega\tau_G)\,(1 + j\omega\tau_R) \tag{2-32}$$

Thus it appears that we may modify the low-frequency model by dividing I_{GDC} and V_{GDC} by $(1 + j\omega\tau_G)$ and dividing the induced voltage in the receptor circuit by $(1 + j\omega\tau_R)$. Although this will extend the results of the low-frequency model to higher frequencies we still must require that the line be electrically short ($\ell \ll \lambda$) and weakly coupled ($k \ll 1$). Also we do not know precisely how far in frequency this result may be extended.

As for the solutions for $V_R(0)$, similar remarks apply except that $V_R^{IND}(0)$ is multiplied by the factor F_L and $V_R^{CAP}(0)$ is multiplied by the factor F_C. These factors are inconsequential for electrically short lines only if $\alpha_{\ell G} = 1$; that is, the generator line is matched. If $\alpha_{\ell G} \neq 1$, these factors may be significant [7].

For the moment let us assume that the line is electrically short ($\ell \ll \lambda$), weakly coupled ($\ell \ll 1$) and $F_L = F_C = 1$. Then the solutions in (2-29) and (2-30) can be written in the form

$$V_R(\ell) \doteq \frac{j\omega\, M_\ell}{(1 + j\omega\tau_G)\,(1 + j\omega\tau_R)} \tag{2-33a}$$

$$V_R(0) \doteq \frac{j\omega M_0}{(1 + j\omega\tau_G)\ (1 + j\omega\tau_R)} \qquad (2\text{-}33b)$$

Note that the responses vary linearly with frequency (20 dB/decade) up to a point where $\omega = \min\ (\frac{1}{\tau_G}, \frac{1}{\tau_R})$. At this point, the response becomes constant (0 dB/decade) up to the point at which $\omega = \max\ (\frac{1}{\tau_G}, \frac{1}{\tau_R})$. At this point the response falls off linearly with frequency (-20 dB/decade). This behavior is summarized in Fig. 2-9. Note that if the upper breakpoint, $\omega = \max\ (\frac{1}{\tau_G}, \frac{1}{\tau_R})$ occurs at a frequency where the line is electrically short as shown in Fig. 2-9, the maximum response occurs between the two breakpoints. Thus a simple way of bounding the result would be to use the low-frequency model of Fig. 2-4 to compute the response up to the first breakpoint and use that value of crosstalk for all higher frequencies. For the example shown in Fig. 2-6, this works quite well in predicting the maximum crosstalk. However, there will occur cases which violate the above assumptions. These are shown in Fig. 2-8. Only the case shown in Fig. 2-8 (a) would be predicted by this method. If one used this method to predict the maximum crosstalk for cases in Fig. 2-8 (b) and (c), possibly severe underprediction would occur; that is, the maximum crosstalk would be much greater than that predicted by the model in Fig. 2-9.

Thus the bounding of crosstalk in this simplest of all possible classes of transmission line is extremely complicated. In considering a model for this case for use in IEMCAP it would appear that the simple, low-frequency model shown in Fig. 2-4 would be the most appropriate. Because of the unknown wire configurations in a bundle and the neglecting of the effects of other wires in the bundle it makes little sense to try to accurately predict the ideal case (Fig. 2-1). Thus the proposed model is one in which the crosstalk increases linearly with frequency. The circuit model is given in Fig. 2-4.

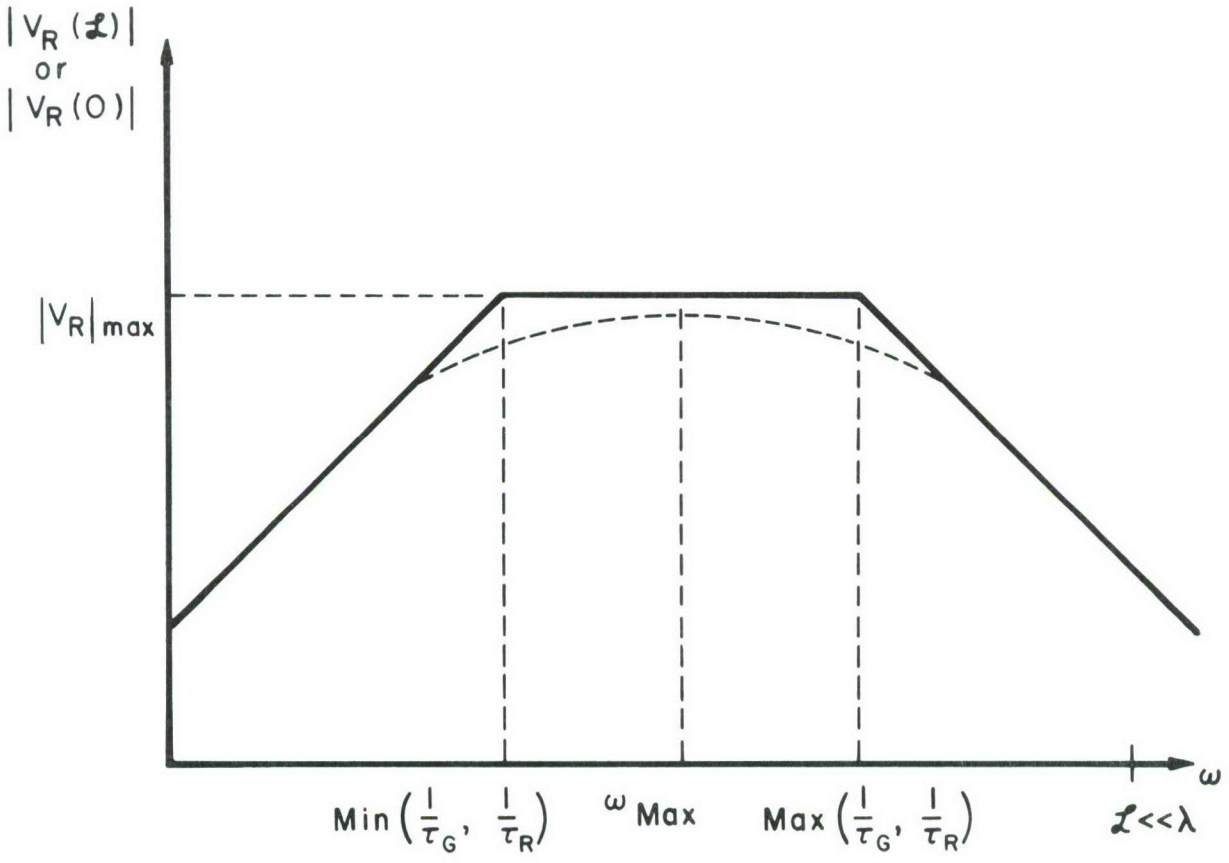
$|V_R(\ell)|$
or
$|V_R(0)|$
$|V_R|_{max}$
ω
$\text{Min}\left(\frac{1}{\tau_G}, \frac{1}{\tau_R}\right)$
ω Max
$\text{Max}\left(\frac{1}{\tau_G}, \frac{1}{\tau_R}\right)$
$\ell << \lambda$

Fig. 2-9.

It is of interest to limit the predictions of this model where they become unrealistic. We have shown above that bounding the crosstalk for this ideal case is far from simple. Perhaps the simplest choice of a bound would be unity coupling. More will be said about this later.

2.2 Untwisted, Shielded Wires

The cases to be considered are shown in Fig. 2-10. The generator/receptor wire may be unshielded or shielded. An investigation of these cases was given in [10, 11]. These configurations are shown having pigtails on either end of the shield. The pigtail sections are considered to be exposed sections of the shielded wire.

It was shown in [10, 11] that for an electrically short line one can superimpose the coupling over the shielded section and the coupling over the pigtail sections. The coupling over the pigtail sections can be treated as in the previous section - a segment of unshielded wires.

A coupling model for the contribution over the shielded section for an electrically short line can similarly be obtained. Let us consider the case in Fig. 2-10 (b) of an unshielded generator wire and a shielded receptor wire. The coupling depends on whether the shield is ungrounded, single end grounded or double end grounded. If the shield is ungrounded it is assumed to have no effect on capacitive and inductive coupling. In fact, it does have a small effect given by the voltage division ratio between the shield-to-ground capacitance and the generator wire-to-shield mutual capacitance. But this is usually small (6 dB) as shown in [10, 11]. If the shield is single-end grounded, it is assumed to eliminate any capacitive coupling to the shielded wire but not affect the inductive coupling. If the shield is double-end

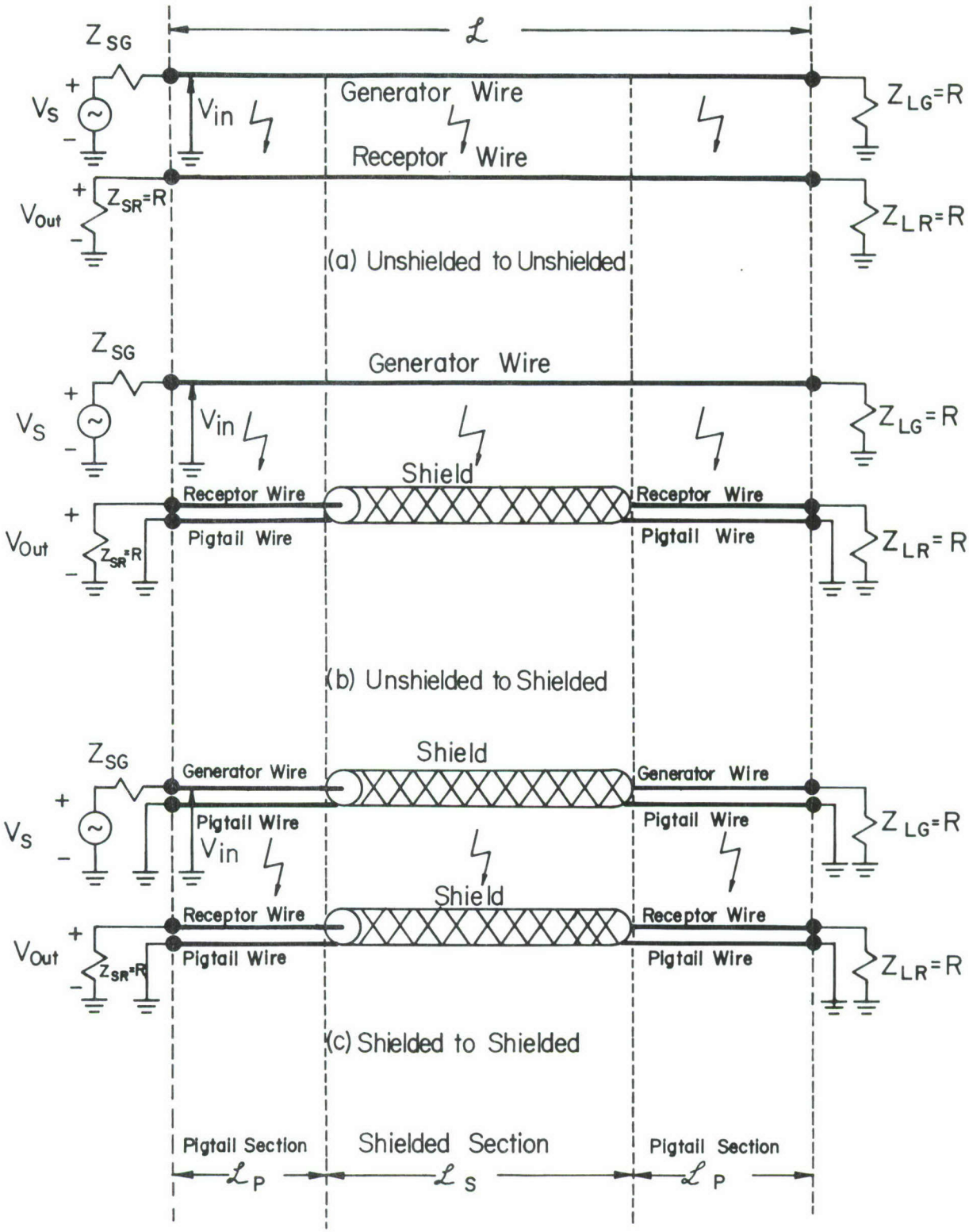

Fig. 2-10. Three cases illustrating crosstalk to shielded wires.

grounded, the capacitive coupling is removed and the inductive coupling is modified by the shield impedance, Z_{SH}, and self inductance above ground, L_S:

$$V_R^{IND}(0) = - \frac{Z_{0R}}{Z_{0R} + Z_{\ell R}} \; j\omega l_m \ell \, I_G \, \frac{Z_{SH}}{Z_{SH} + j\omega L_S} \tag{2-34a}$$

$$V_R^{IND}(\ell) = \frac{Z_{\ell R}}{Z_{0R} + Z_{\ell R}} \; j\omega l_m \ell \, I_G \, \frac{Z_{SH}}{Z_{SH} + j\omega L_S} \tag{2-34b}$$

$$\begin{aligned} V_R^{CAP}(0) &= V_R^{CAP}(\ell) \\ &= 0 \end{aligned} \tag{2-34c}$$

The above model was shown to provide reasonable predictions in [10, 11]. A more detailed modeling of the line using the transmission line model was shown in [11, 12] to provide very accurate predictions for carefully controlled configurations. It was also demonstrated in [12] that the location and orientation of the pigtail wires can have a dramatic influence on the crosstalk. A worst case model would assume that the pigtail wires go directly to ground at the ends of the shields and do not pass along the pigtail sections (which they usually do in a connector installation). For shields on both wires, the model in (2-34) is modified by multiplying by another factor $Z_{SH}/(Z_{SHG} + j\omega L_{SG})$ due to the shield on the generator wire [11].

2.3 Twisted, Unshielded Wires

The subject of modeling twisted pairs was investigated in several reports by the author. The unbalanced twisted pair configuration shown in Fig. 2-11 was shown to be adequately modeled, for electrically short lines, by a sequence of loops [13, 14, 15, 16]. The consequence was that only the differential mode induced current needed to be modeled, the inductive coupling was reduced by the ratio of the loop length to total line length and the capacitive coup-

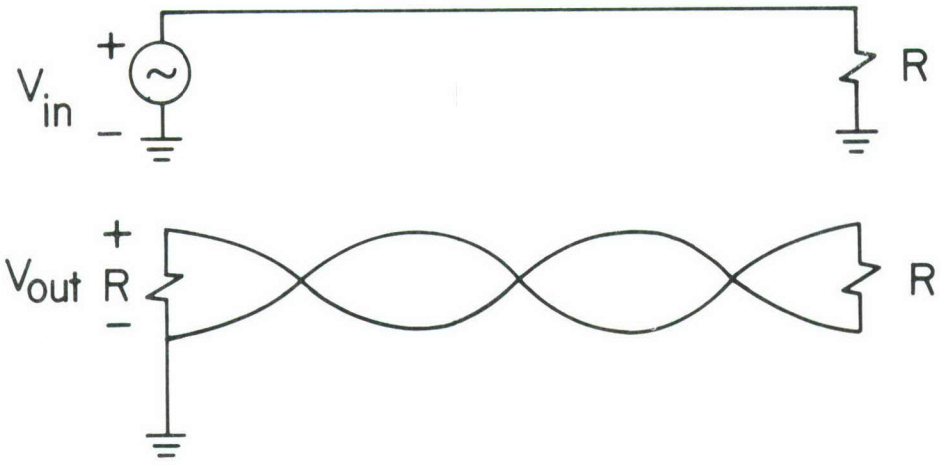

(a) The Unbalanced, Twisted Pair

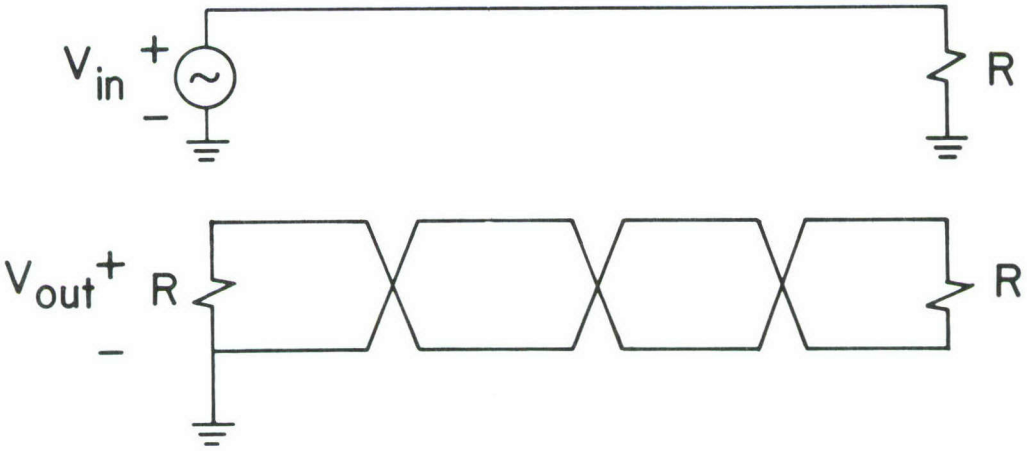

(b) The "Abrupt-Loop" Model

Fig. 2-11. The unbalanced, twisted pair.

ling was the same as to a single wire. The effect of twisting thus lowers the inductive coupling drastically but does not affect the capacitive coupling.

For the balanced twisted pair shown in Fig. 2-12, the balancing of the terminations reduced the capacitive coupling also. Thus the line was essentially modeled as only a single loop and differential mode coupling calculated (perfect balance is assumed) [17, 18].

2.4 Twisted, Shielded Wires

Twisted pairs which have overall shields have not been investigated by the author or apparently to any significant degree in the open literature. There is no reason, however, to believe that the above concepts would not apply here (at sufficiently low frequencies).

An ungrounded shield should have little effect. A single-end grounded shield should eliminate capacitive coupling (which may already be eliminated in the balanced case), and a double-end grounded shield would cause the common-mode inductive coupling in the unbalanced case to be multiplied by $Z_{SH}/(Z_{SH} + j\omega L_{SH})$ and have no effect on the differential mode, inductive coupling in the balanced case.

2.5 Branched Cables

It is reasonable to assume that for electrically short lines which have branches that one can superimpose the coupling contributions over the uniform segments. This was verified for the case of pigtails [11]. If one cannot make this assumption, consideration of the loading on each segment provided by the attached segments becomes a very difficult problem if implemented in IEMCAP. In IEMCAP one may construct very elaborate branchings and if one could not make the above assumption, one would be required to "reflect" impedances to the ends of every segment involved. This would dramatically

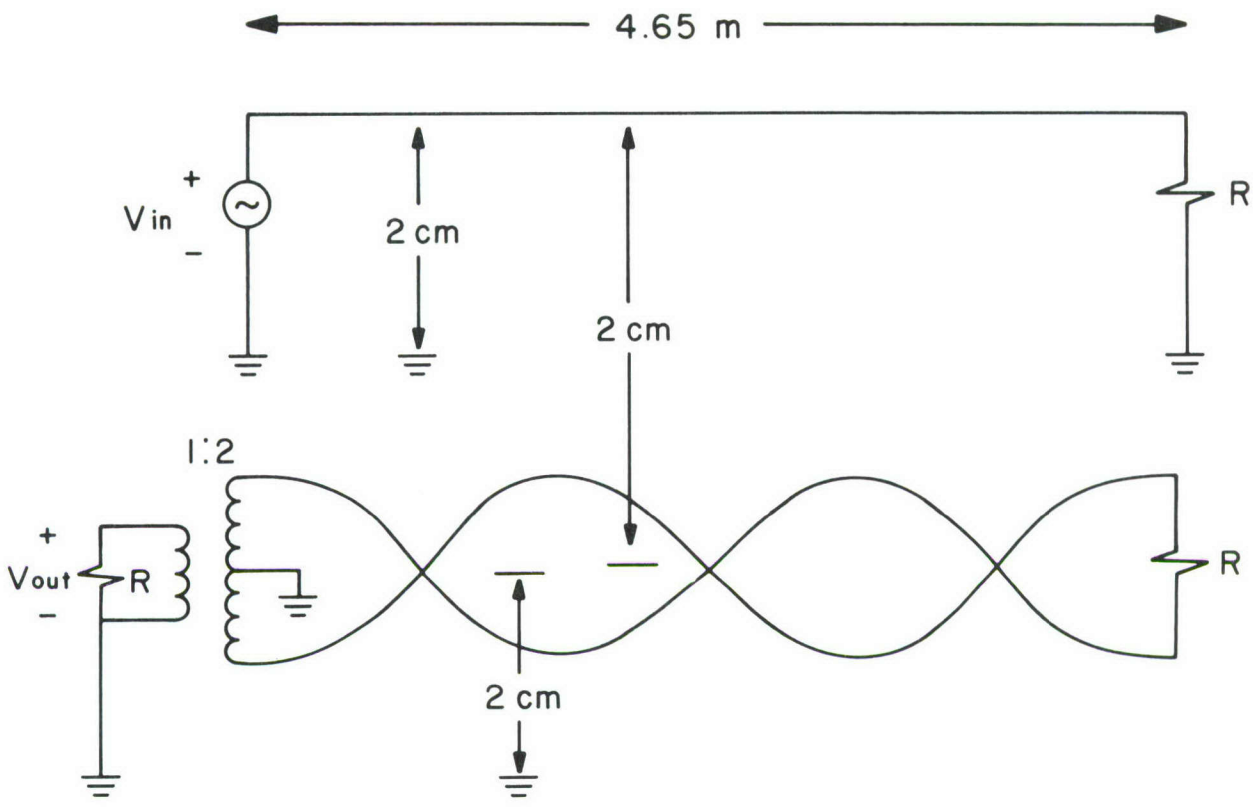

Fig. 2-12. The balanced, twisted pair.

affect the coding difficulties.

2.6 Recommendations for Revision of the Wire-to-Wire Coupling Subroutine (WTWTFR)

This section contains recommendations for changes in the wire-to-wire coupling subroutine (WTWTFR) in IEMCAP. The changes are intended to accomplish four objectives: (1) to modularize that subroutine, (2) to speed up computation, (3) to provide models which have more sound theoretical basis than those presently included in IEMCAP, and (4) to correct certain errors presently in the current models in IEMCAP. The first objective - to modularize the subroutine - is important from the standpoint of future maintenance of the code. The other three objectives concern relatively accurate and speedy predictions. It is important that the models have a sound theoretical basis rather than have the ability to predict only certain limited, empirical data. One then has some confidence that the models will predict some, as yet, uninvestigated situation.

The subroutine which was initially delivered by the contractor contained numerous theoretical inconsistencies and model prediction errors. These were thought to be corrected via a completely rewritten subroutine [19]. The models in that revised subroutine were based on the modeling efforts to that date. Shielded wires and twisted pairs had not been extensively investigated from the standpoint of models for predicting crosstalk. Thus models for those portions of the subroutine were based on limited modeling data which existed at the time [20].

Since that initial revision, several modifications were made to correct coding errors and to add additional features. The original revision was designed to handle pigtails on shielded wires which were three inches (3")

in length. No provision was made for peripherally bonded shields (zero-length pigtails) or variable lengths of pigtails from shield to shield. Recently a revision was made to WTWTFR to allow for variable length pigtails [21]. It has been determined that this revision did not correctly handle pigtails for inductive coupling. In the original revision, the restriction of 3" pigtails on all shield terminations allowed an optimization of the code which would not have been possible with variable length pigtails. Since that code structure and the models relied heavily on the restriction that all shield pigtail terminations be the same it is not a simple matter to change that code to now handle variable length pigtails. Moreover, adding the capability of variable length pigtails by modifying the original code would not take advantage of the optimization which the assumption of 3" pigtails allowed. It would seem, therefore, that one should rewrite and optimize the structure of the code for the variable length pigtail case.

Much additional work has been done on the modeling of crosstalk involving shielded wires and twisted pairs since that original code revision as outlined above. This additional work has shown that some of the models for these cases contained in the original revision are not correct and some models were unnecessarily complicated for the prediction accuracies which one would reasonably expect on practical systems. In addition, some long-held, fundamental notions concerning the superposition of inductive and capacitive coupling (which were fundamental to the original revision) were shown to be incorrect [7].

Thus because of the additional modeling experience and the discovery of the error of certain fundamental model premises, the WTWTFR models need

modification. Because of the extensiveness of these modifications as well as the other reasons alluded to above, it seems advisable to completely rewrite the WTWTFR subroutine. In doing so it is also advisable that it be modularized and optimized. Modularization is critically important from the standpoint of future maintenance. It is possible, but very difficult, for anyone who is not intimately (and currently) familiar with the present code to make changes to it much less track the effects of those changes through the code. Modularization would remedy this problem to a large degree.

2.6.1 Recommended Configurations and Model Assumptions

The present code contains models intended to handle single wires with ground return and twisted pairs (balanced and unbalanced). Shields (single or double) may surround these wires and the shields may be ungrounded, single end grounded or double end grounded. A number of variations from the ideal are also supposedly considered. Shields are considered braided and a "shield penetration factor" is used to attempt to model the penetrations through the holes in these shields. Although this type of penetration no doubt exists, the model in WTWTFR for this has not been theoretically justified. This is an extraordinarily difficult problem which is not amenable to some simple factor such as the above. For this reason, it is recommended that the shield penetration factor remain as presently modeled. Once more theoretically sound models for this effect are obtained they may be incorporated into a modularized code.

In the case of twisted pairs, the current code considers "Unbalanced" and "Balanced" twisted pairs. The specific terminal configurations which these are intended to address has not been clear. In addition, for both these, their deviation from the ideal caused by stray (or intentional)

impedances to ground has been considered on a somewhat unjustifiable basis. A balanced twisted pair is usually considered to be one in which the impedances at one end from each wire to ground are the same. This results in only "differential mode" currents and voltages. Any "unbalance" creates "common mode" currents which return through the ground plane and wire voltages with respect to the ground plane which are not equal. The present "unbalanced twisted pair" model in the code is a somewhat common model but the common mode currents and voltages are computed by adding some heuristically derived stray elements. In a practical (and usually large) system one can only guess at these stray unbalance elements. Even if these stray elements could be accurately ascertained, one would have the large data entry and data gathering problem of inputting and determining them for each twisted pair deployed in the system. Also one is constrained to consider only one configuration for the stray elements in order to derive code equations for that model. If the configuration chosen for these stray, unbalance, nonideal elements does not fit a users actual configuration then the equations for coupling do not apply to that user's problem. Since there are a large number of possible configurations for these strays, it is recommended that these nonideal elements not be considered; that is, we assume a twisted pair to be either perfectly balanced or unbalanced according to a specific model for which system design data is usually obtainable. It is unrealistic to ask the user to gather data or make good estimates of these nonideal parameters for every wire pair deployed in the system. Furthermore the error incurred in inaccurate estimates of these parameters may well be larger than that incurred by other ill-defined but necessary parameters such as relative wire positions in a bundle.

It must be kept in mind that the purposes of IEMCAP are (1) to provide a system configuration file and (2) to provide estimates of potential problem areas so that a more detailed analysis can be used to determine whether a problem will likely exist.

In view of the above rationale, a list of recommended system wiring types for Emitter circuits and Receptor circuits are shown in Fig. 2-13. These represent the most common types of wiring configurations. What needs to be addressed now is the specific terminal configurations at the ends of the wires. The terminal configuration can be more important than the wiring type in controlling EMI. We have chosen the termination configurations for emitters as those shown in Fig. 2-14. The terminations for the receptors are shown in Fig. 2-15.

First consider the emitters shown in Fig. 2-14. The single wire above ground is driven by a 1 volt source (with respect to ground) and terminated in an impedance Z_{LG} with respect to ground. A common mode current, I_C, returning through the ground plane, computed for DC, represents the magnetic field effect (inductive coupling) on neighboring wire circuits. A common mode voltage, V_C, with respect to ground, computed for DC, represents the electric field effect (capacitive coupling) on neighboring wire circuits. For frequencies where the line is not electrically short, these items vary from their DC values. However to consider this variation (up to the 18 GHz frequency limit of the code) would require a transmission line model which would severely complicate the code. It would not necessarily provide more accurate predictions due to the usual host of variations in other important parameters which are present in any practical system.

The assumed terminal configuration for the balanced twisted pair emitter

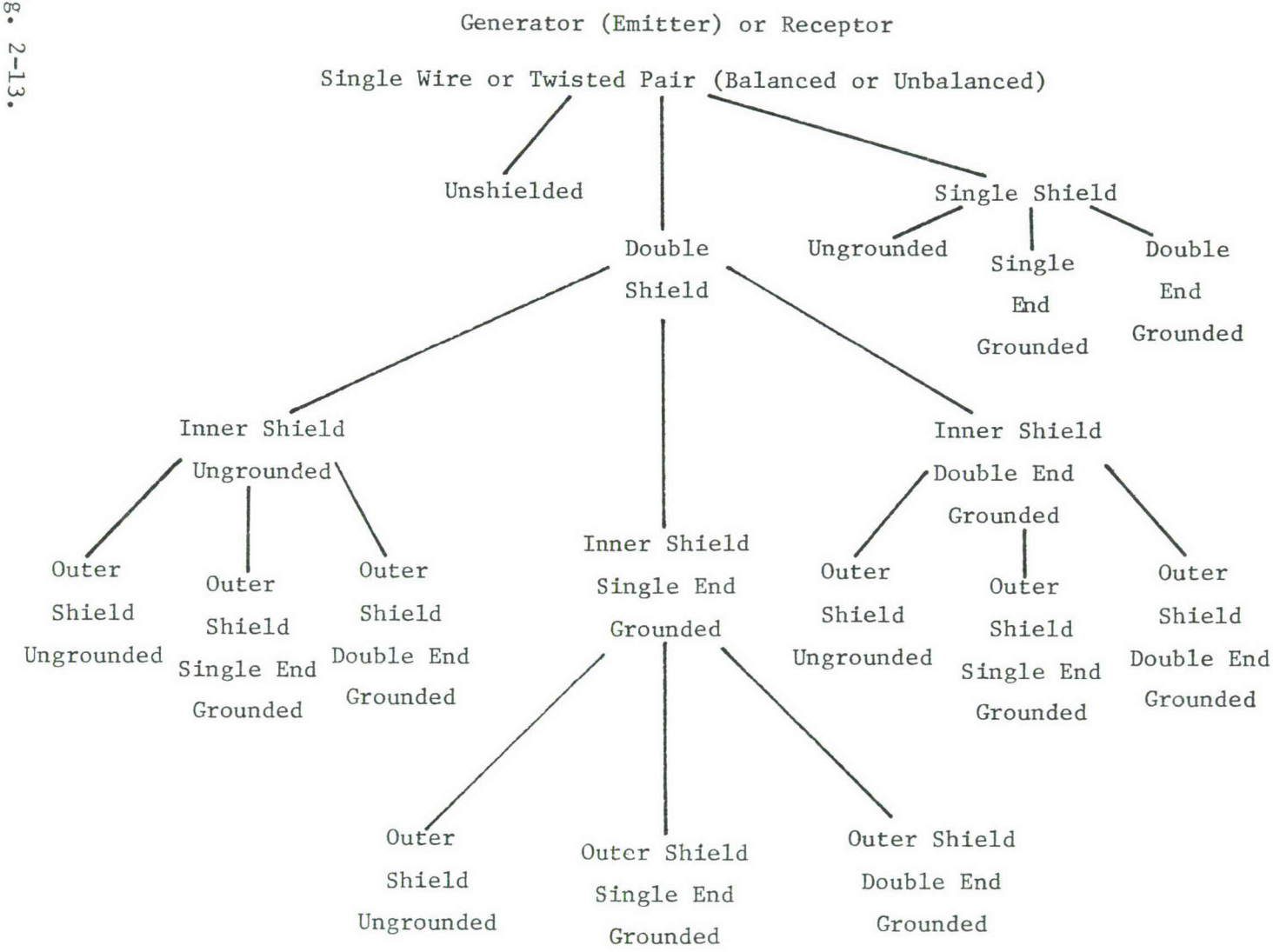
Generator (Emitter) or Receptor
Single Wire or Twisted Pair (Balanced or Unbalanced)
Unshielded
Single Shield
Ungrounded
Single End Grounded
Double End Grounded
Double Shield
Inner Shield Ungrounded
Outer Shield Ungrounded
Outer Shield Single End Grounded
Outer Shield Double End Grounded
Inner Shield Single End Grounded
Outer Shield Ungrounded
Outer Shield Single End Grounded
Outer Shield Double End Grounded
Inner Shield Double End Grounded
Outer Shield Ungrounded
Outer Shield Single End Grounded
Outer Shield Double End Grounded

Fig. 2-13.

Emitter Circuit Types

(I) Single Wire

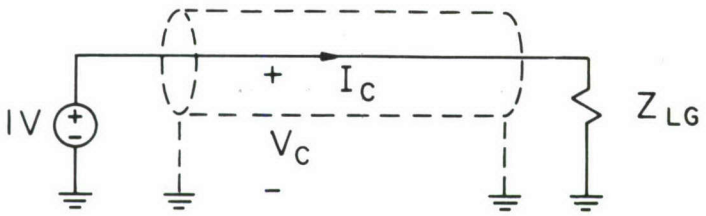

(II) Unbalanced Twisted Pair

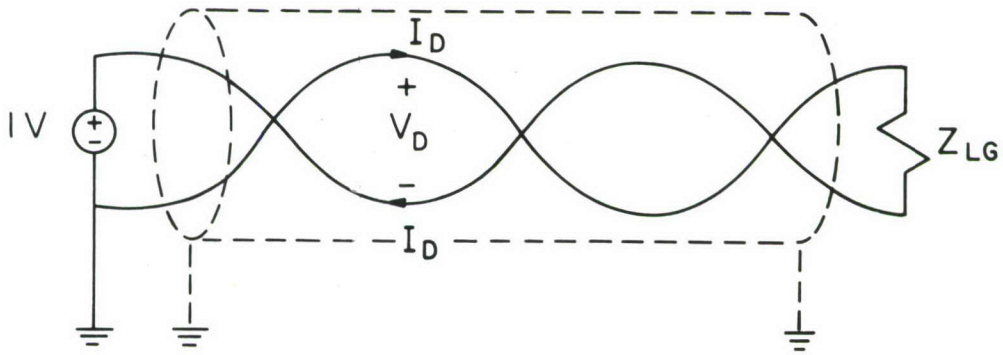

(III) Balanced Twisted Pair

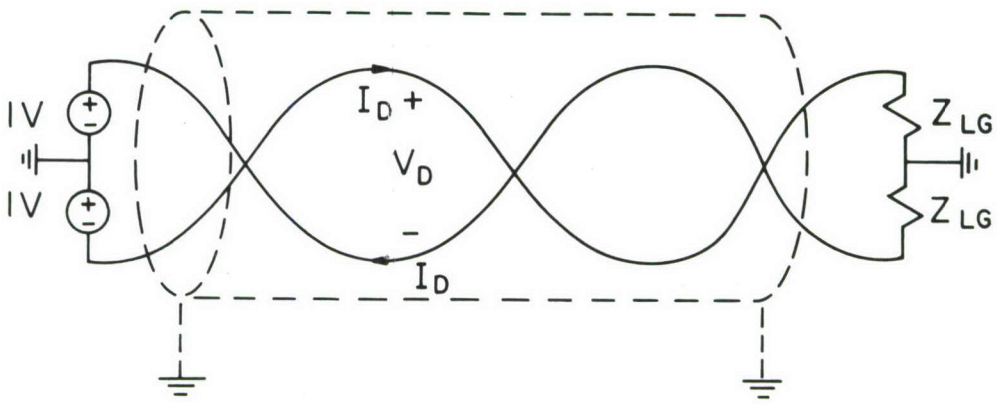

Fig. 2-14. The emitter circuit wire types.

Receptor Circuit Types

(I) Single Wire

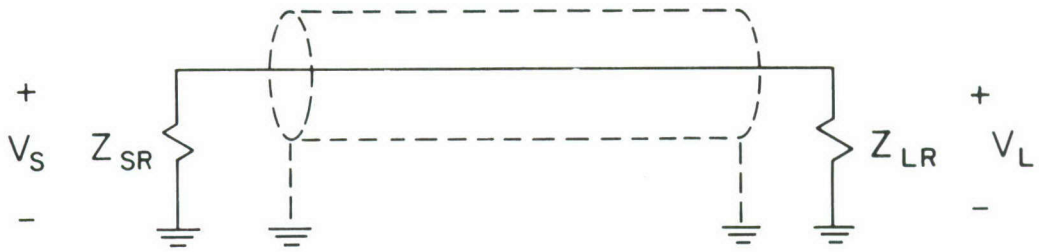

(II) Unbalanced Twisted Pair

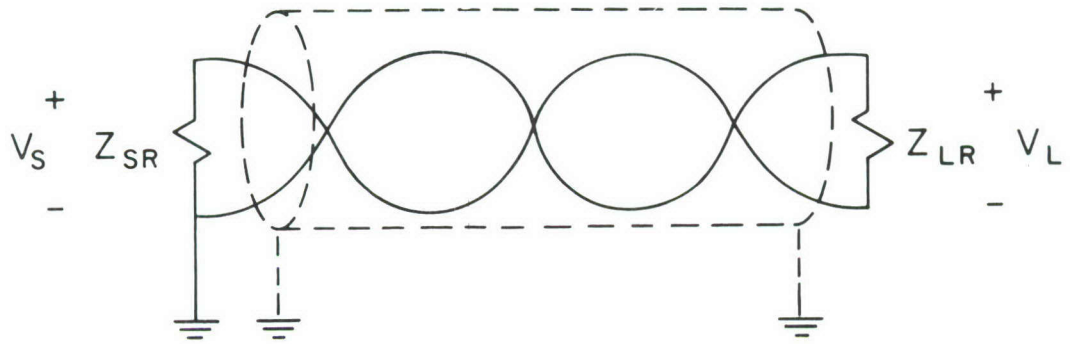

(III) Balanced Twisted Pair

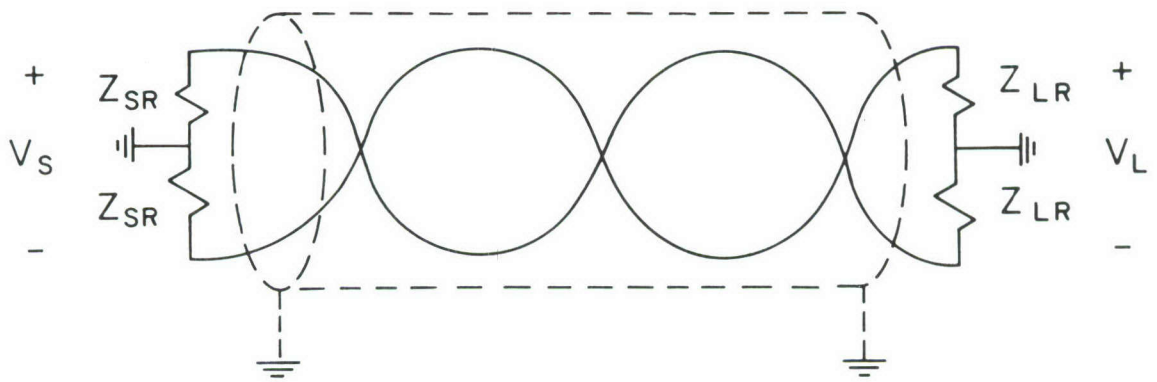

Fig. 2-15. The receptor circuit wire types.

is also shown in Fig. 2-14. Here it is assumed that perfect balance is attained. To assume any unbalance would require that the user estimate the nonideal parameters and that several models for the different configurations of the stray elements be provided. Because of the perfect balance assumption, only a differential current, I_D, and voltage, V_D, are present to affect neighboring circuits. No common mode current is assumed to flow through the ground plane.

The unbalanced twisted pair configuration is shown in Fig. 2-14. Here one end of the twisted pair is grounded while the other end is not grounded to intentionally avoid ground loop or common mode currents. The differential mode current, I_D, and differential mode voltage, V_D, are the only variables to affect neighboring wire circuits.

Each of these three emitter configurations may be surrounded by a single or double shield each of which may be ungrounded, single end grounded or double end grounded. The effect of a shield is as described previously. A shield affects the portion of the emitter current which returns through the ground plane only if it is double end grounded. In this case, the effective current is the unshielded common mode current multiplied by the factor

$$\frac{Z_{SH}}{Z_{SH} + j\omega L_S}$$

where Z_{SH} is the per-unit-length shield impedance and L_S is the per-unit-length shield self inductance above ground. This was shown for the single wire above ground case in [11]. Its extension to twisted pairs is easy to see if one applies the single wire result to each wire and its associated I_D. The above factor applies to currents which return via the ground plane (common mode currents). Thus the twisted pairs (unbalanced or

balanced) are not affected. Thus the above term only multiplies I_C for the single wire case in which a double-end grounded shield encloses the wire.

A shield affects the emitter voltage (V_C or V_D) only if it is grounded at least at one end. In this case, V_C or V_D (as appropriate) is set to zero. An ungrounded shield is assumed to have no effect. In reality, there is a minor effect of an ungrounded shield due to voltage division from the shield to ground capacitance and the wire to shield capacitance as discussed above. This is omitted but can be easily included if it is felt to be necessary.

The receptor circuit terminal configurations are shown in Fig. 2-15. They are very similar to the emitter configurations. A shield has no effect on inductive (magnetic field) coupling unless it encloses a single wire and is double end grounded [11]. If the shield is double end grounded, its effect is effectively modeled by multiplying the inductive coupling computed without the shield by the above factor where Z_{SH} and L_S are the impedance and self inductance (above ground) of this receptor shield. The shield, regardless of grounding configuration, has no affect on inductive coupling for these ideal twisted pair circuits since no current may flow through the ground plane. However a shield around any of these receptor circuits eliminates capacitive coupling so long as it is grounded at least at one end. An ungrounded shield is assumed to have no effect on capacitive coupling.

The models for coupling to these receptor circuits are extensions of the low-frequency model proven for the simplest case of a three-conductor line discussed in section 2.1. It was shown in [6] that the solution to the distributed parameter, transmission line model reduces to that of Fig. 2-4 in the limit as frequency is reduced. Precisely where, in frequency, this be-

comes valid is difficult to predict and a function of the values of the termination impedances [7]. Nevertheless, we are assured that "for a sufficiently small frequency" this result will be true. This is essentially a first order approximation to Faraday's and Ampere's laws. This low-frequency result also implies weak coupling; the effect of the receptor circuit on the generator circuit does not come into play.

This basic low frequency model will be extended (assumed to apply) to the other configurations. Certainly as frequency is reduced, a point will be reached at which it does apply. The detailed models are given in Appendix A. The differences between each generator-receptor configuration are contained in the per-unit-length mutual inductances and mutual capacitances as well as the specific terminal configuration. These mutual elements are computed in Appendix B.

One other item is appropriate for discussion. The common length for coupling, $\mathcal{L}$ in Fig. 2-4, is computed when twisted pairs are involved according to the following idea. The usual notion of the effect of a twisted pair is in terms of whether the line contains an odd or even member of half twists [13-18]. Cancellation of inductive coupling effects is assumed to be complete if the twisted pair contains an even number of half twists. This is because the emf induced in one half twist ideally cancels that induced in the neighboring half twist. Thus the effective line length is reduced for twisted pairs to that of one half twist (assuming for worst case that the line contains an odd number of half twists). If the pitch (length) of the twist is p then the length multiplying the per-unit-length mutual inductance is p/2. This also applies to the case of balanced twisted pairs and capacitive coupling. For unbalanced twisted pairs this applies to inductive coupling only.

Since the current source injected into the grounded wire representing capacitive coupling is cancelled by the short circuit, the common length is effectively the total length for capacitive coupling for unbalanced twisted pairs [13, 14].

These common coupling lengths may prove to be too optimistic in practice. Thus one might choose in a later revision to use the total line length as the common coupling length; that is, model a twisted pair as an untwisted pair.

The final item which needs to be discussed is common impedance coupling. Consider a generator and receptor circuit which share a common <u>return</u> as shown in Fig. 2-16 (a). Suppose that the frequency is sufficiently small that the distributed impedance of this return can be lumped as Z_{CI}. Since Z_{CI} is usually much smaller than Z_{SR} or Z_{LR}, virtually all of the generator current

$$I_G \doteq \frac{1}{Z_{LG}}$$

passes through the common impedance Z_{CI} and develops a voltage $V_{CI} = Z_{CI}I_G$ between the two ends of the receptor circuit. This voltage is divided across Z_{SR} and Z_{LR} to produce a "floor" of direct coupled, interference voltage as illustrated in Fig. 2-16 (b). This common impedance coupling floor represents a minimum coupling level. To include this effect we simply add this common impedance coupling to the above computed inductive and capacitive coupling when <u>both</u> the generator <u>and</u> emitter are single wire circuits. If <u>either</u> the generator <u>or</u> the receptor is a twisted pair (balanced or unbalanced) then no common impedance coupling is added for the reason that, based on the model assumptions, there is no common path through ground to provide this coupling.

2.6.2 <u>Pigtails on Shielded Wires</u>

The basic philosophy for treating pigtails (sections of shielded wires

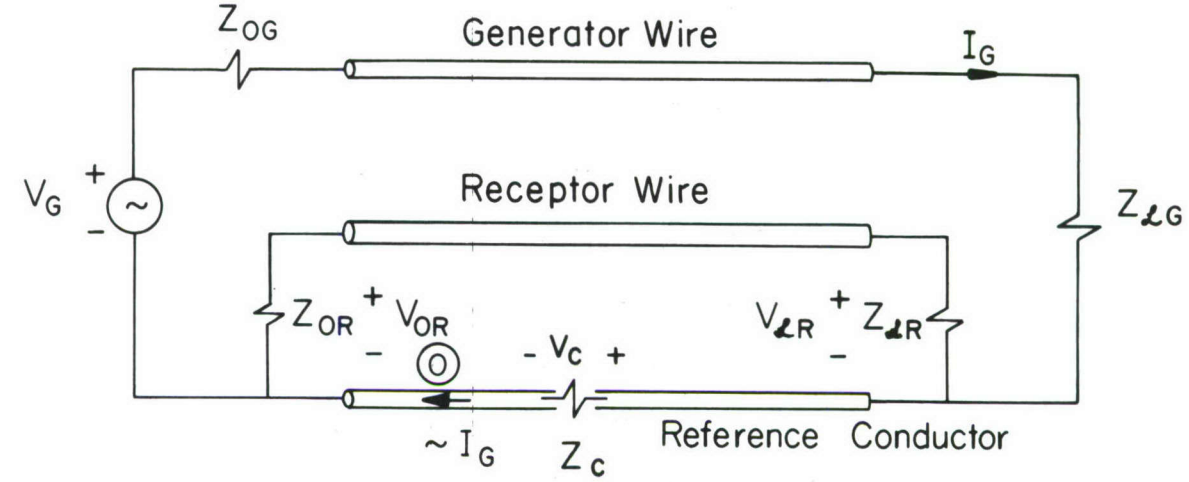

(a)

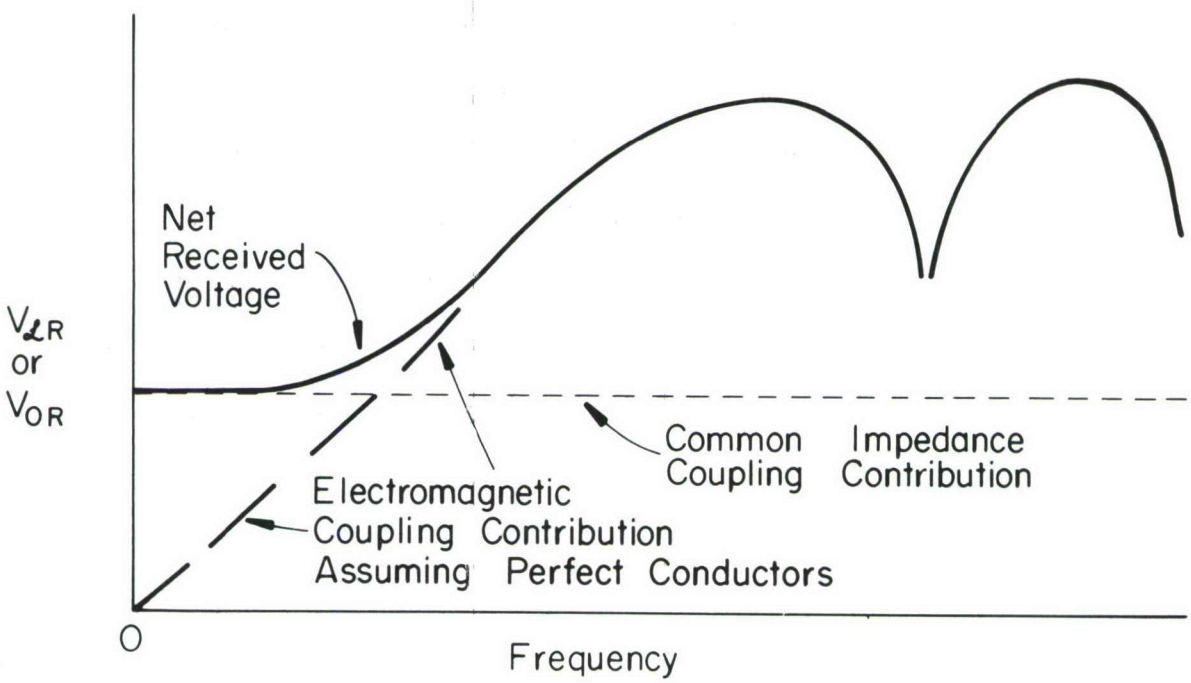

(b)

Fig. 2-16. Common impedance coupling.

where the inner wire is exposed) is illustrated in Fig. 2-17. A fundamental assumption is that the entire bundle is electrically short. If this is the case, then the load impedances at the extreme ends of the wires may be moved to the ends of each bundle segment. It was shown in [10, 11] that for this case (a sufficiently low frequency) one can superimpose the coupling over the indicated uniform sections of this bundle segment to obtain the total coupled voltages at the ends of this bundle segment. This is the basic philosophy for handling pigtail sections that was used in the original revision of IEMCAP. However, the restriction of fixed length (3") on all shields was used to optimize the coding. To allow variable length pigtails as is intended in the present code is a bit more difficult.

In keeping with the present input data structure of the code we will assume a shielded wire to have a pigtail at each bundle point where it is terminated of length given in the wire table for that type of shielded wire. Thus every shielded wire defined in the wire characteristics table has its own pigtail length. In the case of a shielded emitter (receptor) wire this is designated in the following discussion and in the present code as PIGE (PIGR). For a particular bundle segment, the number of terminations of a shielded emitter (receptor) wire is given by IEENDS (IRENDS). These parameters will be used to compute the common segment lengths over this bundle segment.

A typical case is illustrated in Fig. 2-17. Since this bundle segment is assumed to be electrically short, the individual four sections may be interchanged without affecting the result. Thus, what is important is not their sequence of occurrence but the common lengths of similar segments. In Fig.

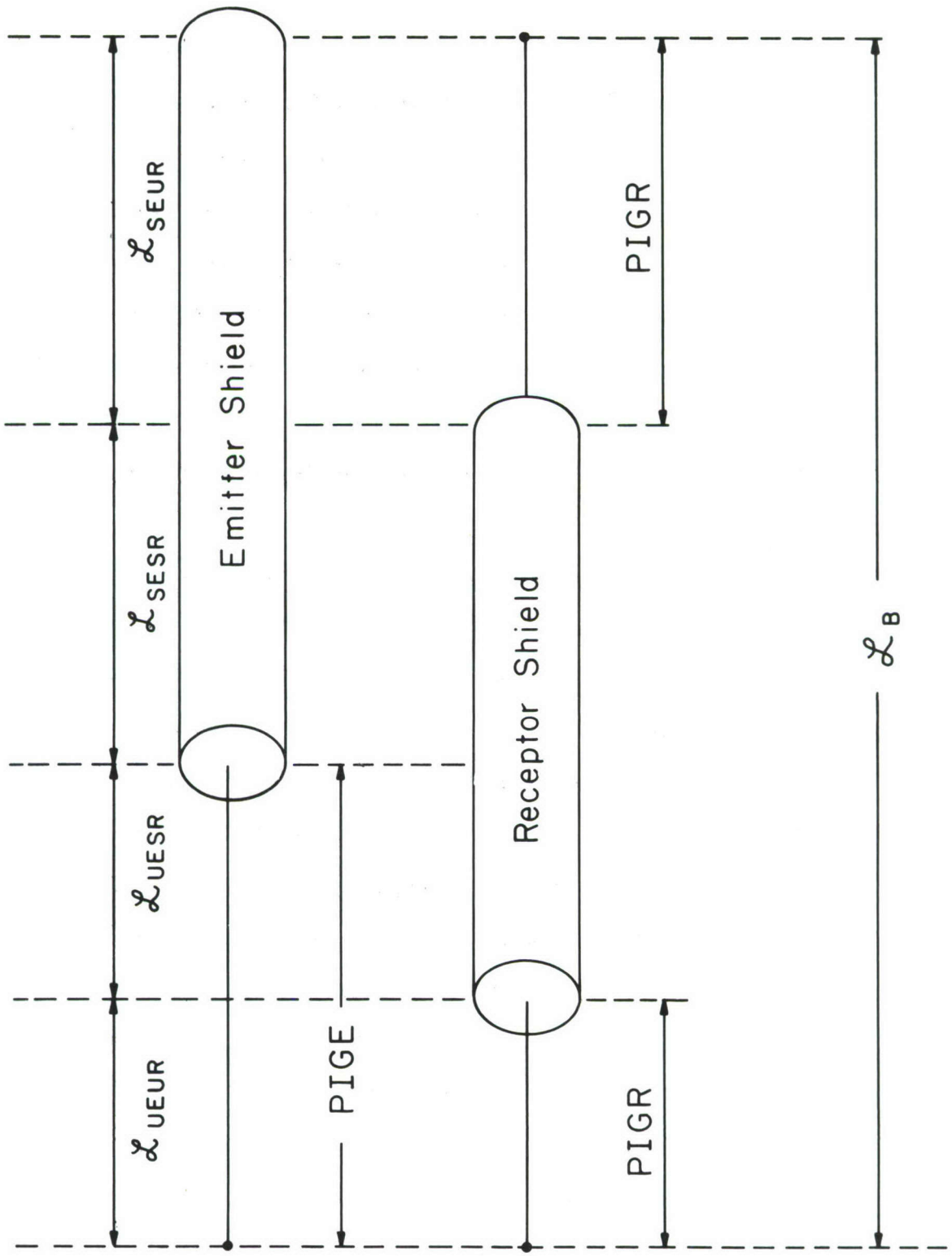

Fig. 2-17. Common lengths for pigtail coupling calculations.

2-17, $\mathcal{L}_{UEUR}$ denotes the section in which the emitter is unshielded (pigtail) and the receptor is unshielded (pigtail). Similarly $\mathcal{L}_{SEUR}$ denotes the section in which the emitter is shielded and the receptor is unshielded (pigtail). The determination of these four basic common lengths is detailed in Appendix A for all possible combinations of IEENDS (0, 1 or 2) and IRENDS (0, 1 or 2).

Once these common lengths are determined, then the basic models of the previous section are used to compute the individual four coupling contributions where the bundle segment length $\mathcal{L}_B$ in those models is replaced by each of these four common section lengths. The four coupled voltages are then added together (magnitudes).

Shielded single wires are shown in Fig. 2-17 for illustration. The method applies without revision for shielded twisted pairs.

2.6.3 Disadvantages of the Proposed Models

The models proposed are theoretically defensible so long as the excitation (analysis) frequency is "sufficiently small". Where this assumption breaks down is extremely difficult to ascertain. Other, more sophisiticated lumped models would also suffer from this disadvantage although the upper frequency limit for these more sophisticated lumped models may be somewhat higher in some cases. Still the upper frequency limit of validity would be difficult to determine and not unique to all values of load impedances. To remove this upper frequency limit, one would need to use a distributed parameter, coupled line, transmission line model. The increase in coding difficulty to implement this model over the simple one suggested is enormous (for all the configurations which IEMCAP is intended to handle). Even if the transmission line model were used, practical system variabilities such as relative wire position in a bundle would probably render any predictions of

this model as inaccurate as those of the simple model. Thus implementing the suggested model is probably the only sensible thing to do. Prediction errors will be made, particularly at the higher frequencies. However, predicting accurate results for some unknown and variable system is virtually impossible. The problem is not uniquely solvable unless one applied IEMCAP to well-controlled and precisely definable systems which is not its intended application.

These simple models however do provide some unrealistic results at certain frequencies. For example, many of the models predict the coupling to increase linearly with frequency (20 dB/decade). At the lower frequencies this is true. However if extended to higher frequencies, the coupling may exceed unity. This, in itself, is not unrealistic; voltage transfer ratios (which are what the models predict) can exceed unity (consider transformers, for example). No problem occurs unless the current transfer ratio exceeds unity, then also the power gain would exceed unity: a clearly unreasonable result.

It is difficult to "bound" these predictions such that the power gain never exceeds unity because of the assumption of weak coupling; that is, all the power delivered by the 1 volt voltage source at the end of the emitter circuit is transferred to its load, Z_{LG}. In reality, most of the power delivered by this voltage source is delivered to Z_{LG} with only a very small portion delivered via crosstalk to the receptor circuit. However limiting the power gain to each receptor load to not exceed unity has no basis for these models. Even if it did, how would we apportion this power gain to each end of the receptor circuit? There is no seemingly satisfactory answer to this problem so it is suggested that the computed voltage transfer ratios

not be allowed to exceed unity.

Another highly optimistic result is obtained by our assumption that the shields are solid. In reality, the holes in braided shields will allow increased coupling. Again, modeling this phenomenon with a simple but defensible model is not obvious. Perhaps one has to "live with" this problem. Of some comfort is that for shields having pigtails which are not of zero length, the pigtail coupling will probably take over or dominate at the higher frequencies rendering the imperfect shield question a moot point [10]. For zero length pigtails on both emitter and receptor shields one will have an optimistic view of the protection afforded by the shields.

Underlying these model deficiencies is the basic problem of variability or inaccuracy of input data for the models. It has been shown that the variability in crosstalk due to minor variations in relative wire positions in a bundle can cause as much as 40 dB change in crosstalk.[22]. So in light of this, perhaps the other model deficiencies are not out of line with what one would reasonably expect as prediction errors for practical systems.

III. REVISION OF THE FIELD-TO-WIRE COUPLING SUBROUTINE FTWTFR

The subroutine FTWTFR is intended to calculate terminal currents induced in cable bundles due to (1) environmental fields or (2) antennas (directly illuminating a wire via exposure of that wire through an aperture). The model is based on the transmission line model outlined in [23, 24, 25].

The current subroutine in IEMCAP is essentially the original one delivered by McAir [1]. Although the model is based on the transmission line model [23, 24, 25], it is supposedly a bound of the predictions of that model rather than an exact solution of that model. No explanation or derivation of this was given in the documentation [1]. Private conversations with Dr. R. Pearlman of McAir provided insight into a possible derivation. That estimated derivation is described in [29]. This derivation does not represent a satisfactory result for several reasons. First the result apparently assumes uniform plane wave illumination of the wires. In the interior of an aircraft or other closed system where the wires are illuminated, it is highly doubtful that the fields will resemble uniform plane waves. Also the result was obtained by considering only three propagation directions and polarizations of the uniform wave and taking the maximum result. Other orientations were not considered. An attempt was made by McAir to provide a bound on this bound by determining a maximum current induced as though this wire above ground were an antenna having a gain of unity or an effective area of the loop formed by the wires. No justification was provided for this result.

Thus it is not clear that the field-to-wire subroutine provides a measure or at least a realistic bound on this coupling. An additional problem with this subroutine is its model for shielded wires. The above result for currents induced in unshielded wires is multiplied by a "shielding effectiveness factor". No justification was given in [1] for this factor. It is

suspected that this was obtained by using certain empirical data for various shielded wires given in an earlier McAir report [30]. The shielding effectiveness factor in [1] fits the empirical data in [30]. However the empirical data in [30] was for unilluminated shields. Whether this term is used properly in FTWTFR is not clear. The shielding effectiveness in [30] appeared to be defined as the ratio of the incremental current on the outside of the shield to the incremental current on the inside of the shield. Relating this factor (correctly) to the field-to-wire problem is not as straightforward as implied in [1].

Consequently it would appear that the field-to-wire subroutine should be rewritten and the models placed on a more theoretically sound and defensible basis. We shall do this in later sections.

3.1 The Transmission Line Model

The problem is defined in Fig. 3-1 (a). Two wires of length $\mathcal{L}$ and separated by a distance d have loads, Z_0 and $Z_{\mathcal{L}}$. An incident field illuminates the line. This incident field need not be a uniform plane wave. The electric and magnetic field intensities of the incident field are denoted by E^i and H^i, respectively. The per-unit-length model of the line is shown in Fig. 3-1 (b). The quantities ℓ and c are the per-unit-length inductance and capacitance, respectively, of the line. Note that the total quantity is the per-unit-length quantity multiplied by the section length, Δx. Two sources induced by the incident field are present. The portion of the per-unit-length voltage source

$$\phi_n = \mu \int_0^d H_z^i \, dy \tag{3-1}$$

represents the per-unit-length component of the incident magnetic flux normal

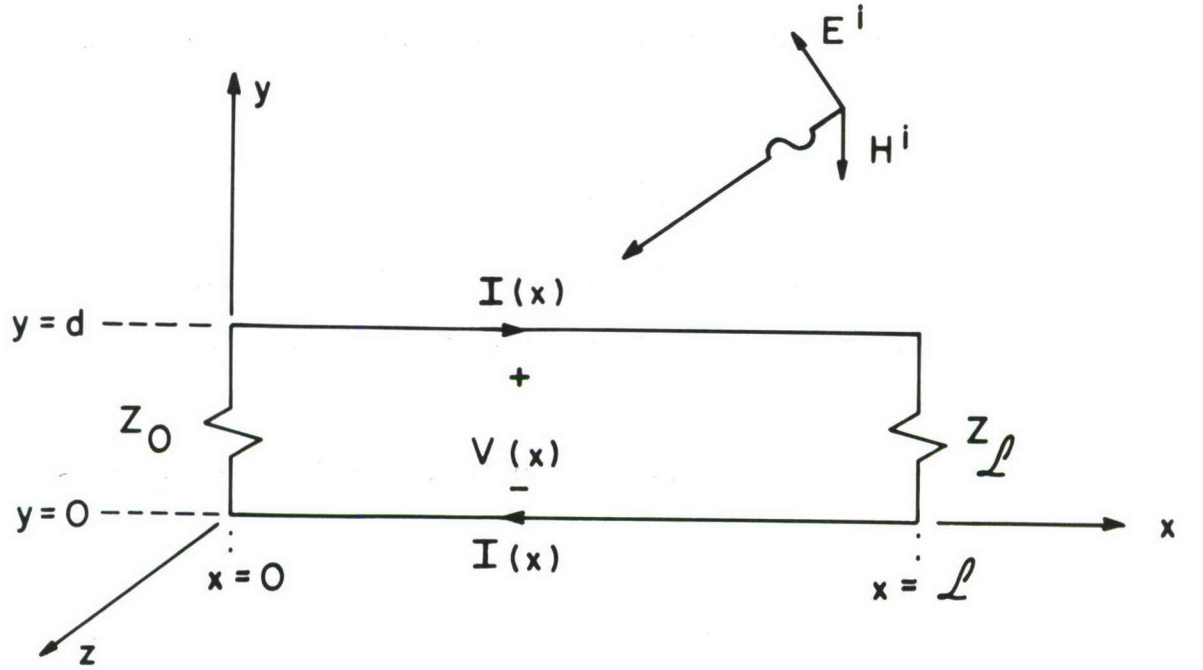

(a)

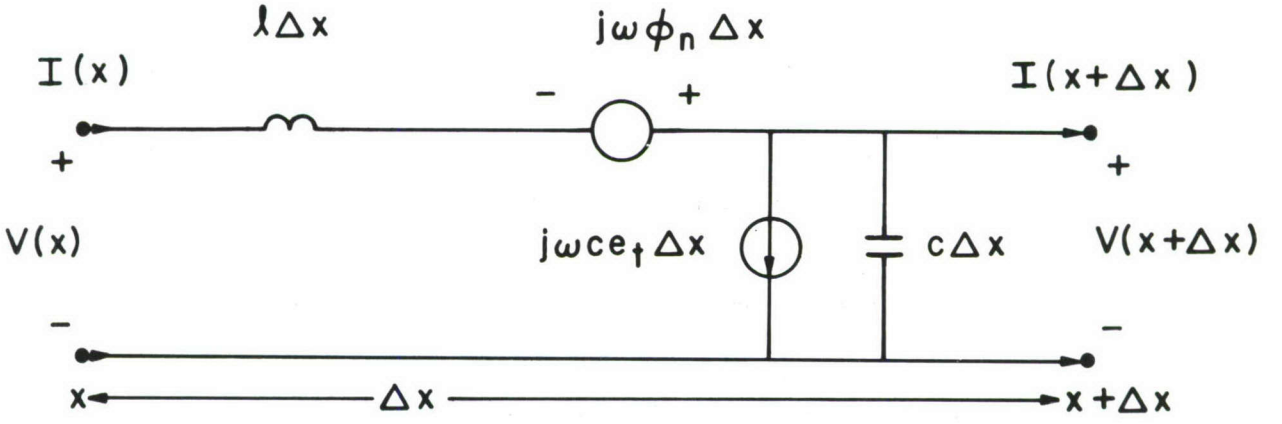

(b)

Fig. 3-1. Field-to-wire problem description and the per-unit-length circuit.

to the line. Multiplying this by $j\omega\Delta x$ gives the rate of change of the total magnetic flux which, by Faraday's law, is representable as an induced emf. The current source

$$j\omega c e_t \Delta x = j\omega c \int_0^d E_y^i \, dy \, \Delta x \tag{3-2}$$

represents a displacement current induced by the incident electric field to flow between the wires. By Ampere's law this is representable as an induced current source.

The differential equations of the line are obtained from the model as $\Delta x \to 0$ and become

$$\frac{dV(x)}{dx} + j\omega \ell \, I(x) = j\omega \phi_n(x) \tag{3-3a}$$

$$\frac{dI(x)}{dx} + j\omega c \, V(x) = -j\omega c e_t(x) \tag{3-3b}$$

The exact solution of these coupled differential equations with the terminal conditions:

$$V(0) = -Z_0 \, I(0) \tag{3-4a}$$

$$V(\mathcal{L}) = Z_{\mathcal{L}} \, I(\mathcal{L}) \tag{3-4b}$$

incorporated yields the terminal currents [23-28]:

$$I(0) = \frac{1}{\Delta} \left\{ \int_0^{\mathcal{L}} \left[\cos \beta(\mathcal{L}-\tau) + j \frac{Z_{\mathcal{L}}}{R_c} \sin \beta(\mathcal{L}-\tau)\right] e_\ell(\tau) \, d\tau \right.$$
$$\left. + \left[\cos\beta\mathcal{L} + j \frac{Z_{\mathcal{L}}}{R_c} \sin\beta\mathcal{L}\right] e_t(0) - e_t(\mathcal{L}) \right\} \tag{3-5a}$$

$$I(\ell) = [\cos \beta\ell + j \frac{Z_0}{R_C} \sin \beta\ell]\, I(0)$$

$$- j \frac{1}{R_C} \int_0^{\ell} \sin \beta(\ell-\tau)\, e_\ell(\tau)\, d\tau$$

$$- j \frac{1}{R_C} \sin (\beta\ell)\, e_t(0) \qquad (3\text{-}5b)$$

$$= \frac{1}{\Delta} \{ \int_0^{\ell} [\cos \beta\tau + j \frac{Z_0}{R_C} \sin \beta\tau]\, e_\ell(\tau)\, d\tau$$

$$+ e_t(0) - [\cos \beta\ell + j \frac{Z_0}{R_C} \sin \beta\ell]\, e_t(\ell)\}$$

where

$$\Delta = (Z_0 + Z_\ell) \cos \beta\ell + j\, (R_C + \frac{Z_0 Z_\ell}{R_C}) \sin (\beta\ell) \qquad (3\text{-}6a)$$

$$e_t(0) = \int_0^d E_y^i\, (0, y)\, dy \qquad (3\text{-}6b)$$

$$e_t(\ell) = \int_0^d E_y^i\, (\ell, y)\, dy \qquad (3\text{-}6c)$$

$$e_\ell(x) = E_x^i\, (x, d) - E_x^i\, (x, 0) \qquad (3\text{-}6d)$$

and

$$\beta = \frac{2\pi}{\lambda} \qquad (3\text{-}6e)$$

and

$$R_C = \sqrt{\frac{\ell}{c}} \qquad (3\text{-}6f)$$

is the line characteristic resistance.

This model has been compared to results computed by a method of moments code in [27, 28] and to experimental results in [29] and found to be an accurate representation of the line. However this model of the simplest possible configuration (two wires) does not yield simple results for the ter-

minal currents. It is as difficult to produce bounds on this result as it was to produce bounds on the simplest case of crosstalk in the previous chapter.

To illustrate this let us assume matched loads $Z_0 = Z_{\ell} = R_C$. (Results for an unmatched line should be no simpler than for a matched line). In this case, (3-5) reduce to

$$I(0) = \frac{1}{2R_C} \left\{ \int_0^{\ell} e^{-j\beta\tau} e_{\ell}(\tau)\, d\tau + e_t(0) - e^{-j\beta\ell} e_t(\ell) \right\} \qquad (3\text{-}7a)$$

$$I(\ell) = \frac{1}{2R_C} \left\{ \int_0^{\ell} e^{-j\beta(\ell-\tau)} e_{\ell}(\tau)\, d\tau + e^{-j\beta\ell} e_t(0) - e_t(\ell) \right\} \qquad (3\text{-}7b)$$

In order to produce bounds, we must specify the structure of the incident field. For illustration let us suppose that the incident field is a uniform plane wave described by [26]

$$\vec{E}^i = [E_x^i \vec{a}_x + E_y^i \vec{a}_y + E_z^i \vec{a}_z]\, e^{-j\beta(\gamma_x x + \gamma_y y + \gamma_z z)} \qquad (3\text{-}8)$$

where γ_x, γ_y, γ_z are the direction cosines of the propagation vector. Since E_z^i contributes nothing to induced currents and $z = 0$ we assume

$$\vec{E}^i = [E_x^i \vec{a}_x + E_y^i \vec{a}_y]\, e^{-j\beta(\gamma_x x + \gamma_y y)} \qquad (3\text{-}9)$$

Substitution into (3-7) yields the following results for the magnitudes of the induced currents:

$$|I(0)| = \frac{d\ell}{2R_C} \beta \left| (1+\gamma_x) E_y^i - \gamma_y E_x^i \right| \left| \frac{\sin(\gamma_y \beta d/2)}{(\gamma_y \beta d/2)} \right| \left| \frac{\sin[(1+\gamma_x)\beta\ell/2]}{(1+\gamma_x)\beta\ell/2} \right| \qquad (3\text{-}10a)$$

$$|I(\mathcal{L})| = \frac{d\mathcal{L}}{2R_C}\,\beta\left|(\gamma_x-1)E_y^i - \gamma_y E_x^i\right| \left|\frac{\sin(\gamma_y\beta d/2)}{(\gamma_y\beta d/2)}\right| \left|\frac{\sin[(1-\gamma_x)\beta\mathcal{L}/2]}{(1-\gamma_x)\beta\mathcal{L}/2}\right| \quad (3\text{-}10b)$$

Note that the above results for the magnitudes of the induced, terminal currents (for matched loads) have been placed in the following form:

$$|I| = Kf \left|\frac{\sin(\pi\tau_1 f)}{\pi\tau_1 f}\right| \left|\frac{\sin(\pi\tau_2 f)}{\pi\tau_2 f}\right| \quad (3\text{-}11)$$

If we convert this to decibel form we have

$$\begin{aligned} |I|_{dB} &= 20\log_{10}(|I|) \\ &= 20\log_{10}(K) + 20\log_{10}(f) \\ &\quad + 20\log_{10}\left(\left|\frac{\sin(\pi\tau_1 f)}{\pi\tau_1 f}\right| \left|\frac{\sin(\pi\tau_2 f)}{\pi\tau_2 f}\right|\right) \end{aligned} \quad (3\text{-}12)$$

This can be plotted as shown in Fig. 3-2(a) in a log-log or Bode plot format. Note that the latter term in (3-12) is the familiar spectrum of a trapezoidal pulse having, for example, a rise time of τ_2 and a pulse width (between 50% points) of τ_1. Although the actual spectrum has nulls, one can bound the peaks with three segments as shown in Fig. 3-2(a). Suppose $\tau_2 < \tau_1$. The first segment has a slope of 0 dB/decade out to $f = \frac{1}{\pi\tau_1}$. Then the slope becomes -20 dB/decade out to $f = \frac{1}{\pi\tau_2}$. After this the slope is -40 dB/decade. On the log-log or Bode plot, one can simply add the three sketches which comprise (3-12) as shown in Fig. 3-2 (b). This shows that a maximum occurs between $\frac{1}{\pi\tau_1}$ and $\frac{1}{\pi\tau_2}$. In fact, it can be easily shown that the maximum occurs at the geometric mean of the two break frequencies

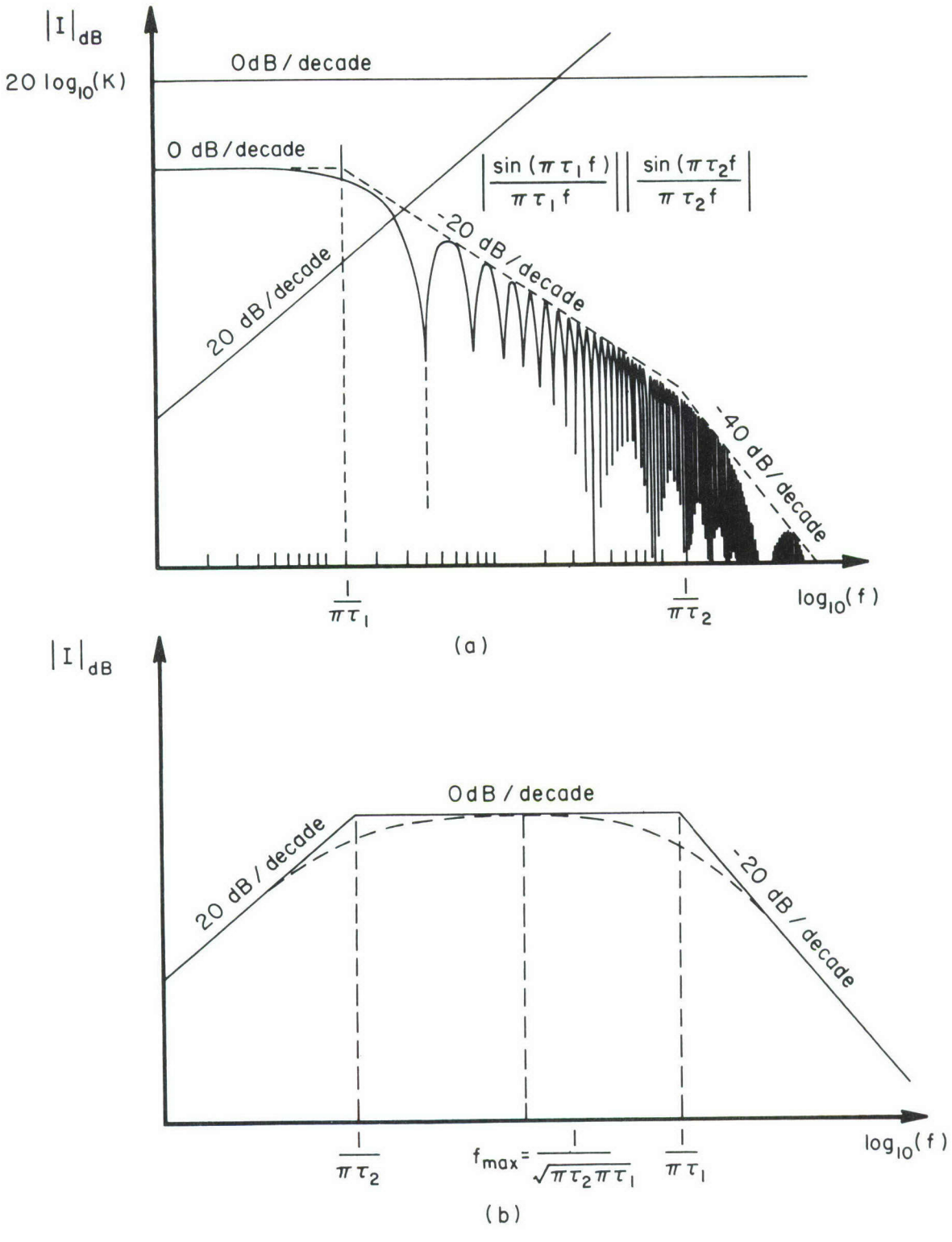

Fig. 3-2. Bounding the frequency response.

$$f_{max} = \frac{1}{\pi\sqrt{\tau_1 \tau_2}} \qquad (3\text{-}13)$$

Now, returning to our original problem, observe that (3-10) and (3-11) are of the same form. For a given orientation of the incident field, namely, for γ_x, γ_y, E_x^i, E_y^i, one can determine the frequency at which maximum coupling occurs to the line by constructing the Bode plots shown in Fig. 3-3. One should be reminded that this is not a "tight" bound on the actual coupling since, for ease of plotting, we have bounded the product of the two $\frac{\sin x}{x}$ terms as shown in Fig. 3-2 (a).

In the previous development we have seen how truly complicated this seemingly simple problem is. We were only able to bound the result when the loads are matched. In actual cables, not only will we have more than two wires but it is highly doubtful that the loads will be matched to the line characteristic impedance. (For example, consider a power transmission circuit.) If, however, we relax this requirement of matched loads, the result becomes very complicated even for a well-defined, uniform plane wave excitation. In an actual system not only will the line loads probably not be matched but we will probably not have uniform plane wave excitation of the line. Even if we did, there is not enough information in the IEMCAP data input to determine the direction of propagation relative to the line or the polarization of the incident field relative to the line. Consequently it seems more reasonable to develop simple models which speed computation time and have accuracies consistent with the accuracy of other models in the code. Such a proposed model is the subject of the next section.

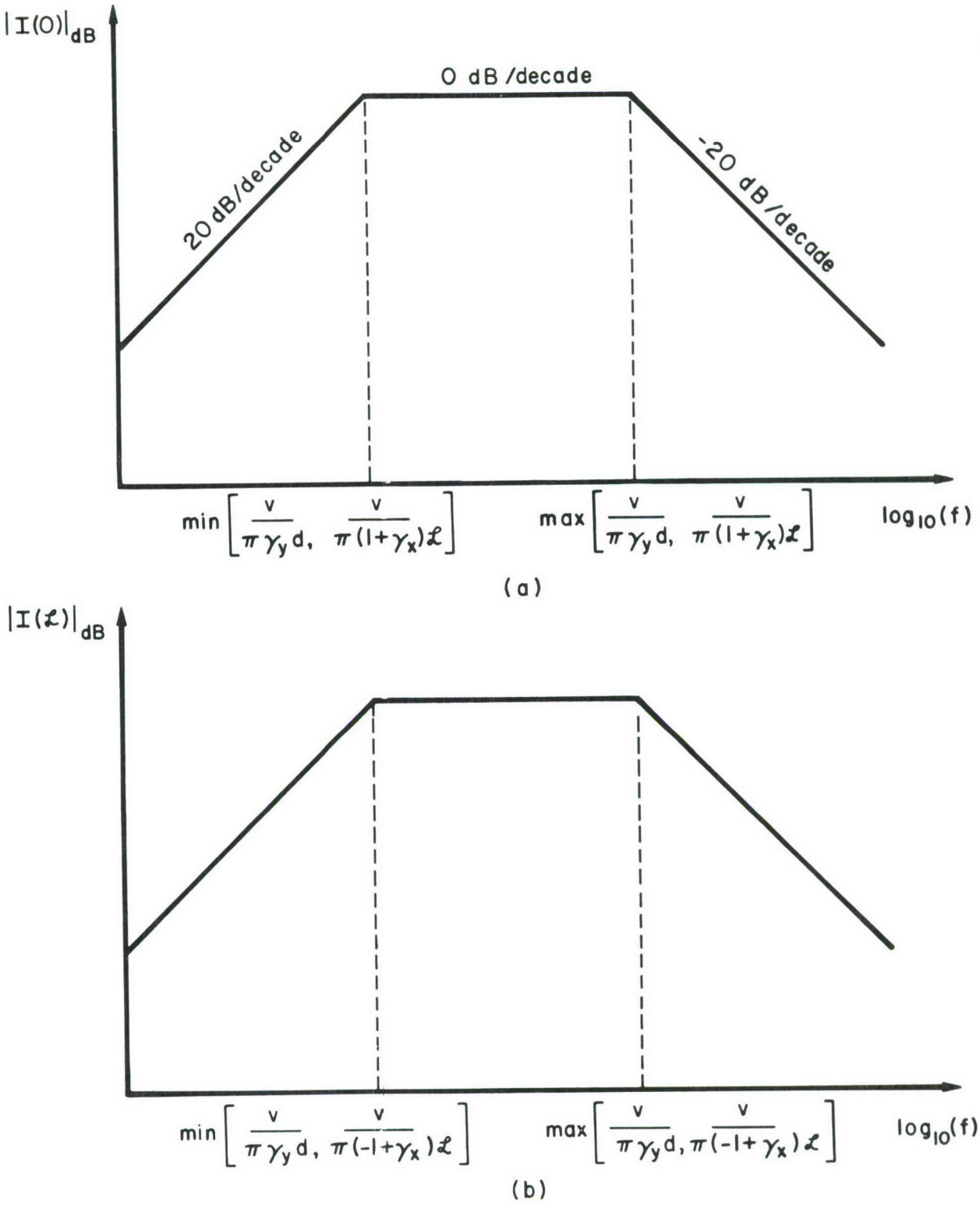

Fig. 3-3. Bounds on the induced, terminal currents.

3.2 A Proposed, Low-Frequency, Field-to-Wire Model for IEMCAP for Unshielded, Untwisted Wires

In developing this model we must keep in mind the available data. The IEMCAP provides (via user input or simple calculations) the electric field in the vicinity of a cable bundle segment. This field level arises from one of several sources. The user specifies two environmental field levels - the internal environmental field and the external environmental field. These are specified by providing up to 90 frequencies and the associated electric field levels at those frequencies. If only the external field is specified, the internal field levels default to 40 dB below the corresponding external field levels. If only the internal field is specified, the external field defaults to 40 dB above that.

The coupling to cable bundle segments is computed for each segment and the contributions added to yield the composite coupling (induced current) at a port connected to these two wires (or, strictly speaking, wire with ground plane return). Coupling to wire segments from external fields (either external environmental fields or antenna generated fields) occurs over a bundle segment only if that bundle segment is exposed to an aperture. If the segment is exposed by an aperture, the electric field over the portion of the line length equal to the aperture length is computed from the antenna via the Friis transmission equation in subroutine ACTFER and from the specified external environmental field in subroutine ENVIRN. Both contributions are used in the FTWTFR subroutine to generate the induced currents. If the segment is exposed via an aperture, no internal environmental field coupling is computed. If the segment is not exposed via an aperture, only internal environmental fields produce the incident electric field at the segment and

in this case the field illuminates the entire bundle segment.

In any case, subroutines ENVIRN and ACTFER provide the incident electric field (and length of illumination of the segment) to subroutine FTWTFR which then computes the contribution to induced port currents over this segment via the above model theory. Thus we will concentrate on subroutine FTWTFR and its available input data.

Note that the available input data to FTWTFR is the incident electric field in the vicinity of this bundle segment (and the length of the illuminated segment is the aperture length in the case of aperture illumination). We have no information on (1) the structure of the field nor (2) its polarization, etc. However, to accurately determine induced currents via the above transmission line model (or even bound the results with reasonable bounds) we must have considerably more information than this.

To illustrate how important this information can be, we have shown experimental results reported in [29] in Fig. 3-4, 3-5, 3-6. The experiment is shown in Fig. 3-4. It consists of a #20 gauge wire mounted 5 mm above a ground plane. The length of the wire is 25 cm and a uniform plane wave at a frequency of 1.2 GHz illuminates the line. Thus the line length is one wavelength. The line is terminated at both ends in 50 Ω (R_C = 192 Ω). The induced currents for parallel and normal polarization are shown for parallel polarization in Fig. 3-5 and for normal polarization in Fig. 3-6. Note the sensitivity of the response to the direction of propagation relative to the line axis. This clearly shows that unless one has precise information on the incident field (and a carefully controlled line) one has little hope of accurate predictions.

In light of the available data for the FTWTFR subroutine and the above

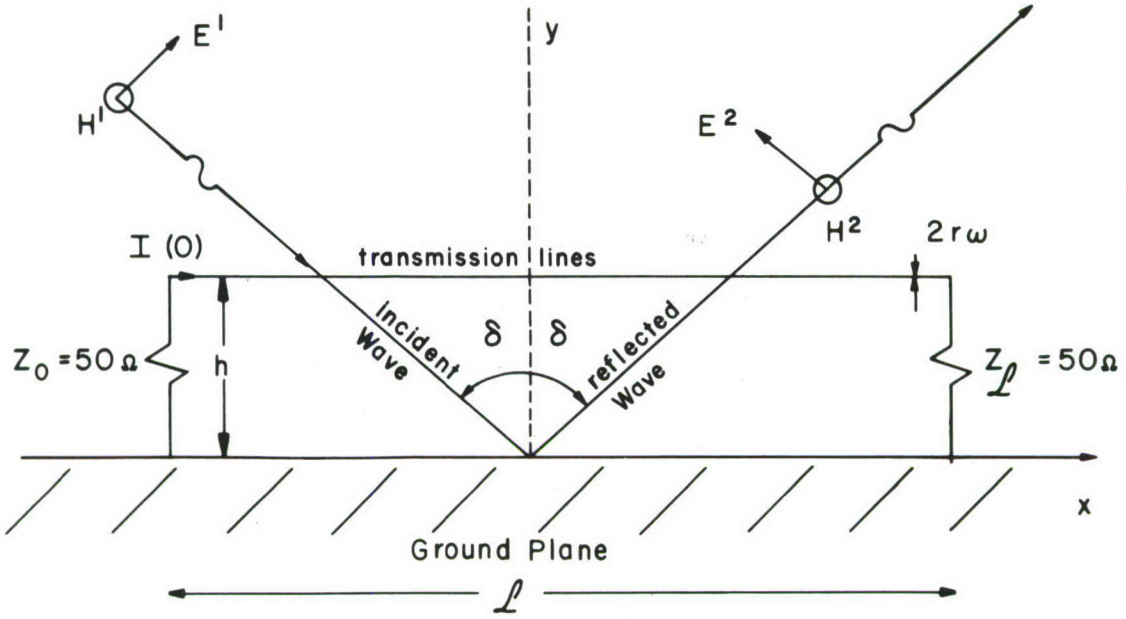

(a) Side View

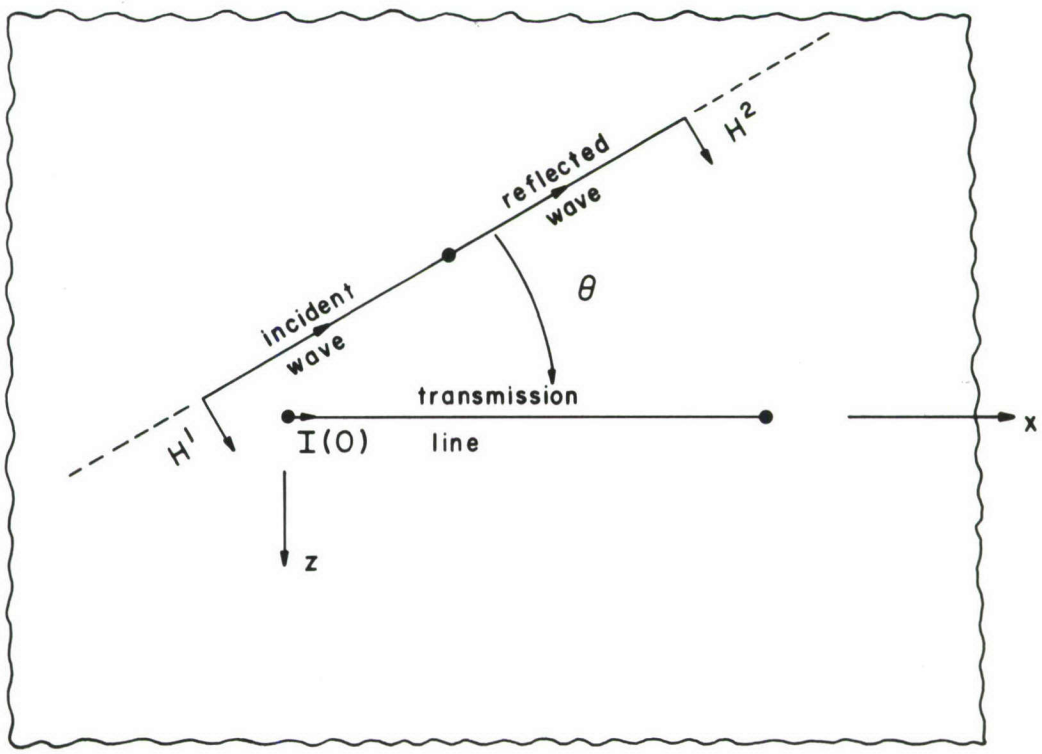

(b) Top View

Fig. 3-4. The experimental configuration (parallel polarization).

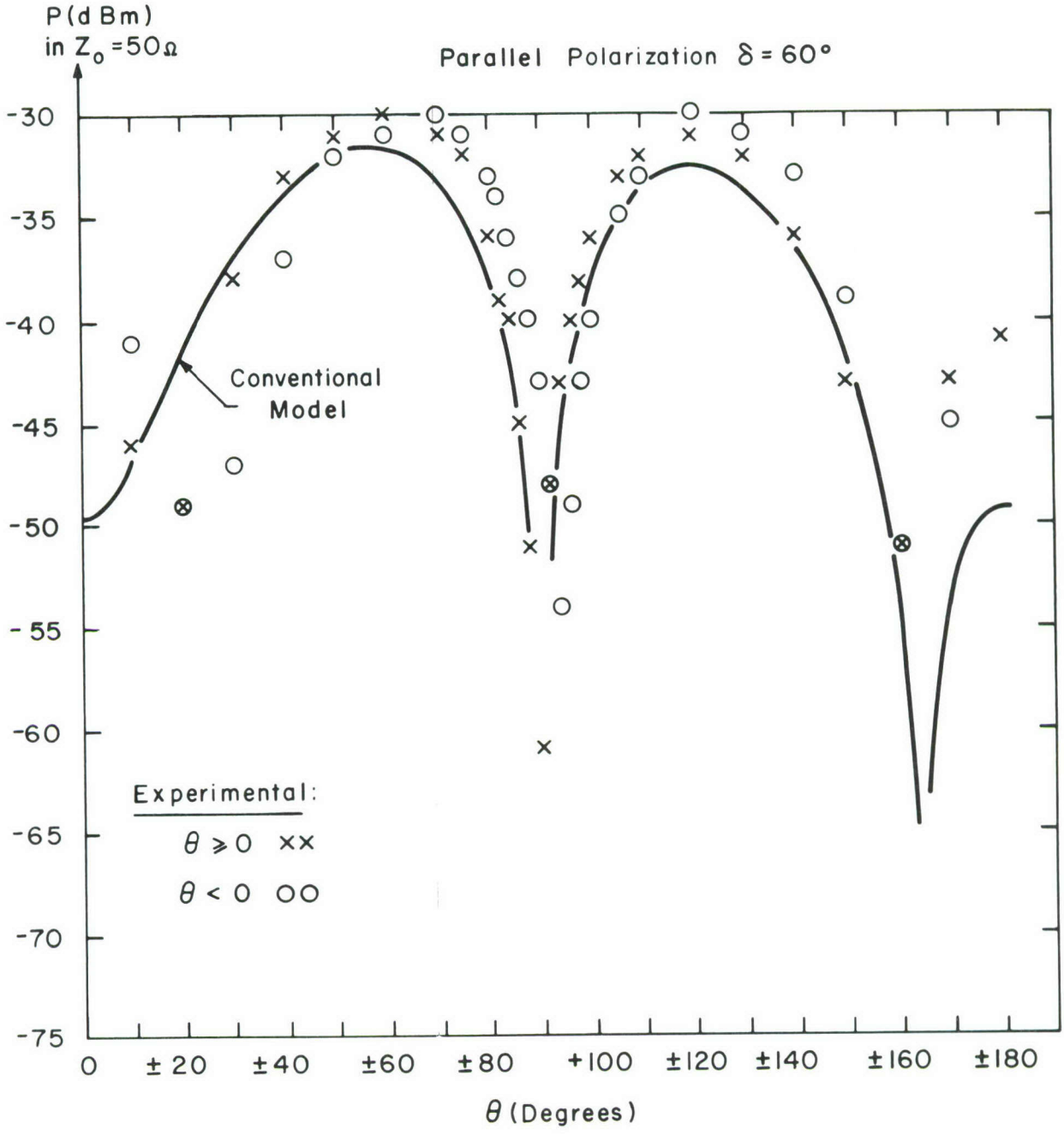

Fig. 3-5. Predictions of the model for parallel polarization and $\mathcal{L}$ = 25 cm, k = 5 mm, f = 1.2 GHz, $\delta = 60^{\circ}$.

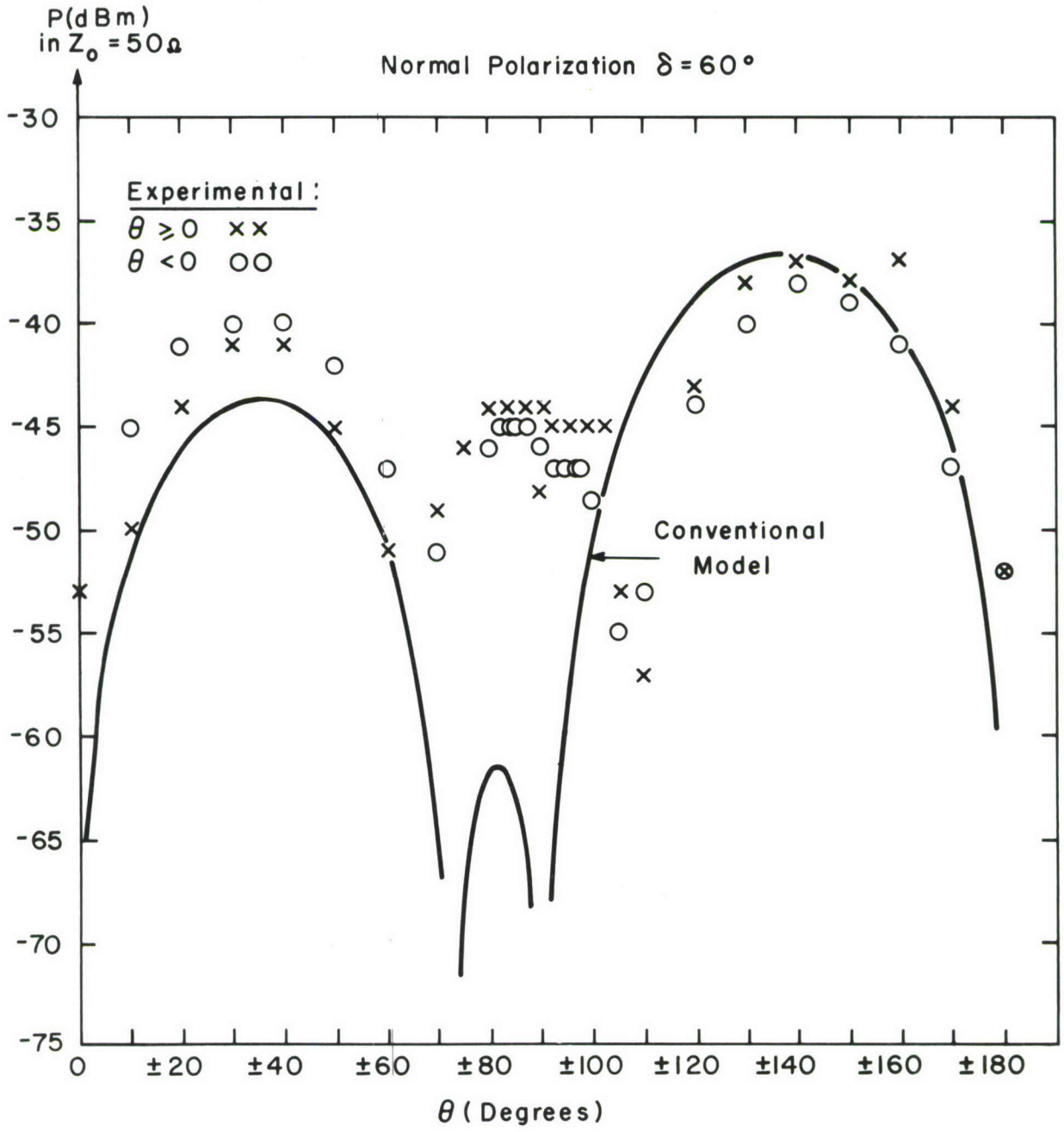

Fig. 3-6. Predictions of the model for normal polarization and $\mathcal{L}$ = 25 cm, k = 5 mm, f = 1.2 GHz, $\delta = 60^{\circ}$.

points, we propose the following model for unshielded, untwisted wires. The model is arrived at by reconsidering the per-unit-length model shown in Fig. 3-1 (b). First we assume that the line is electrically short and replace Δx with $\mathcal{L}$; that is, we lump the distributed sources. This is shown in Fig. 3-7 (a). Next we assume that the fields H_z^i and E_y^i are independent of the y direction. Thus

$$\phi_n = \mu \int_0^h H_z^i \, d_y = \mu H_z^i h \tag{3-14a}$$

$$e_t = \int_0^h E_y^i \, d_y = E_y^i h \tag{3-14b}$$

This modification is shown in Fig. 3-7(b). And finally, in the absence of any other information, we assume

$$H_z^i = \frac{E_y^i}{\eta} \tag{3-15}$$

where η is the wave impedance. We assume

$$\eta = 377 \tag{3-16}$$

and $E_y^i = E^i$ is the incident electric field provided to FTWTFR. The reduction is shown in Fig. 3-7 (c) where we have used the following facts:

$$\frac{\mu}{\eta} = \frac{1}{v} \tag{3-17}$$

where

$$v = 3 \times 10^8 \tag{3-18}$$

and

$$c = \frac{1}{vR_C} \tag{3-19}$$

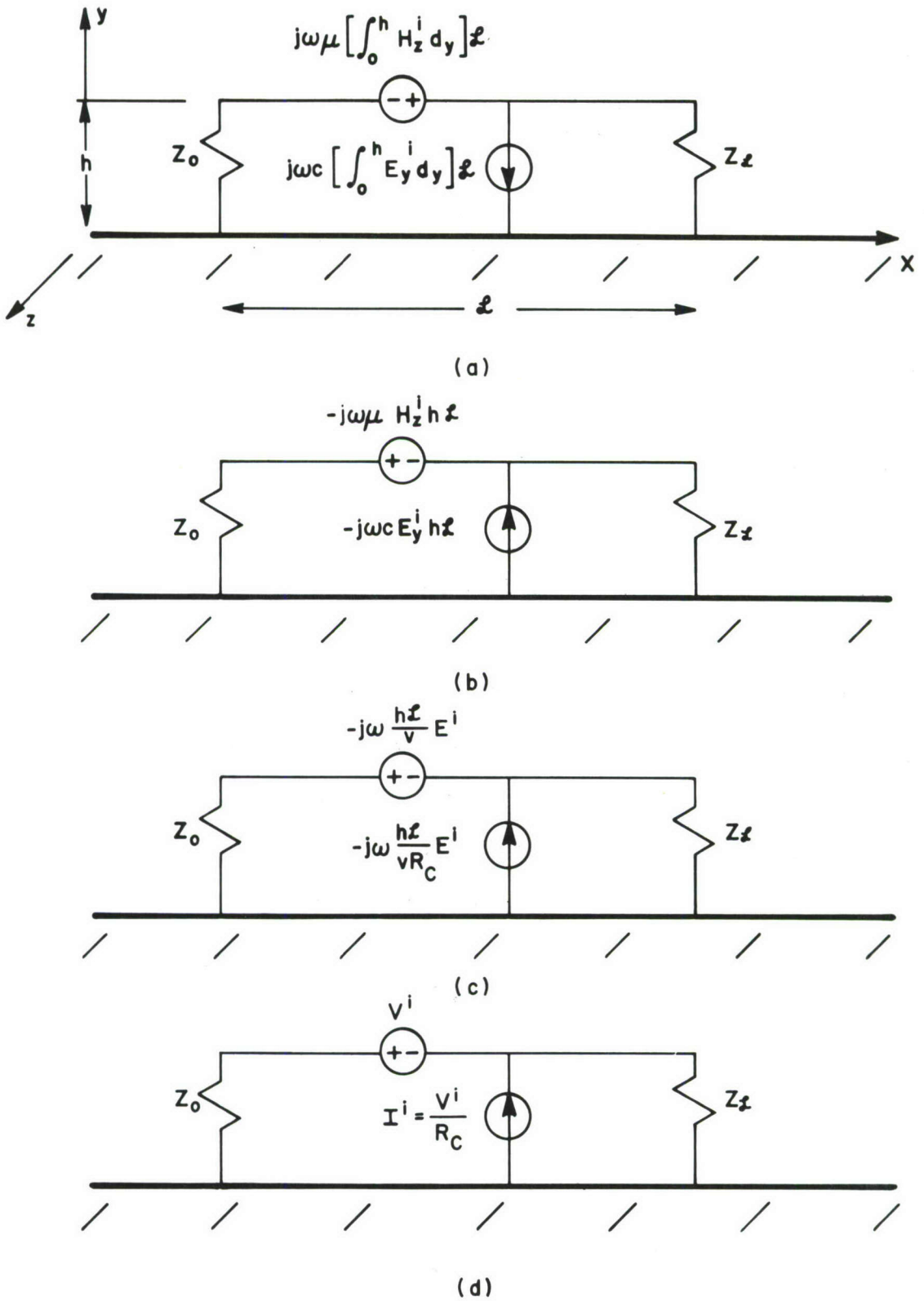

Fig. 3-7. A low-frequency approximation.

where the line characteristic resistance is

$$R_C = 60 \ln\left(\frac{2h}{r_w}\right) \tag{3-20}$$

and r_w is the wire radius.

Note that a voltage source is induced:

$$V^i = -j \frac{\omega}{v} A E^i \tag{3-21a}$$

where A is the area of the loop:

$$A = h\ell \tag{3-21b}$$

and a current source is induced

$$I^i = V^i/R_C \tag{3-21c}$$

These observations will be important in later adaptations of this basic model to twisted and/or shielded wires.

There are two contributions to the induced currents as was the case for wire-to-wire coupling. The voltage source represents magnetic field effects and may be viewed as an "inductive coupling" contribution, whereas the current source represents electric field effects and may be viewed as a "capacitive coupling" contribution. We add the magnitudes of these contributions and obtain

$$\begin{aligned} |I(0)| &= |I(0)|^{IND} + |I(0)|^{CAP} \\ &= \frac{V_m^i}{Z_0 + Z_\ell} + \frac{Z_\ell}{Z_0 + Z_\ell} I_m^i \\ &= V_m^i \left[\frac{1 + Z_\ell/R_C}{Z_0 + Z_\ell}\right] \\ &= \frac{V_m^i}{R_C}\left[\frac{R_C + Z_\ell}{Z_0 + Z_\ell}\right] \end{aligned} \tag{3-22a}$$

$$|I(\ell)| = V_m^i \left[\frac{1 + Z_0/R_C}{Z_0 + Z_\ell}\right] = \frac{V_m^i}{R_C}\left[\frac{R_C + Z_0}{Z_0 + Z_\ell}\right] \tag{3-22b}$$

where

$$V_m^i = \frac{\omega A}{v} E^i = \frac{\omega}{v} h\ell E^i \tag{3-22c}$$

It is rather interesting to note that this is precisely the same as the present model in FTWTFR over the low-frequency range where the response varies linearly with frequency which was apparently derived using a different rationale.

The difference is in the bounds imposed on the model. In light of the expected accuracies of IEMCAP, both in expected predictions and in available input data, and in view of the lack of information provided to FTWTFR, we propose that the bound for this model be set at the induced currents which would result from this line collecting the maximum power from an incident wave. If we use the actual loop area to be the effective area:

$$A_e = h\ell \tag{3-23}$$

The maximum average power collected from a passing uniform plane wave would be

$$P_{max} = \frac{1}{2}\frac{E^{i^2}}{377} A_e = \frac{1}{2}\frac{E^{i^2}}{377} h\ell \tag{3-24}$$

Assuming the dimensions to be electrically small, define the line voltage V_{max} such that

$$P_{max} = \frac{1}{2} \frac{V_{max}^2}{Z_0 || Z_\ell} \tag{3-25}$$

(We assume the loads to be purely resistive as is done in IEMCAP.) Thus the load currents would be

$$|I(0)|_{max} = \frac{V_{max}}{Z_0} = E^i \sqrt{\frac{Z_\ell}{Z_0(Z_0 + Z_\ell)}} \frac{h\ell}{377} \tag{3-26a}$$

$$|I(\ell)|_{max} = \frac{V_{max}}{Z_\ell} = E^i \sqrt{\frac{Z_0}{Z_\ell(Z_0 + Z_\ell)}} \frac{h\ell}{377} \tag{3-26b}$$

The resulting model is shown in Fig. 3-8. These predictions were compared to results computed by the exact model and a method of moments code which were given in [28] for uniform plane wave excitation and various angles of incidence, polarization and terminal impedances. In the low-frequency regions the results compared within 6 dB. In all cases, this model bounded those predictions. The maximum "overprediction" was on the order of 20 dB whereas most bounds were within 6 dB of the actual maxima.

The present version of FTWTFR contains a similar bound [1]:

$$|I(\ell)|_{max} = \frac{\max\left[\frac{\lambda}{\sqrt{4\pi}}, \ell\right]}{\sqrt{377\ Z_\ell}} \tag{3-27}$$

Although no derivation or justification of this was given in [1], it seems that the following would be a logical procedure to arrive at this result.

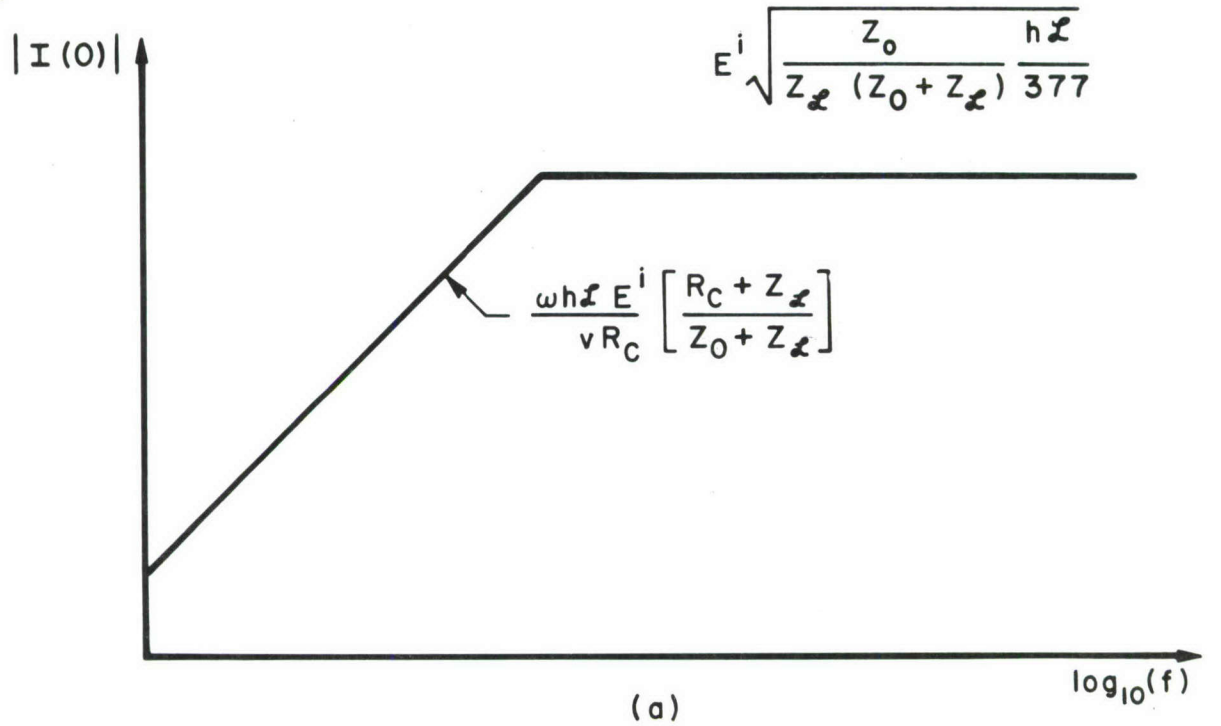

(a)

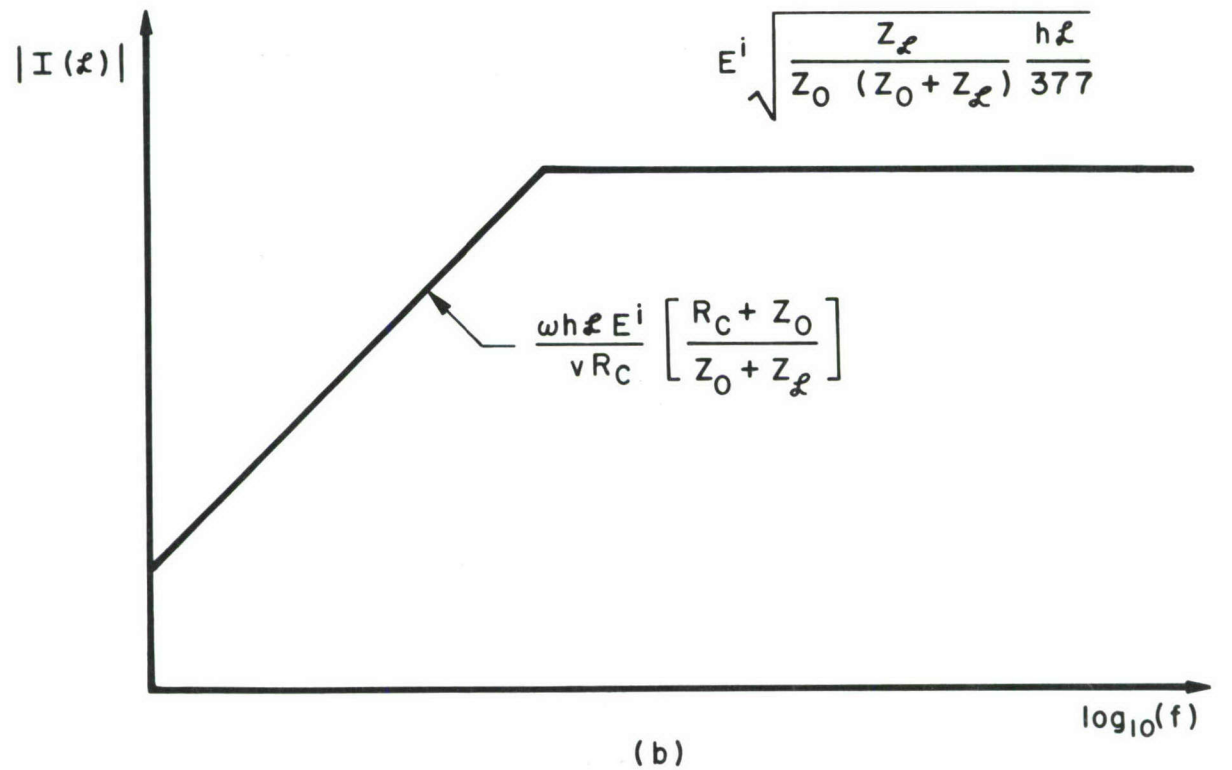

(b)

Fig. 3-8. Bounds on the induced currents.

Suppose we assume the wire with ground to be a collecting aperture with effective area A_e. Thus from an incident uniform plane wave, the collected average power would be

$$P = \frac{1}{2} \frac{E^{i^2}}{377} A_e \tag{3-28}$$

If all of this collected power is delivered to one of the loads then

$$P = \frac{1}{2} |I(\ell)|^2 Z_\ell \tag{3-29}$$

and

$$|I(\ell)| = E^i \frac{\sqrt{A_e}}{\sqrt{377 Z_\ell}} \tag{3-30}$$

Now

$$A_e = \frac{\lambda^2}{4\pi} G \tag{3-31}$$

If we assume the gain to be unity, G = 1, then $A_e = \lambda^2/4\pi$. On the other hand if we assume the maximum aperture to be the physical aperture then $A_e = \ell h$. Thus the present result in FTWTFR in (3-27) appears to have been derived from this process. However there are two fundamental errors; not all of the collected power is delivered to only one of the two loads (thus (3-29) is incorrect) and the maximum aperture is ℓh and not ℓ as (3-27) implies. Thus the proposed bound, (3-26), seems to be consistent with the previous philosophy and corrects errors apparent in that derivation.

3.3 Unshielded, Twisted Pairs

We use a philosophy similar to the wire-to-wire model for this case; we only consider induced, differential mode signals. First consider the case of an unbalanced, twisted pair. We model the line as a sequence of alternating loops as shown in Fig. 3-9 (a). We then compute the induced sources in the line as in the previous section with the exceptions that (1)

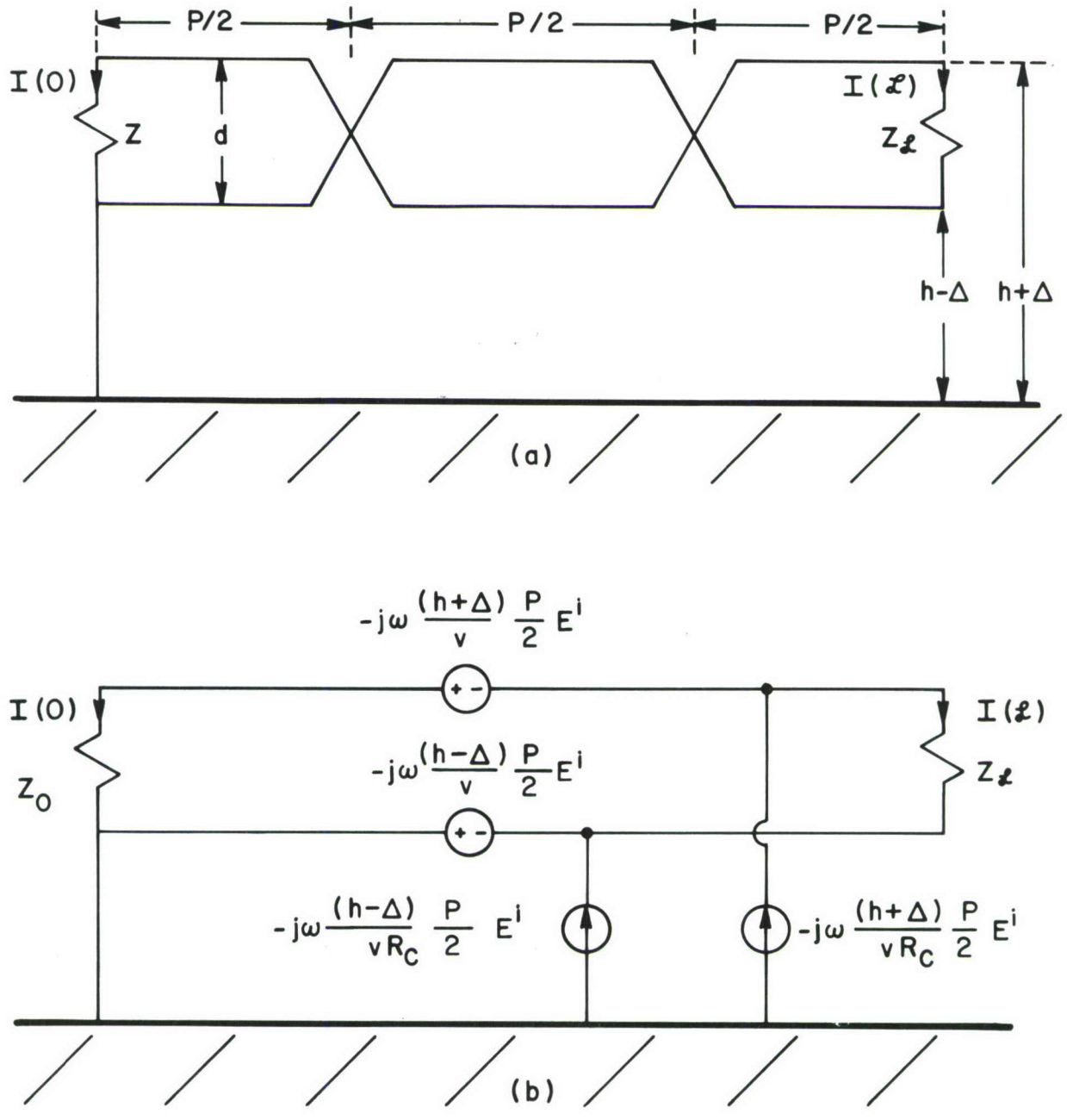

Fig. 3-9. The unbalanced, twisted pair model.

the (bundle) height above ground, h, in that model is replaced by the height of each wire above ground, $h+\Delta$ and $h-\Delta$ where $\Delta = d/2$ and d is the wire separation, (2) the characteristic resistance of each line above ground is

$$R_C = 60\ \ell n \left(\frac{2(h \pm \Delta)}{r_w} \right) \tag{3-32}$$

where r_w is the wire radius, and (3) the line length, $\mathcal{L}$, is replaced by P/2 where P is the pitch of the twisted pair. (We assume exact cancellation for an even number of half twists.) The result is shown in Fig. 3-9 (b). From this we obtain

$$|I(0)|^{IND} = \frac{\frac{\omega(h+\Delta)P}{2v} E^i}{Z_0 + Z_{\mathcal{L}}} - \frac{\frac{\omega(h-\Delta)P}{2v} E^i}{Z_0 + Z_{\mathcal{L}}}$$

$$= - \frac{\frac{\omega dP}{2v} E^i}{Z_0 + Z_{\mathcal{L}}} \tag{3-33a}$$

$$|I(0)|^{CAP} = \frac{Z_{\mathcal{L}}}{Z_0 + Z_{\mathcal{L}}} \quad \frac{\omega(h+\Delta)P\ E^i}{2v\ R_C}$$

$$\doteq \frac{Z_{\mathcal{L}}}{Z_0 + Z_{\mathcal{L}}} \quad \frac{\omega hP\ E^i}{2v\ R_C} \tag{3-33b}$$

Note that the inductive coupling is the same as the single wire case except that the height above ground is replaced by the wire separation and the line length is replaced by P/2. The capacitive coupling is the same as the single wire case except that the line length becomes P/2. (Note that the induced current source attached to the ground wire has no effect.) Similarly

$$|I(\mathcal{L})|^{IND} = |I(0)|^{IND} \tag{3-33c}$$

$$|I(\mathcal{L})|^{CAP} = \frac{Z_0}{Z_{\mathcal{L}}} |I(0)|^{CAP} \tag{3-33d}$$

and

$$|I(0)| = |I(0)|^{IND} + |I(0)|^{CAP} \tag{3-34a}$$

$$|I(\ell)| = |I(\ell)|^{IND} + |I(\ell)|^{CAP} \tag{3-34b}$$

Note that the induced sources in the single wire above ground model are equivalent to those here where the loop area is A = d P/2 and the characteristic resistance is twice that of a single wire above ground.

The bound on this result is similar to the bound for the previous case of one wire above ground and is derived in a similar fashion treating the loop area between the wires as an antenna:

$$|I(0)|_{max} = E^i \sqrt{\frac{Z_\ell}{Z_0(Z_0 + Z_\ell)}} \frac{d\ P/2}{377} \tag{3-35a}$$

$$|I(\ell)|_{max} = E^i \sqrt{\frac{Z_0}{Z_\ell(Z_0 + Z_\ell)}} \frac{d\ P/2}{377} \tag{3-35b}$$

The balanced twisted pair case is treated similarly. We model the balanced twisted pair case as a sequence of abrupt loops as shown in Fig. 3-10 (a). At this point we need to define what is meant by "induced currents". At the left end we may define induced currents $I_1(0)$ and $I_2(0)$ as shown. Normally the received voltage V(0) is related to the difference of these two induced currents as

$$V(0) = Z_0[I_1(0) - I_2(0)]$$

Thus it seems reasonable that the induced currents would be the differences

$$I(0) = I_1(0) - I_2(0) \tag{3-36a}$$

$$I(\ell) = I_1(\ell) - I_2(\ell) \tag{3-36b}$$

In order to determine the induced sources, we again treat <u>each wire</u>

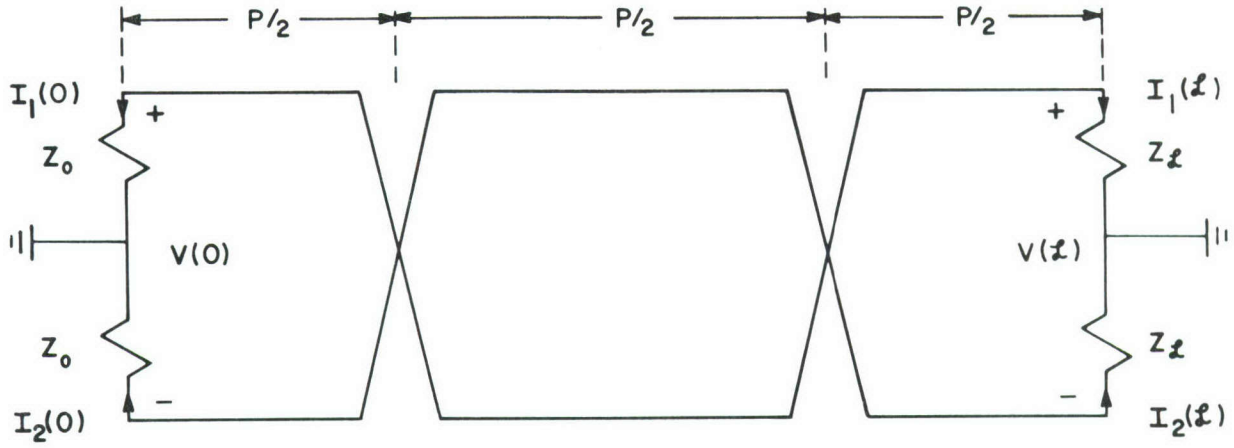

(a)

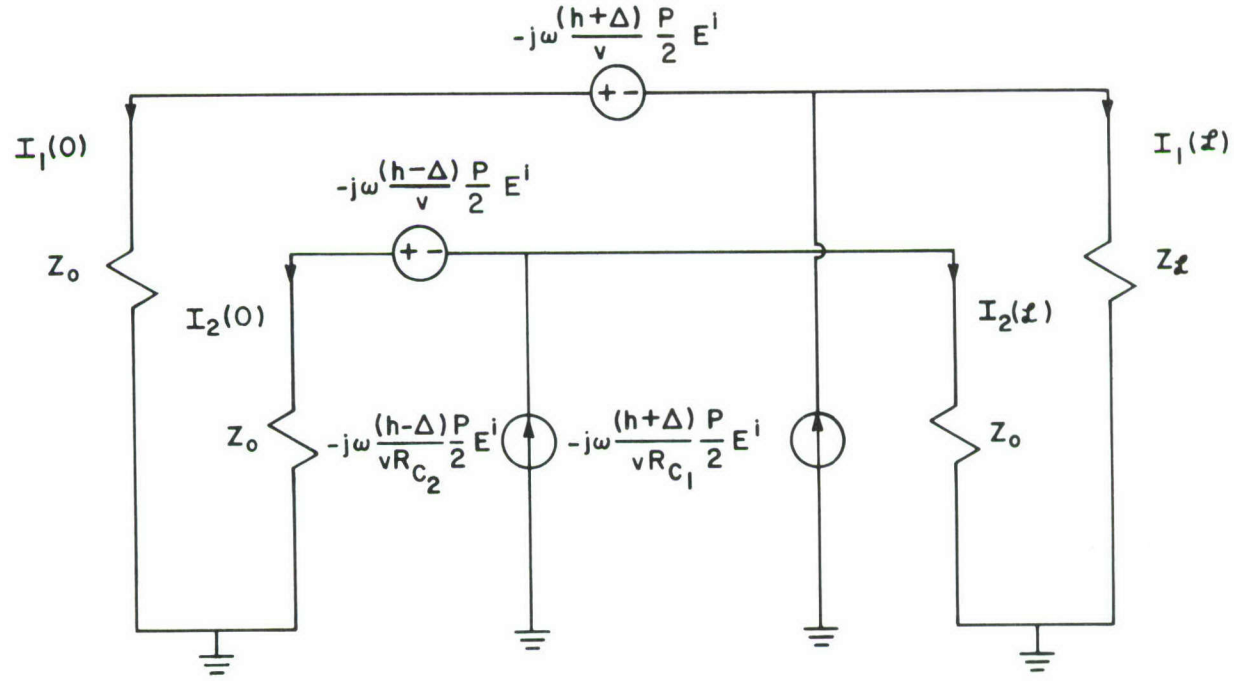

(b)

Fig. 3-10. The balanced, twisted pair model.

above ground separately. One wire is at height h+Δ above ground and the other wire is at height h-Δ above ground where h is the bundle height and Δ is one-half the wire separation. The resulting model is shown in Fig. 3-10 (b) and is based on the one-wire-above-ground model in Fig. 3-7 (c) where

$$R_{C_1} = 60 \ln\left(\frac{h+\Delta}{r_w}\right) \tag{3-37a}$$

$$R_{C_2} = 60 \ln\left(\frac{h-\Delta}{r_w}\right) \tag{3-37b}$$

From this result we obtain

$$|I(0)|^{IND} = \frac{\frac{\omega(h+\Delta)}{v} P/2}{Z_0 + Z_{\mathcal{L}}} E^i - \frac{\frac{\omega(h-\Delta)}{v} \frac{P}{2}}{Z_0 + Z_{\mathcal{L}}} E^i$$

$$= \frac{\frac{\omega dP}{2v}}{Z_0 + Z_{\mathcal{L}}} E^i \tag{3-38a}$$

$$|I(0)|^{CAP} = \frac{Z_{\mathcal{L}}}{Z_0 + Z_{\mathcal{L}}} \frac{\omega(h+\Delta)}{v R_{C_1}} \frac{P}{2} E^i - \frac{Z_{\mathcal{L}}}{Z_0 + Z_{\mathcal{L}}} \frac{\omega(h-\Delta)}{v R_{C_2}} \frac{P}{2} E^i$$

$$= \frac{Z_{\mathcal{L}}}{Z_0 + Z_{\mathcal{L}}} \frac{\omega P}{2v} \left[\frac{h+\Delta}{R_{C_1}} - \frac{h-\Delta}{R_{C_2}}\right] E^i$$

$$= \frac{Z_{\mathcal{L}}}{Z_0 + Z_{\mathcal{L}}} \frac{\omega P(h+\Delta)}{2v R_{C_1}} \left[1 - \frac{h-\Delta}{h+\Delta} \frac{R_{C_1}}{R_{C_2}}\right] E^i \tag{3-38b}$$

$$\doteq \frac{Z_{\mathcal{L}}}{Z_0 + Z_{\mathcal{L}}} \frac{\omega hP}{2v R_C} \left[1 - \frac{h-\Delta}{h+\Delta} \frac{R_{C_1}}{R_{C_2}}\right] E^i$$

and

$$|I(0)| = |I(0)|^{IND} + |I(0)|^{CAP} \tag{3-39}$$

Note that the inductive coupling is the same as for the unbalanced case.

Similarly

$$|I(\mathscr{L})|^{IND} = |I(0)|^{IND} \tag{3-40a}$$

$$|I(\mathscr{L})|^{CAP} = \frac{Z_0}{Z_{\mathscr{L}}} |I(0)|^{CAP} \tag{3-40b}$$

and

$$|I(\mathscr{L})| = |I(\mathscr{L})|^{IND} + |I(\mathscr{L})|^{CAP} \tag{3-41}$$

Again the induced sources are equivalent to the single wire above ground case except that the loop area A and the characteristic resistance R_C are different.

The bounds on these currents are computed from the difference of the bounds on the currents in each line:

$$|I(0)|_{max} = E^i \sqrt{\frac{Z_{\mathscr{L}}}{Z_0(Z_0 + Z_{\mathscr{L}})} \frac{(h+\Delta)\ P/2}{377}} - E^i \sqrt{\frac{Z_{\mathscr{L}}}{Z_0(Z_0 + Z_{\mathscr{L}})} \frac{(h-\Delta)\ P/2}{377}} \tag{3-42a}$$

$$|I(\mathscr{L})|_{max} = E^i \sqrt{\frac{Z_0}{Z_{\mathscr{L}}(Z_0 + Z_{\mathscr{L}})} \frac{(h+\Delta)\ P/2}{377}} - E^i \sqrt{\frac{Z_0}{Z_{\mathscr{L}}(Z_0 + Z_{\mathscr{L}})} \frac{(h-\Delta)\ P/2}{377}} \tag{3-42b}$$

3.4 Shielded Wires

In this section we address the effect of a shield on the field-to-wire coupling. The three cases are shown in Fig. 3-11 where the shield may be either a single or a double shield. As with wire-to-wire coupling, we must address the effect of pigtails. (This is not addressed in the current FTWTFR subroutine.) In a fashion similar to wire-to-wire coupling, we will superimpose the field-to-wire coupling contributions over the pigtail sections and

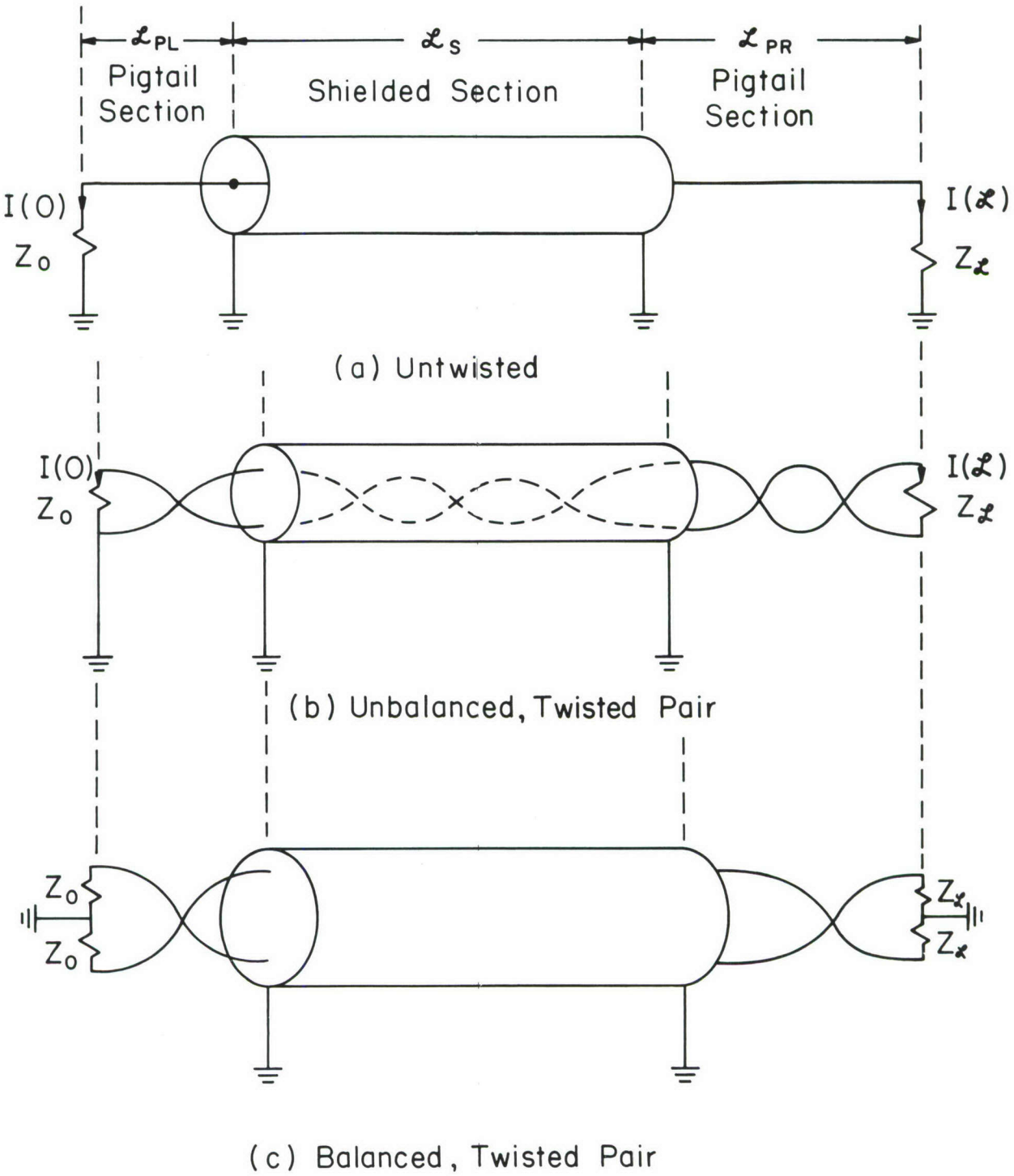

Fig. 3-11. Modeling coupling to pigtail sections.

over the shielded sections. The pigtail coupling over the pigtail sections is addressed via the unshielded line models of the previous sections and using line lengths of $2\ell_p$ for single wires and min $\{2\ell_p, P/2\}$ for twisted pairs where ℓ_p is the pigtail length and P is the pitch of the twisted pair. We now address the coupling to the shielded section.

First consider the case of a shielded, single wire shown in Fig. 3-12 (a). The shield length is denoted as ℓ_s ($\ell_s = \ell_B - 2\ell_p$) and the height above ground is denoted as h, the bundle height. The philosophy here is similar to the wire-to-wire case. We insert the induced sources and compute the induced currents. If a shield is grounded at least at one end, we remove the induced current sources, i.e., the analogous capacitive coupling is taken to be zero. Similarly, a shield affects the "inductive coupling" only if the shield is double-end grounded. Otherwise, the shield is assumed to have no effect on the unshielded, inductive coupling. Thus for a double-end grounded shield, the unshielded result is corrected by multiplying the induced voltage source by the shielding factor

$$S = \frac{Z_{SH}}{Z_{SH} + j\omega L_S} \tag{3-43}$$

where the shield self impedance is Z_{SH} and the self inductance of the shield above ground is

$$L_S = \frac{\mu_o}{2\pi} \ln\left(\frac{2h}{r_s + t_s}\right) \tag{3-44}$$

where r_s is the shield inner radius and t_s is the shield thickness.

These results can be derived in two ways. First consider the equivalent circuit in 3-12 (c). The incident field is assumed to induce V^i in the two

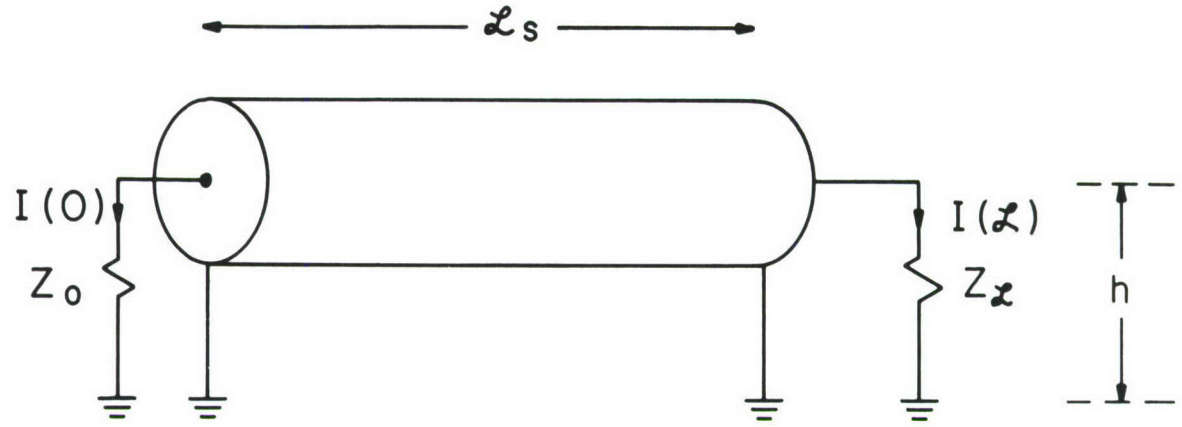

(a)

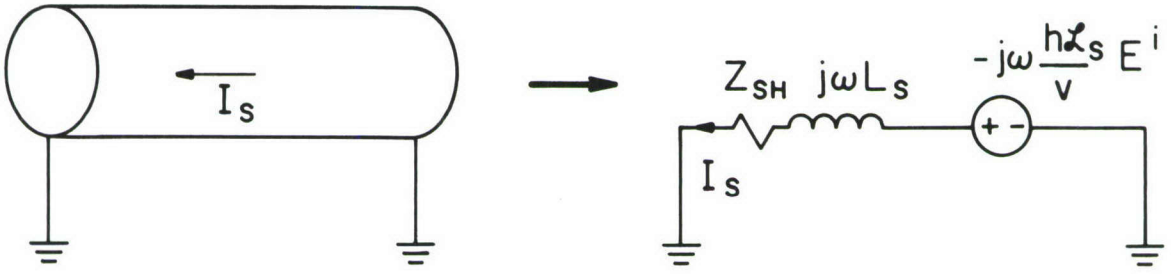

(b)

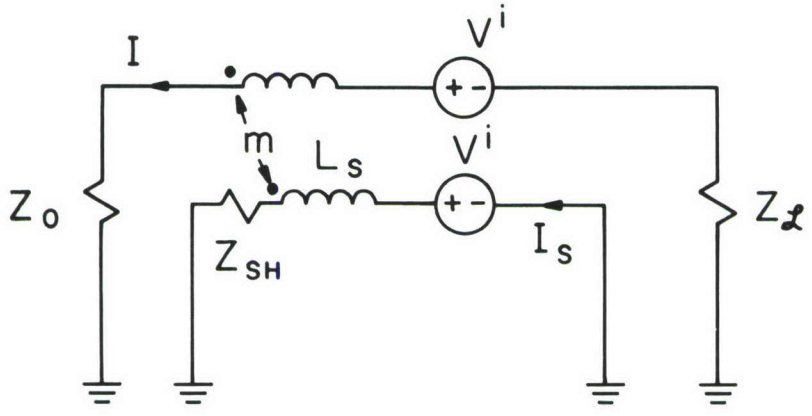

(c)

Fig. 3-12. Including the effect of a shield.

loop areas bounded by the inner wire and bounded by the shield. A shield current is induced to flow which interacts with the interior wire-ground plane loop to induce another contribution. From the circuit of Fig. 3-12 (c) one can write

$$(Z_0 + Z_\ell)I + j\omega M I_s = V^i \tag{3-45a}$$

$$(Z_{SH} + j\omega L_S)I_s + j\omega M I = V^i \tag{3-45b}$$

Solving yields

$$[(Z_0 + Z_\ell) - j\omega M]I = [(Z_{SH} + j\omega L_S) - j\omega M]I_s \tag{3-46}$$

or

$$I_s = \frac{(Z_0 + Z_\ell) - j\omega M}{(Z_{SH} + j\omega L_S) - j\omega M} \quad I \tag{3-47}$$

Substituting (3-47) into (3-45a) gives

$$I = \frac{Z_{SH} + j\omega(L_S - M)}{(Z_0 + Z_\ell)(Z_{SH} + j\omega L_S) + \omega^2 M^2} \quad V^i \tag{3-48}$$

Noting, as was the case for wire-to-wire coupling, that the self-inductance of the shield above ground, L_S, and the mutual inductance between the shield and the inner wire, M, are one and the same, we obtain, neglecting the higher order term $\omega^2 M$,

$$I = \frac{V^i}{(Z_0 + Z_\ell)} \quad \frac{Z_{SH}}{Z_{SH} + j\omega L_S} \tag{3-49}$$

Thus the unshielded magnetic field coupling is modified by multiplying by the shielding factor in (3-43). Note that this result requires a nonzero shield current I_s. This will occur only if the shield is double-end grounded. Otherwise the shielding factor is unity.

An alternative derivation of this result is obtained from Fig. 3-13 (a). We first assume that the terminations are completely housed within the shield

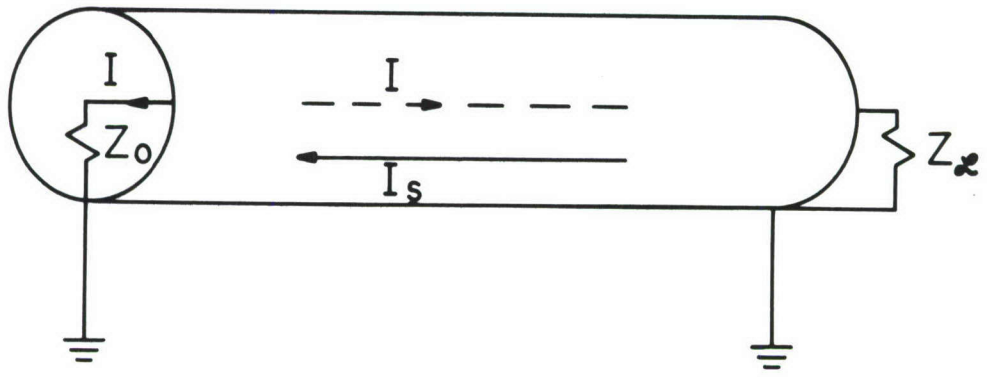

(a)

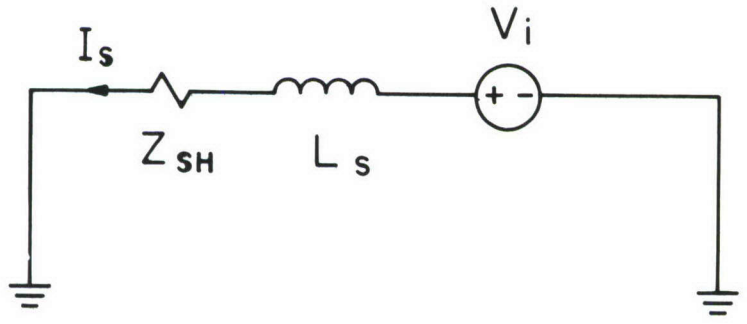

(b)

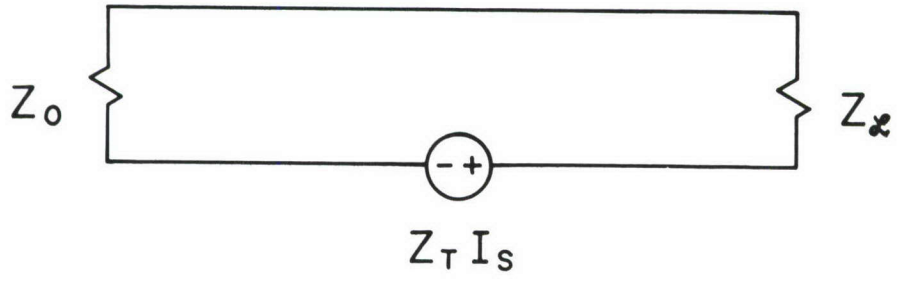

(c)

Fig. 3-13. Use of surface transfer impedance, Z_T, to compute coupling.

and do not connect directly to the ground. In this case the induced source, V^i, lies only in the shield-ground plane loop. The induced shield current is then

$$I_s = \frac{V^i}{Z_S + j\omega L_S} \tag{3-50}$$

The effect of this shield current is passed through the shield via the shield surface transfer impedance, Z_T, resulting in a voltage source induced on the interior surface of the shield, $Z_T I_s$ [11]. This produces the induced current I:

$$\begin{aligned} I &= \frac{Z_T I_s}{Z_0 + Z_\ell} \\ &= \frac{V^i}{Z_0 + Z_\ell} \frac{Z_T}{Z_S + j\omega L_S} \end{aligned} \tag{3-51}$$

Note that for a sufficiently small frequency such that the shield wall thickness is less than a skin depth. The shield and transfer impedances are approximately equal, i.e.,

$$Z_T \doteq Z_{SH} \tag{3-52}$$

Thus (3-51) and (3-49) are equivalent. We shall presume (3-52) to be true.

For balanced or unbalanced twisted pairs we presume a shield, regardless of its grounding configuration, to have no effect on inductive coupling. The reason is the same as for the wire-to-wire coupling case; no net induced current returns through the ground plane for these ideal configurations. Thus the magnetic flux produced by the shield current has no counteracting effect. Thus the shielding factors apply only for single wires with shields that are double-end grounded. If the shield is ungrounded it is assumed to have no effect.

This simplifies the models considerably. We simply multiply the un-

shielded results by the various shielding factors which were developed for the wire-to-wire case. The only area left to be addressed is the bound. For the unshielded case, the induced currents increased linearly with frequency. For the shielded case, the induced currents also increase linearly with frequency so long as no shield is double-end grounded. If only one shield is double end grounded, the unshielded result is multiplied by the shielding factor in (3-43) in which case the resulting induced currents increase with frequency up to a frequency at which $Z_{SH} = \omega L_S$. Above this frequency the induced currents remain constant. If both shields are double-end grounded, the unshielded result is multiplied by the inner and outer shield shielding factors, S_o and S_i, as was the case for wire-to-wire coupling. Above a certain frequency, the coupling will decrease linearly with and increase in frequency (-20 dB/decade). Thus we need to be concerned about limiting the uncontrolled increase of coupling with frequency only in the case that no shield is double-end grounded. But in this case, we reduce to the unshielded result (with or without the capacitive coupling induced source depending on whether the shield is ungrounded or single-end grounded). We developed a bound for this previously and will use that bound here.

3.5 Branched Cables

Our philosophy for handling branched cables is identical to that for wire-to-wire coupli g; we will superimpose the coupling contributions to the wire(s) in question from those of each branch segment through which the wire runs.

The current version of IEMCAP does this presently. The only addition needed will be to add pigtail contributions which is not presently done.

3.6 Pigtails

Pigtail coupling is treated as an unshielded section. Thus we will need to pass to the FTWTFR subroutine, parameters for the bundle segment in question, the parameters IRENDS (indicating whether a pigtail is present at 0, 1 or both ends of this segment) and PIGR (the lengths of pigtails specified by the user for this shielded wire).

Once these parameters are passed to FTWTFR, we can compute the sum of the shielded section and pigtail section coupling for each bundle segment. Then we select the minimum of this induced current and the bound for the unshielded case to be the coupling over this segment. The total current induced at a port is then the sum of the induced currents associated with each bundle segment through which this wire passes.

3.7 The FTWTFR Subroutine Revision

The revision of the FTWTFR subroutine is detailed in Appendix C along the lines of the discussion in the previous sections. The details are considerably simpler than for WTWTFR since we need not consider the possible combinations of adjacent wire types as we did in WTWTFR.

The bound will be calculated for each segment and the magnitudes of the induced currents will be added (outside FTWTFR) for all segments through which this wire passes. The segment exposure length will be determined by whether the segment is exposed to an aperture or not as described previously and is presently done in FTWTFR.

IV. System Perturbations

Modern avionics systems are structurally far from the ideal assumed by IEMCAP. For example, cable bundles do not always maintain the same height above the ground plane (fuselage). Furthermore, aircraft structural ribs appear at periodic intervals along the bundle between the bundle and the ground plane [31]. Hydraulic lines (which are "grounded" cylinders) also pass near these cable bundles. Also cable clamps are used at periodic intervals along the bundle to secure it to the fuselage [32].

The essential question regarding the IEMCAP models is whether these "system perturbations" need to be included in the wire-to-wire and field-to-wire models. There are two questions to be answered in this regard. For the anticipated frequencies and dimensions of interest, do these system perturbations significantly effect the wire-to-wire and field-to-wire coupling? If the answer to this question is yes then we need to answer the next question: Will the inclusion of models of these perturbations into the wire-to-wire and field-to-wire coupling subroutines change the predictions of these models significantly and if so, will the predictions be more accurate? This latter question is particularly important to answer. Even though these system perturbations may, in actuality, significantly influence the wire-to-wire and field-to-wire coupling, the present models in IEMCAP may not be sufficiently complex to allow these effects to be modeled. For example, it is known that perturbations placed periodically along a transmission line can cause pass bands and stop bands to appear in the signal transmission properties of the line [33, 34]. The effects of these periodically-placed perturbations generally only occur for frequencies where the line is elec-

trically long [33]. For these frequencies, the wire-to-wire and field-to-wire models presently included in IEMCAP and suggested for revision in this document only provide a course bound. So it appears that even though these perturbations can cause significant effects, it will do little good to include models of these perturbations in the wire-to-wire and field-to-wire subroutines as they are now constituted. If one wishes to model these effects, an entirely different model philosophy from that presently employed (or suggested here) must be employed, e.g. a distributed parameter or multiconductor transmission line model.

The present philosophy of IEMCAP rules out this detailed modeling. Any such detailed modeling is reserved for off-line models in the IAP. Perhaps there is a need to revise those IAP models (which are basically distributed parameter transmission line models) to include these perturbations. This would seem to be the most reasonable course of action.

A survey of IEMCAP users was conducted in the summer of 1982. A questionnaire was mailed to over 35 users to obtain their suggestions for additional perturbations to be considered for modeling. Only 2 were returned. Those two suggested cable trays and junction boxes as perturbations to be modeled as well as other functional revisions not addressed in this report. Based on conversations with industry and the author's observations we will investigate the following non-ideal system perturbations:

(1) structural ribs [31]

(2) cable clamps [32]

(3) hydraulic lines

(4) cable trays

(5) bulkhead/disconnect penetrations

(6) junction boxes.

4.1 Structural Ribs

Coen, Liu and Tesche have modeled the effect of a structural rib in [31]. Their model consists of a capacitance between the wire and ground plane at the point of discontinuity as shown in Fig. 4-1. No closed form expressions for this equivalent capacitance were obtained and numerical solutions had to be used. Curves of numerical results for various ratios of wire radius to wire height above ground, a/b, and rib height to height of the wire above ground, h/b, were given. These were given in terms of the ratio of the rib capacitance C_R to the product of the unperturbed line capacitance c and the height of the wire above ground:

$$\frac{C_R}{bc}$$

From those results we can obtain estimates of the effects of ribs for low frequency line behavior.

As an example, consider a #20 gauge wire (a = 16 mils) suspended a height of 3 inches above the fuselage (b = 3"). Suppose the rib height is 2.5" (h = 2.5"). The per-unit-length capacitance of the unperturbed line is

$$c = \frac{2\pi\varepsilon o}{\ell n(2b/r_w)}$$

$$= 9.373 \text{ pF/m}$$

From the results in Fig. 6 of [31] we obtain

$$\frac{C_R}{bc} \doteq .15$$

Thus

$$C_R = .107 \text{ pF}$$

If we model the line with a Tee network (valid for electrically short

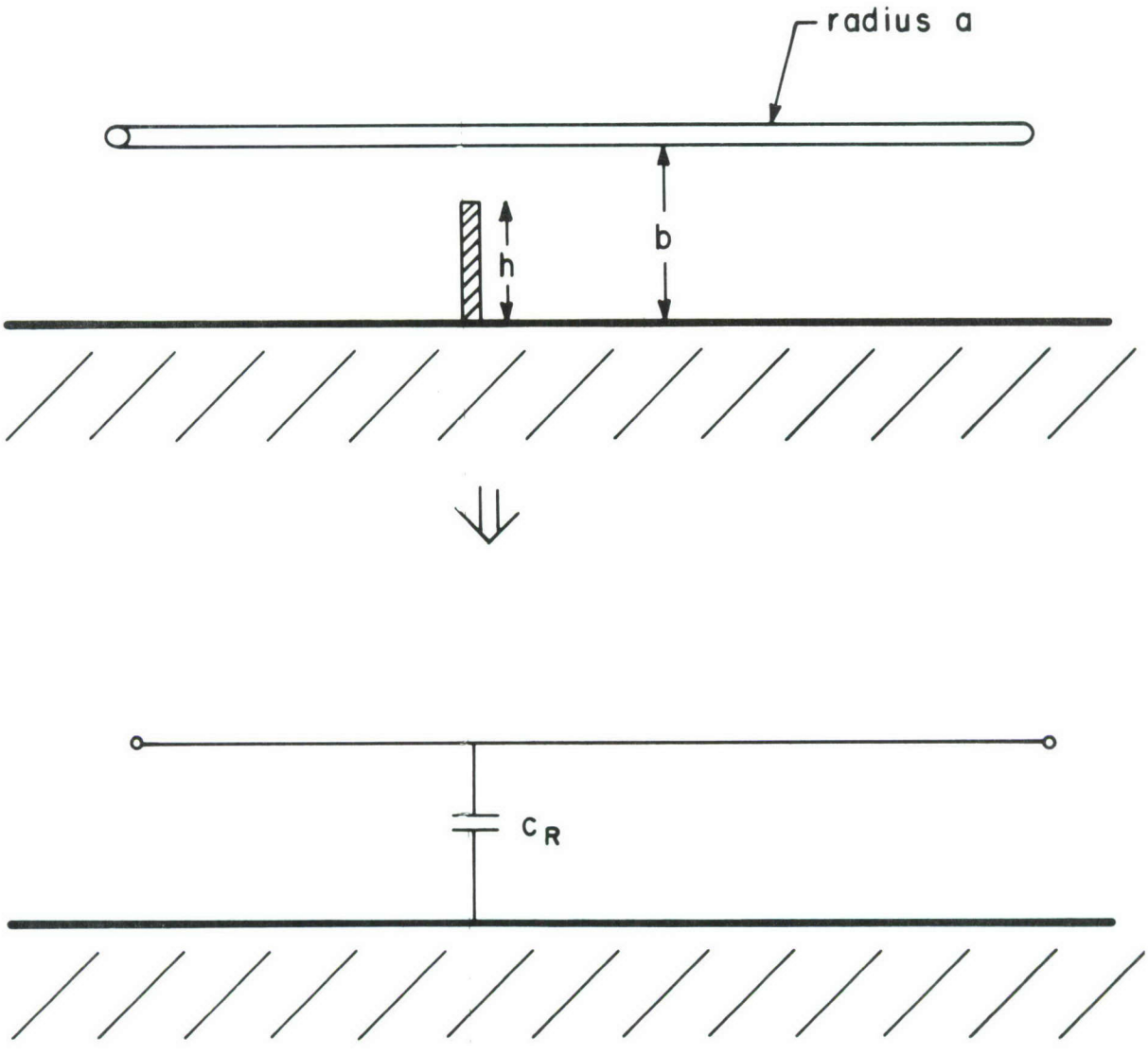

Fig. 4-1. Modeling the effect of a structural rib.

lines) and include the rib capacitance (assuming it is located at the midpoint of the line) we obtain the circuit shown in Fig. 4-2 [3]. Note that the total line to ground capacitance is

$$C_T = C_R + c\ell \quad \text{pF}$$
$$= .107 + 9.373\ell \quad \text{pF}$$

The rib capacitance equals the unperturbed line capacitance for a line length of .023 m or approximately 1/2 inch. Of course this same analysis can be applied to sections of the line between adjacent ribs. Thus if the separation between adjacent ribs is greater than 1/2 inch, their effect on behavior of electrically short lines should be negligible. Certainly then the effect of the rib is inconsequential in any low frequency model for these dimensions.

It is difficult to make any general conclusions for the effect of ribs on an electrically short line but the above dimensions seem reasonable and typical. Consequently it does not appear that structural ribs will significantly affect the behavior of electrically short lines where the models of IEMCAP are valid. The effect of ribs on the high frequency behavior (where the line is electrically long) will be investigated in a later section.

Some experimental work on the effect of ribs is contained in [37]. A 6.1 m line was suspended above a ground plane. The cable was apparently an RG/213 coax. The height of suspension appeared to be 8.9 cm. 50 ribs were periodically placed along the line. It is not clear from the documentation what was done or the effect of the ribs.

4.2 Cable Clamps

Models of cable clamps were obtained by Tesche and Liu in [32]. For typical cable clamp dimensions and frequencies below 1 GHz, the model of a cable clamp can be simplified to a Tee structure shown in Fig. 4-3. In

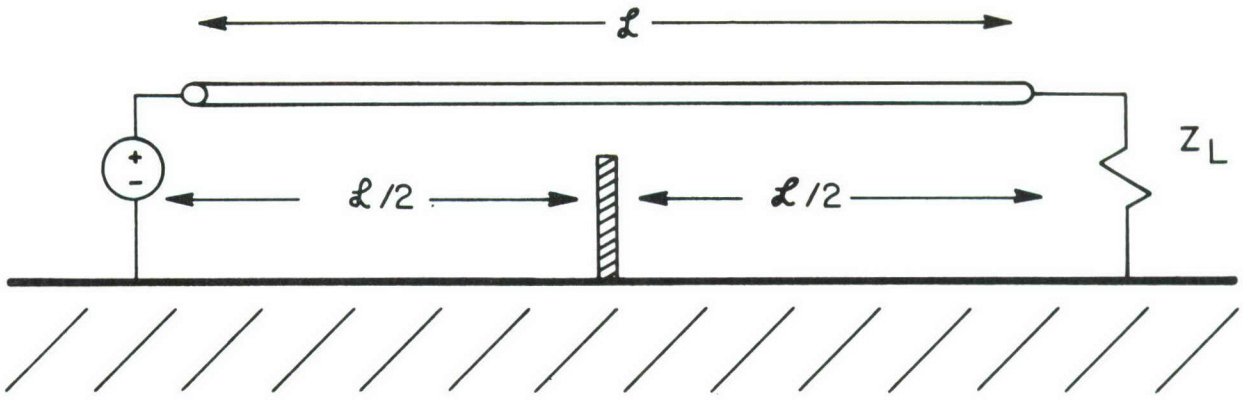

(a)

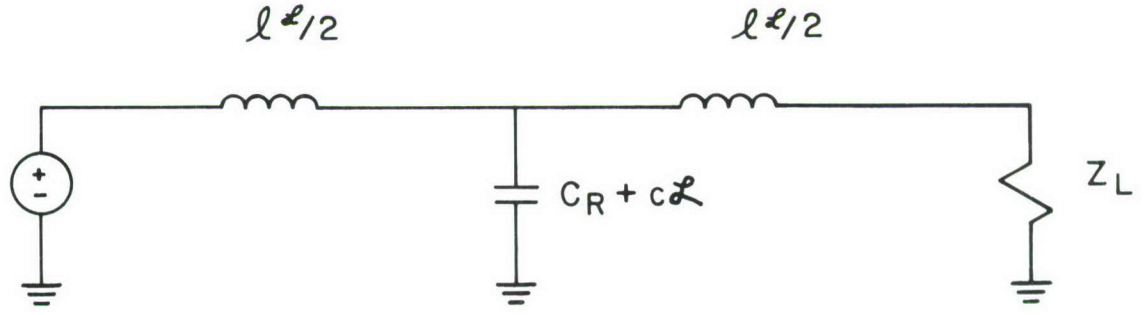

(b)

Fig. 4-2. Including the effect of a rib in the line model.

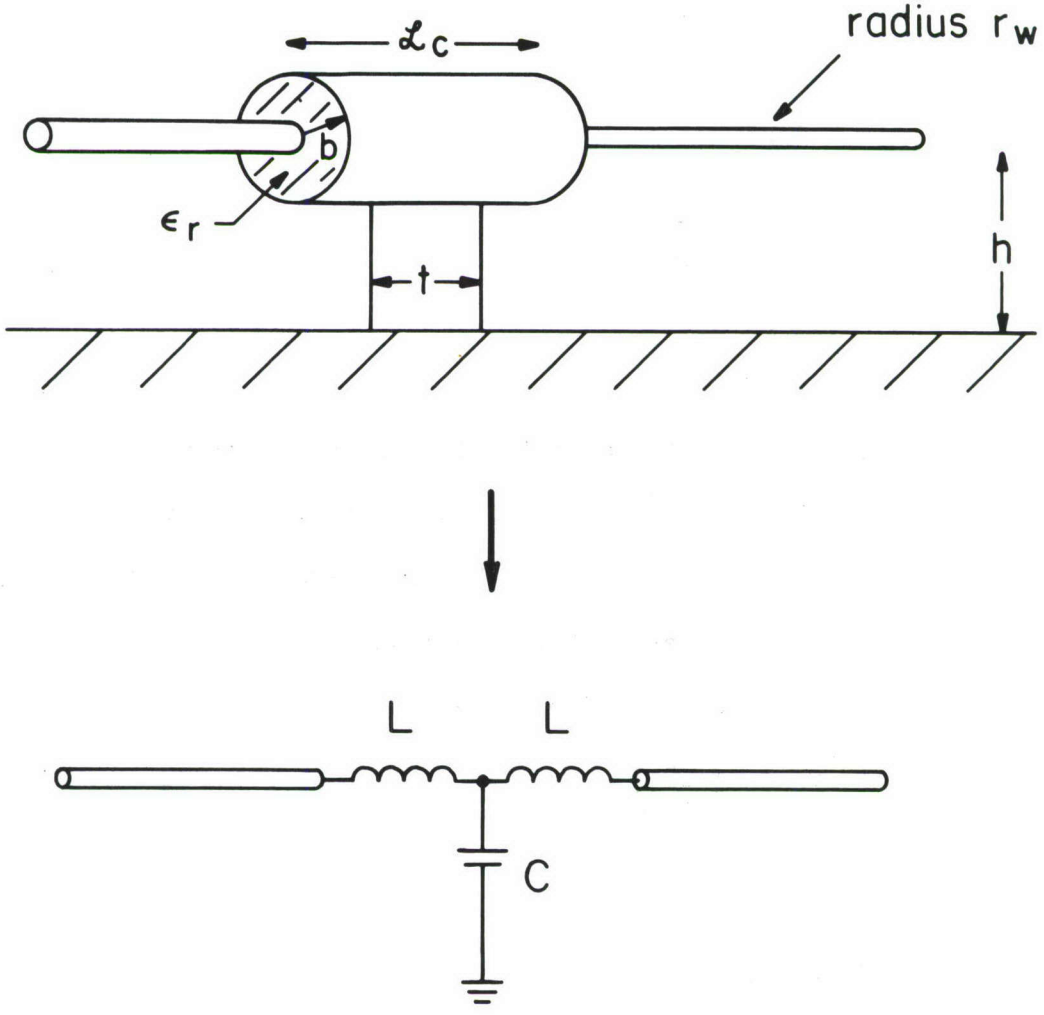

Fig. 4-3. Modeling a cable clamp.

[32], the following dimensions are considered:

$$\mathcal{L}_c = 1.4 \text{ cm}$$

$$b = 2.15 \text{ cm}$$

$$h = 3 \text{ cm}$$

$$r_w = 1.5 \text{ cm}$$

$$t = 1.4 \text{ cm}$$

$$\varepsilon_r = 2.25$$

and the elements of the model become

$$L = 1.7 \text{ nH}$$

$$C = 4.8 \text{ pF}$$

To investigate the effect of the cable clamp on the low-frequency line behavior (electrically short line) we assume the clamp is placed at the center of a line of length $\mathcal{L}$ and model the line with a Tee circuit as shown in Fig. 4-4 [3]. Here ℓ and c are the per-unit-length inductance and capacitance of the unperturbed line. For the above dimensions

$$\ell = \frac{\mu_o}{2\pi} \ln\left(\frac{2h}{r_w}\right)$$

$$= 277.3 \text{ nH/m}$$

$$c = \frac{2\pi\varepsilon_o}{\ln(2h/r_w)}$$

$$= 40.07 \text{ pF/m}$$

The inductance parameter of the clamp, L, can be neglected if it is much less than $\frac{\ell}{2}\frac{\mathcal{L}}{2}$. These terms are equal for line lengths of $\mathcal{L} = 4L/\ell = .025 \text{ m} \doteq 1$ inch. Consequently for these typical clamp and line dimensions, the clamp can be modeled as simply a capacitance C as was the case for a structural rib.

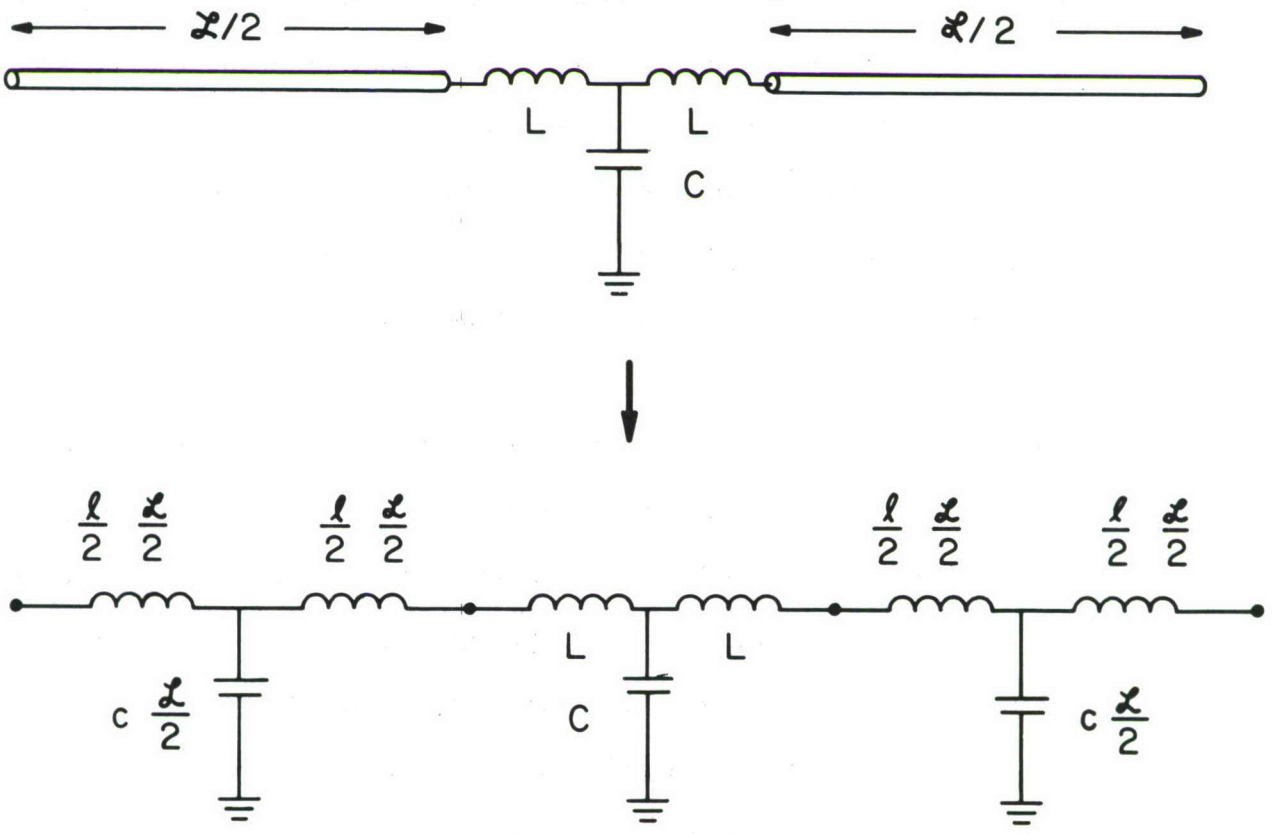

Fig. 4-4. Including the effect of a cable clamp in the line model.

As in Fig. 4-2, the effect of the clamp then can be neglected when $C = c\ell/2$ or

$$\ell < 2\frac{C}{c}$$

$$= .24 \text{ m}$$

$$\doteq 10 \text{ inches}$$

Here the cable clamp capacitance to ground has more of an effect than the structural rib. This is to be expected since the clamp surrounds the wire and reduces fringing of the fields more than the rib.

Nevertheless, it appears from the above calculations that the cable clamps have negligible effect on the behavior of an electrically short line. The effect on high-frequency line behavior will be addressed in a later section.

The author performed an experiment to assess the effect of cable clamps. A 25-wire cable bundle of total length 4 meters was constructed. The bundle consisted of 25 #22 gauge stranded wires (pvc insulation) laced together in a typical cable harness configuration. The cable was suspended above an aluminum ground plane. The load configuration was as shown in Fig. 4-5. Wire #25 was driven at the left end by a sinusoidal source. The right end of wire #25 as well as both ends of wire #14 were terminated in a resistance R. Two values of R were used: $R = 50\ \Omega$ and $R = 1\text{k}\ \Omega$. The other 23 wires were terminated in arbitrarily chosen resistances as shown in Fig. 4-5. The ratio of the output voltage across the load at the left end of wire #14, V_{out}, to the voltage applied to the left end of wire #25, V_{in}, was measured for frequencies from 1 kHz to 400 MHz. The line is one wavelength at 75 MHz.

Next, standard aircraft cable clamps were placed around the bundle and

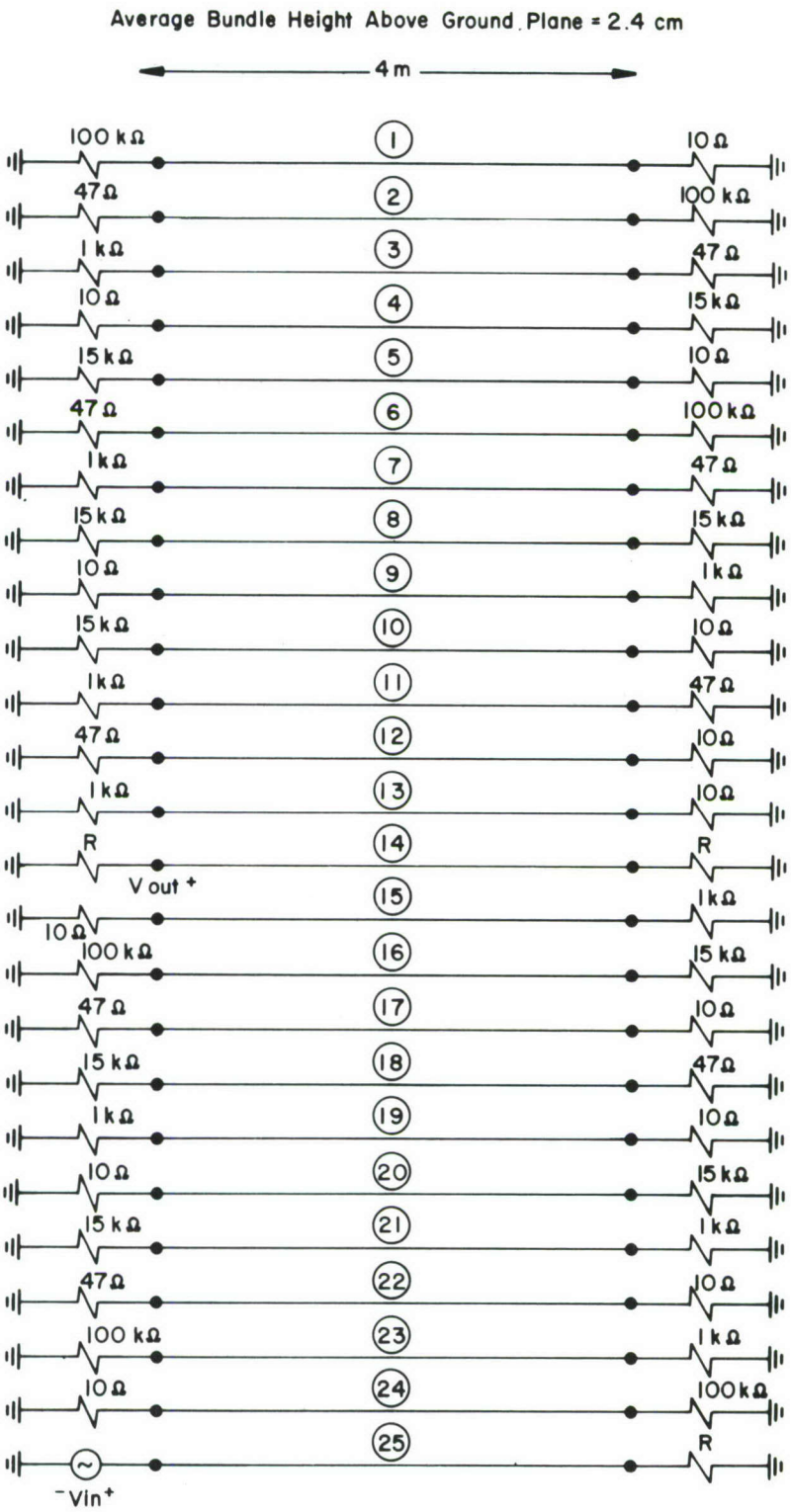

Fig. 4-5. The terminal configuration for the experiment.

screwed to the ground plane. These clamps were purchased at a local, commercial airport and consisted of a rubber insert and surrounding metal flange. The inner hole diameter was approximately 3/4 cm. These clamps placed the bundle at a height of 1 cm above the ground plane. (This was the height of the bundle when the clamps are removed.) The clamps were spaced so that their separation would be one-quarter wavelength at 300 MHz and one-half wavelength at 450 MHz. Thus the clamp separation was 1/4 m or $9\frac{13''}{16}$. This resulted in 15 clamps being placed along the line.

The results for R = 50 Ω are shown in Fig. 4-6, and the results for R = 1 kΩ are shown in Fig. 4-7. Note that for frequencies where the line is electrically short (below, say, 10 MHz) the 15 cable clamps have no effect at all. Note also that for higher frequencies, where the cable is electrically long, the clamps affect the response only at selected frequency points; the overall response pattern is independent of the presence of the clamps. This high-frequency behavior will be investigated in a later section.

4.3 Hydraulic Lines

No published work on modeling the effects of hydraulic lines on cable behavior could be found. Since hydraulic lines could be modeled as "fat wires" shorted to ground at each end, it is conceivable that they could have a dramatic effect on cable coupling if they are routed parallel to the cable bundle. The author has observed numerous instances in which wires with short circuit loads can have a substantial effect on coupling in a cable bundle. This has been seen in shielded-wire crosstalk [11] and in ribbon cables in which a ground-signal-ground arrangement occurs. However, in all these instances the effect has been to reduce the crosstalk rather than enhance it. Considering the complications involved with estimating positions of hydraulic

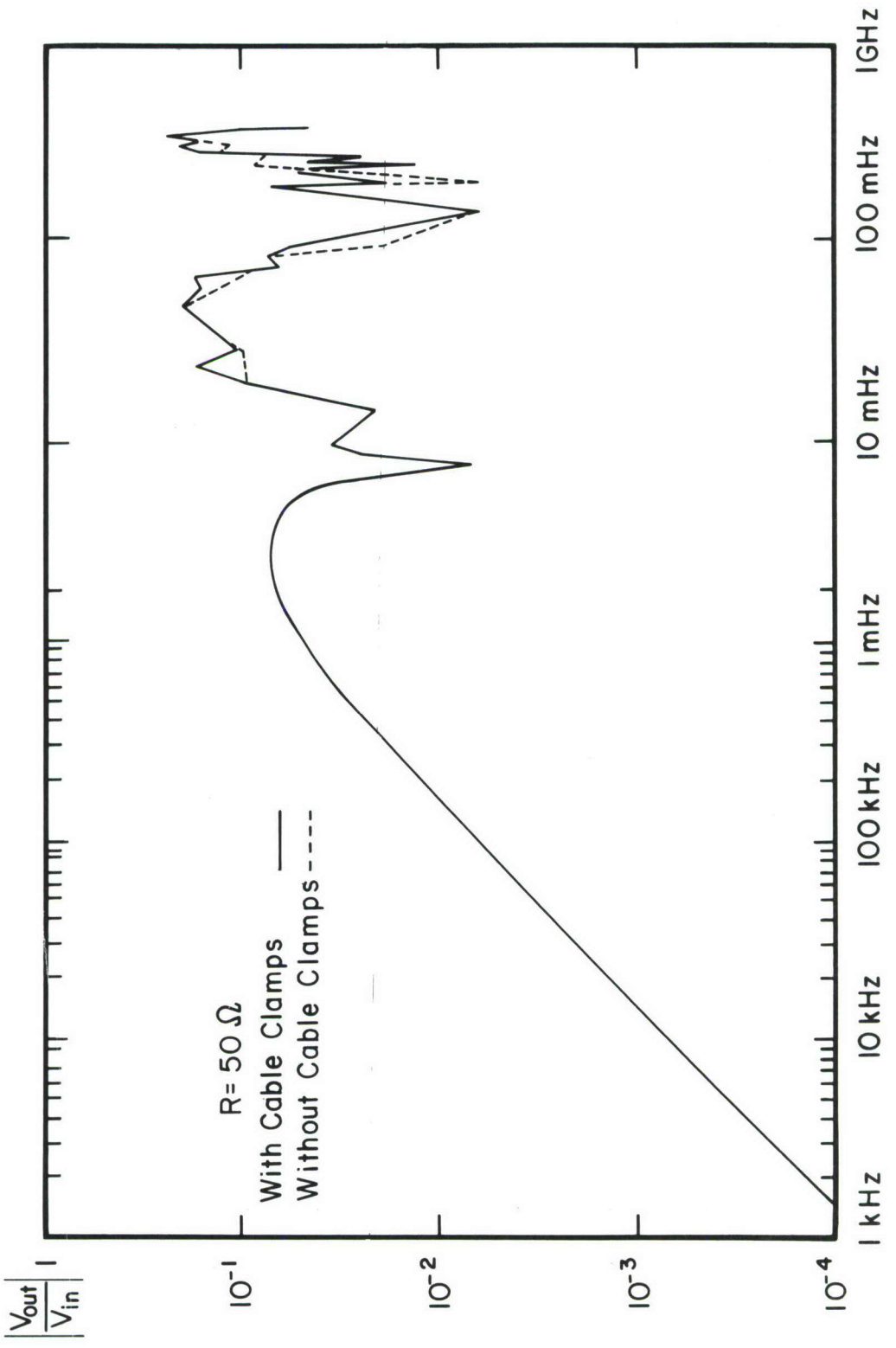

Fig. 4-6. Results for R = 50 Ω.

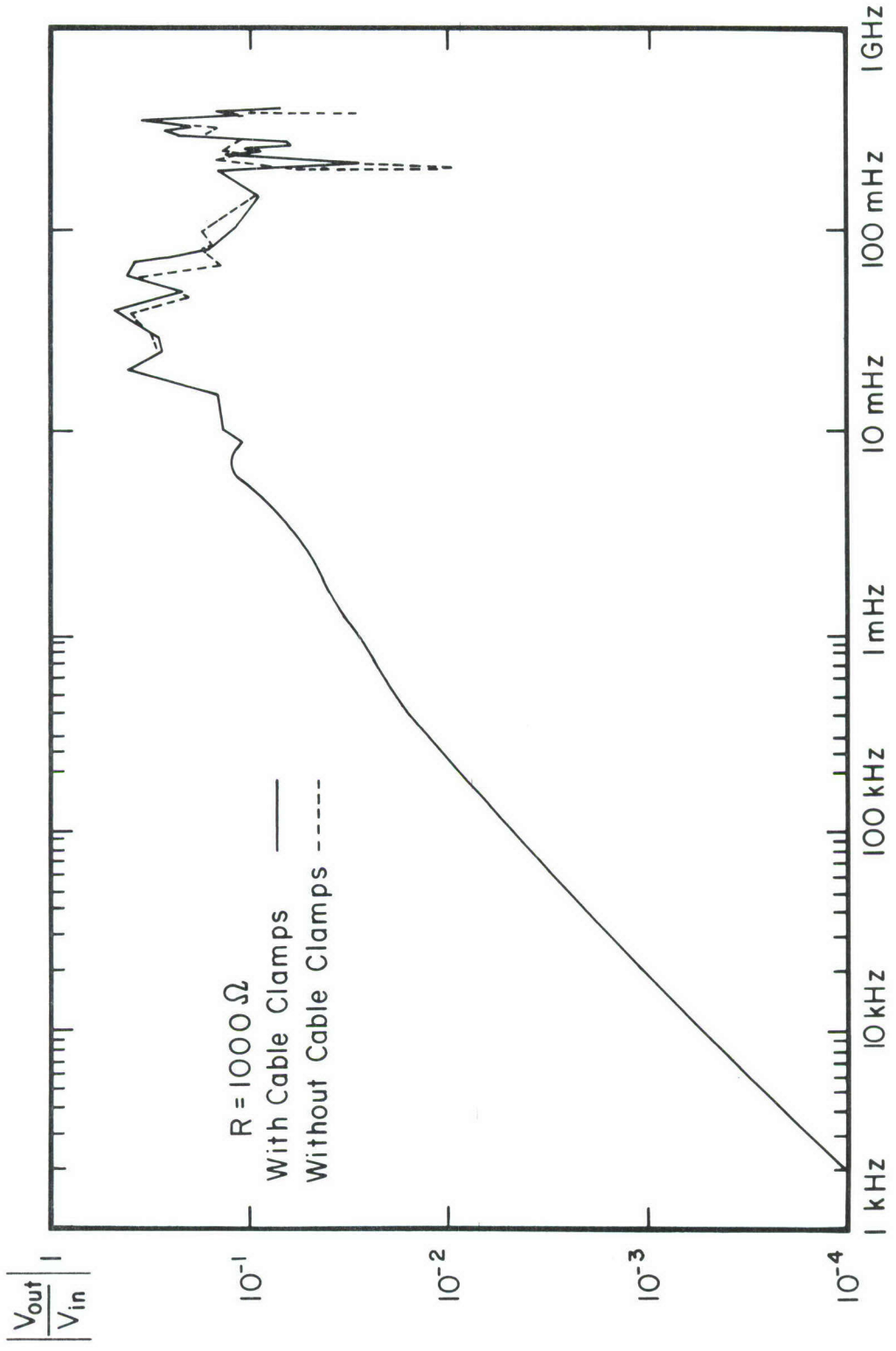

Fig. 4-7. Results for R = 1 k Ω.

lines relative to cables from electrical specifications as well as the additional input data structure required to input these, it is not recommended that they be included in the modeling capability.

4.4 Cable Trays

It was suggested in the IEMCAP user questionnaire responses that modeling of cable trays be considered. If the cable tray is, as is typical, a rectangular trough, very little effect would be expected so long as the bundle is not too near the side walls of the tray. The cable tray would most likely be grounded to the fuselage so that its lower surface would serve as a ground plane which the IEMCAP models assume. In Fig. 4-8, if $h>>s_1$ and $h>>s_2$, one would expect the lumped parameter IEMCAP models to be applicable.

At higher frequencies where the cross-sectional dimensions of the tray are becoming electrically significant, the tray dimensions would be important. Certainly this would be the case for covered trays where waveguide modes would be excited. However, the models in IEMCAP only provide a course bound in this frequency range. Thus it will be of no use to try to simulate these high frequency effects of cable trays with model additions to IEMCAP.

4.5 Bulkhead Penetrations

Bulkheads are essentially walls separating compartments of the aircraft. Their existence may be due to structural considerations, separation of pressurized/unpressurized compartments, etc. In any event, the need arises to pass cable bundles between these compartments.

In the case of the simplest type of penetration between two unpressurized compartments, the penetration may be via a simple hole in the bulkhead as shown in Fig. 4-9 (a). This perturbation can be represented as a lumped capacitance to ground in the same fashion as a structural rib as shown in Fig.

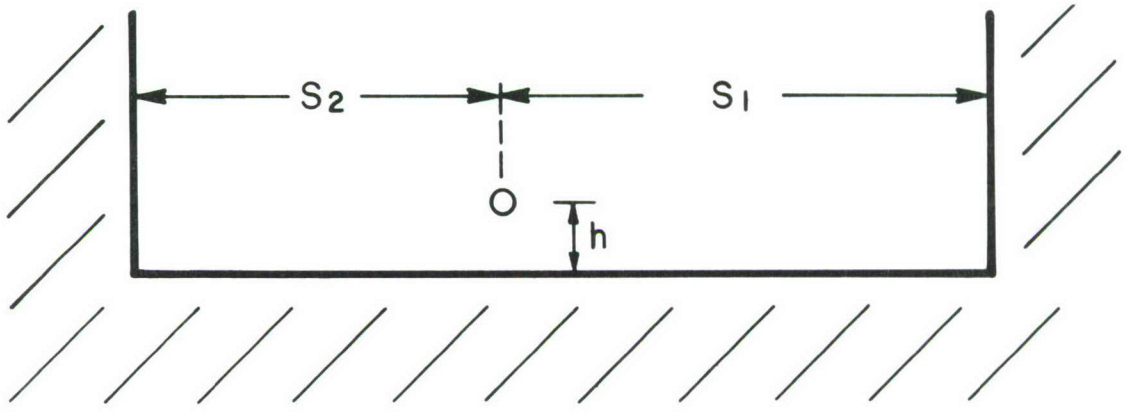

Fig. 4-8. Dimensions of cable trays.

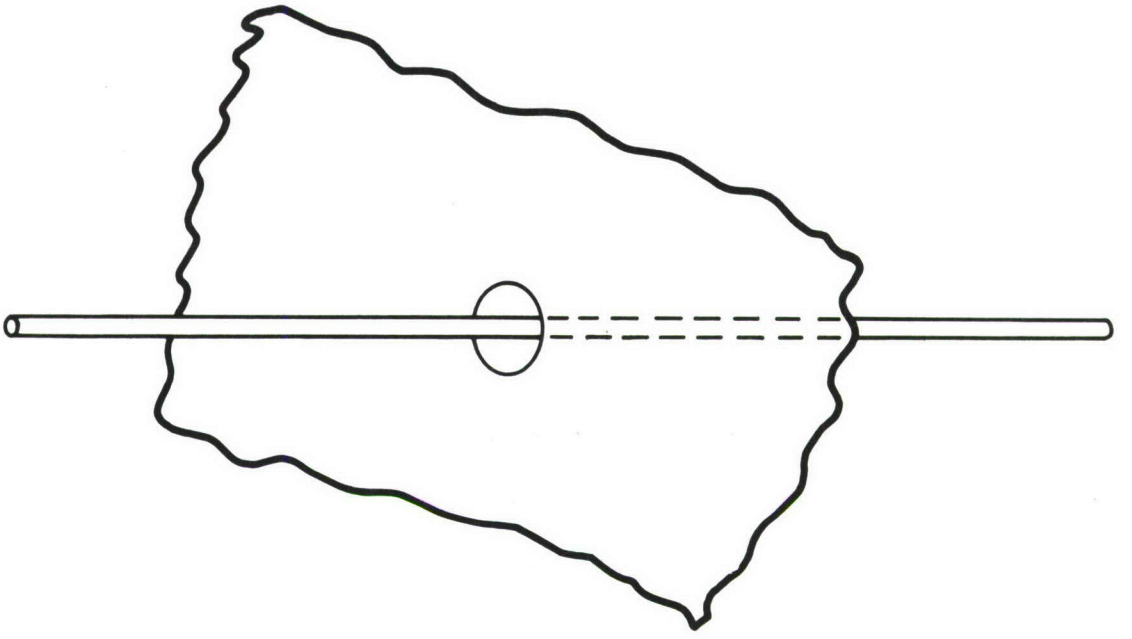

(a)

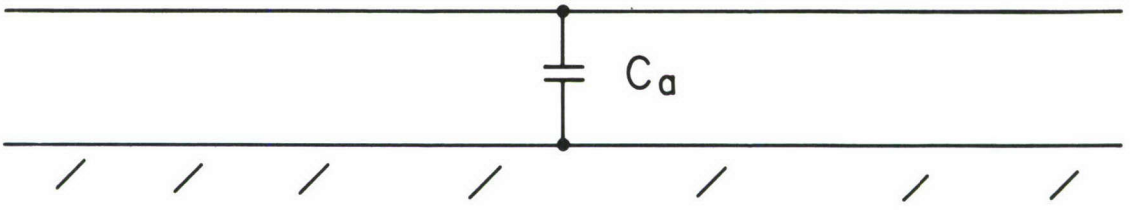

(b)

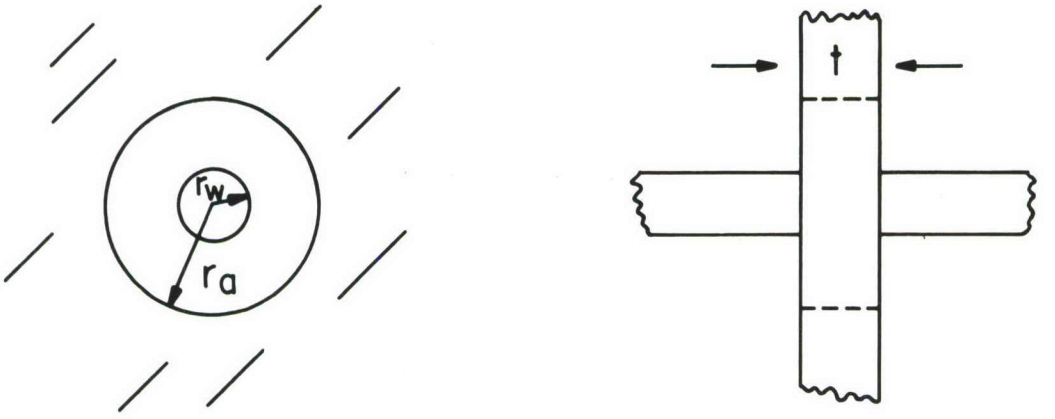

(c)

Fig. 4-9. Modeling a bulkhead penetration.

4-9 (b). A simple way of estimating this capacitance is to take into account the thickness of the bulkhead, t, and its radius, r_a, and model the penetration as a coaxial cable shown in Fig. 4-9 (c):

$$C_a = \frac{2\pi\varepsilon_o\varepsilon_r}{\ell n\left(\frac{r_a}{r_w}\right)} \quad t \qquad (4\text{-}1)$$

This approach was used in [37] and agreed moderately well with experimental results. Of course one, perhaps major, problem with this method of characterizing the bulkhead penetration is that it neglects fringing. Equation (4-1) was derived for an infinite, coaxial line and neglects fringing. However it would be expected to be an upper bound on the true result.

For an aperture of 1 inch, a #20 gauge wire (r_w = 16 mils) and a bulkhead thickness of 5 mils corresponding to 36 gauge aluminum, equation (4-1) gives

$$C_a = 1.7 \times 10^{-15} \quad F$$

The corresponding capacitance for a structural rib calculated previously was 100 times this which had no effect on the low frequency predictions unless the line length was less than 1 inch. Certainly this bulkhead capacitance would be of even less consequence. Thus it appears that bulkhead aperture penetrations have little effect on low frequency crosstalk when the line is electrically short. The high-frequency effect of periodically spaced bulkhead penetrations will be investigated in a later section.

However, bulkhead penetrations can have a substantial effect on low frequency crosstalk. But this is not due to the physical penetration but the wire installation technique in the connectors at a pressure bulkhead disconnect. Quite often it is necessary to pass wiring between two compartments,

at least one of which is pressurized. In this case it is common to install connectors (Cannon plugs) in the bulkhead. The cable attaches to these Cannon plugs.

The problem incurred is not in penetrating the bulkhead but in how shielded wires are installed in the connectors. It is quite common to strip back the shields and connect them to pins in the connector via pigtail wires as shown in Fig. 4-10. In doing so, the interior, shielded wire is exposed to other wires in the bundle over this pigtail section length. These pigtails were shown in earlier reports [10, 11, 12] to have a substantial effect on crosstalk and must be modeled. IEMCAP currently employs models of pigtails which occur at ports. What is needed is a method for incorporating these bulkhead pigtails which do not occur at "ports". A suggestion for implementing this will be given in a later section.

4.6 Junction Boxes

In conversations with engineers in the aerospace industry, the author has obtained the impression that the term "junction boxes" (or J-boxes) is a generic term for points at which wires are interconnected. A common method of doing this is with a "terminal strip" which consists of several screw terminals. These terminal strips may or may not be covered with a metallic or nonmetallic box and hence the term "junction box".

As with the case of bulkhead penetrations, it is not the junction box/terminal strip itself which causes problems but the manner in which shielded wires are terminated which causes the problem. Quite often shielded wires are terminated by stripping back the shields and connecting them to a separate screw terminal as shown in Fig. 4-11. Again these pigtails can have a

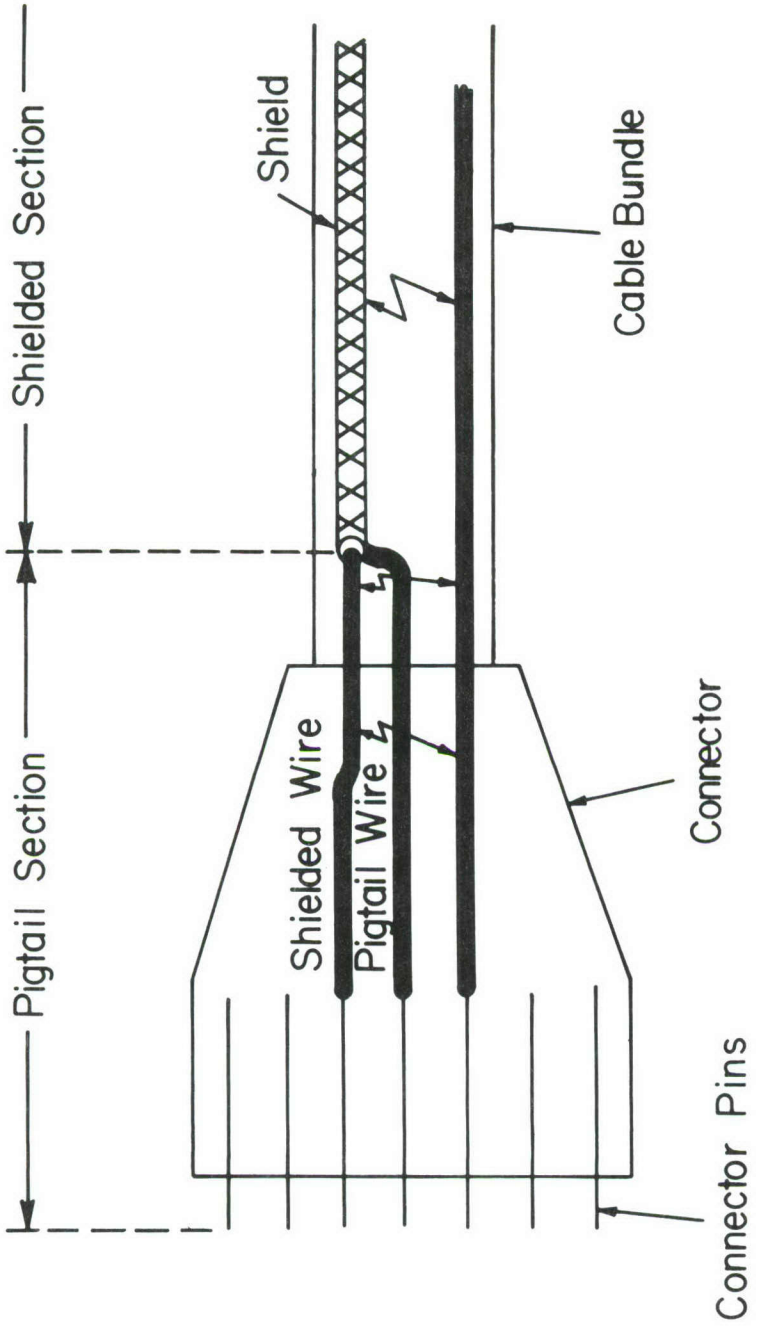

Fig. 4-10. Pigtails occurring in connectors.

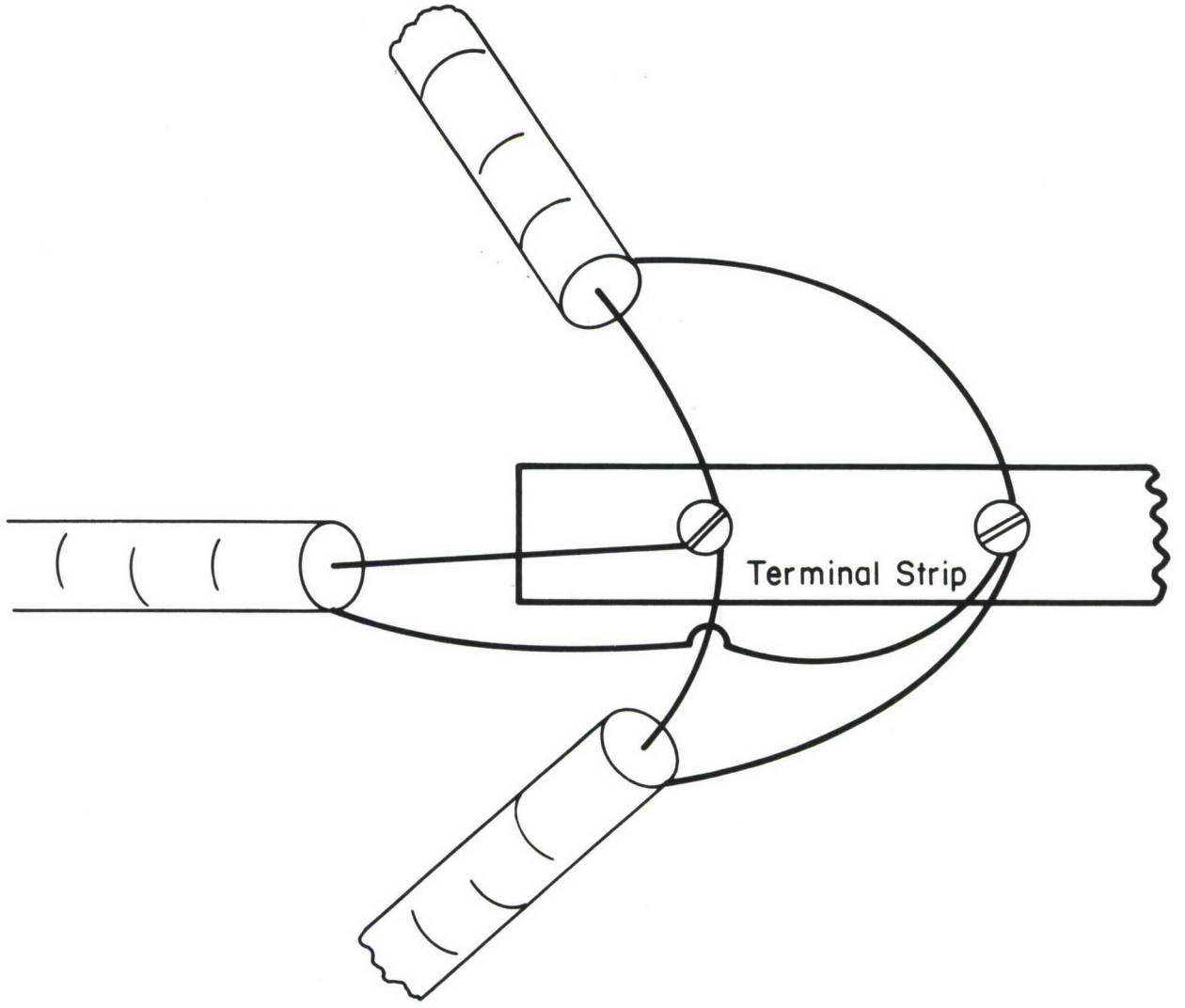

Fig. 4-11. A terminal strip.

serious effect on crosstalk and should be modeled. A method for doing this in IEMCAP will be discussed in a later section.

4.7 Effects of Periodic Perturbations

The effects of periodic perturbations on a transmission line have been investigated indirectly in numerous places. The general category of problems is concerned with wave propagation in periodic structures [35]. A great deal is known about general wave propagation in these structures. The mathematical theorem of Floquet shows that the solution of the transmission line equations for single frequency excitation on an x directed, periodic structure of period T can be represented as waves of the following form [36]

$$V(x) = e^{\pm jkx}\ \phi_V^{\pm}(x) \tag{4-2a}$$

$$I(x) = e^{\pm jkx}\ \phi_I^{\pm}(x) \tag{4-2b}$$

where $\phi_V^{\pm}(s)$ and $\phi_I^{\pm}(x)$ are periodic in x with period T. This results from the fact that the transmission line equations for a two-conductor line are of the form, for single-frequency excitation

$$\frac{dV(x)}{dx} = -\ Z(x)\ I(x) \tag{4-3a}$$

$$\frac{dI(x)}{dx} = -\ Y(x)\ V(x) \tag{4-3b}$$

The periodic line discontinuities cause the per-unit-length impedance, Z(x), and admittance, Y(x), to be periodic in T. The extension to multiconductor lines is straightforward. Thus the fields are plane waves which are "modulated" by the periodicity of the line. Therefore one would expect to investigate, instead of a phase velocity, the group velocity of the line.

Lam in [33] has investigated such a structure. His approach is to model the line and discontinuities as a cascade of two ports as shown in Fig. 4-12. Each two-port is modeled via its chain parameter matrix, ϕ. For the uniform section of line of length ℓ, the chain parameter matrix relates the voltage and current at the right end to those at the left end:

$$\begin{bmatrix} V(x_2) \\ I(x_2) \end{bmatrix} = \underbrace{\begin{bmatrix} \phi_{11} & \phi_{12} \\ \phi_{21} & \phi_{22} \end{bmatrix}}_{\underset{\sim}{\phi}_L} \begin{bmatrix} V(x_1) \\ I(x_1) \end{bmatrix} \tag{4-4}$$

For a lossless line in a homogeneous medium these entries can be easily determined [3]:

$$\begin{aligned} \phi_{11} &= \cos(\beta\ell) \\ &= \phi_{22} \\ \phi_{12} &= j\, R_C \sin(\beta\ell) \\ \phi_{21} &= j\, \frac{1}{R_C} \sin(\beta\ell) \end{aligned} \tag{4-5}$$

where $\beta = \omega/v$ and v is the phase velocity of this uniform section and R_C is the characteristic resistance. The perturbation can be generally modeled as a lumped parameter network so long as its dimensions are electrically small.

The overall chain parameter matrix of the line is the product of these individual chain parameter matrices:

$$\underset{\sim}{\phi} = \underset{\sim}{\phi}_L \, \underset{\sim}{\phi}_p \, \underset{\sim}{\phi}_L \, \underset{\sim}{\phi}_p \, - - - - \tag{4-6}$$

Once the overall chain parameter matrix of the line, $\underset{\sim}{\phi}$, is determined, the terminal relations can be substituted to determine the terminal voltages and currents of the line [3].

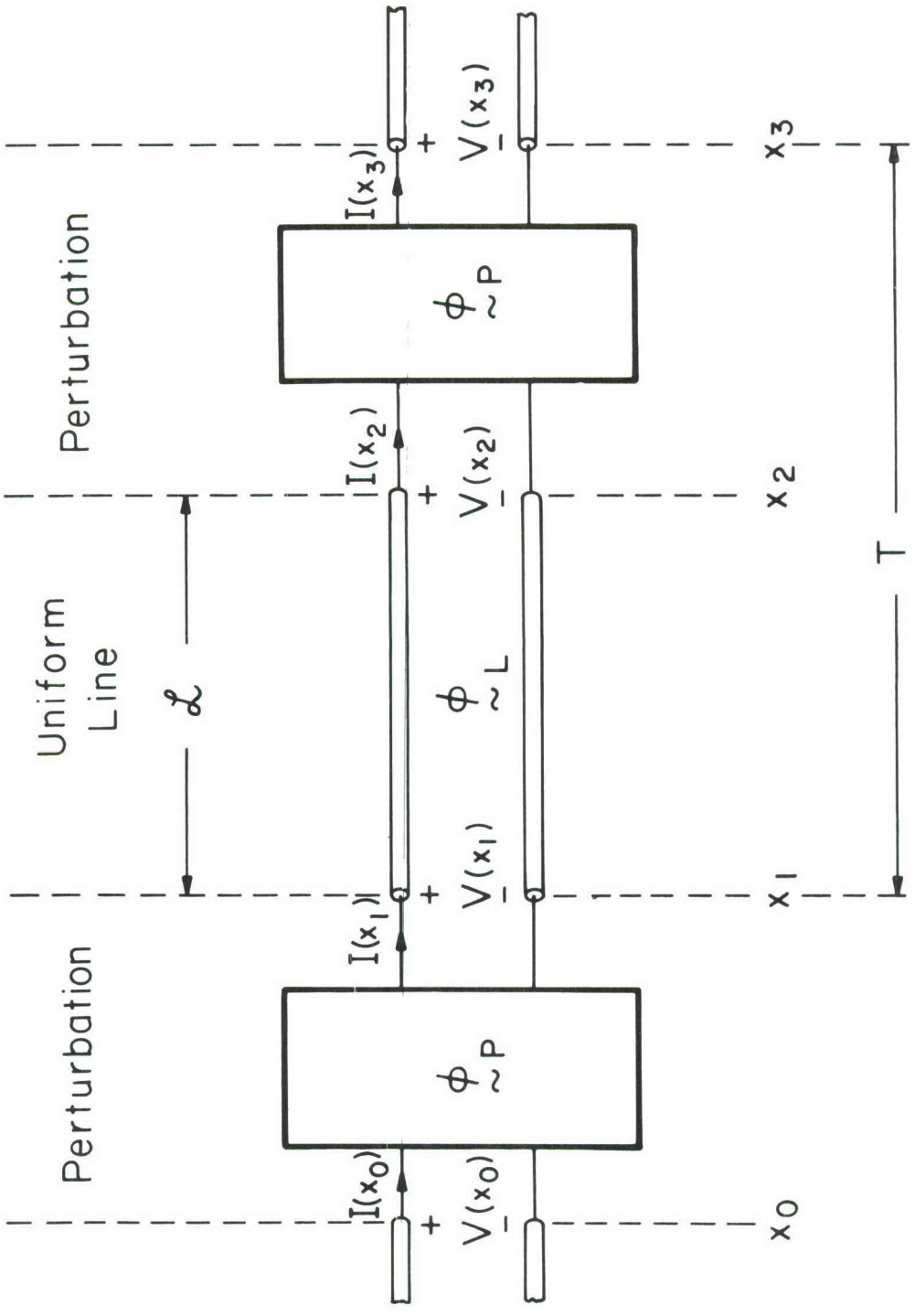

Fig. 4-12. Modeling periodic, line perturbations.

Lam considers an infinite line [33]. Since each section consisting of a uniform line and a perturbation is exactly one period in length, waves which propagate down this line must be such that they differ at the end points by at most a phase factor. Thus

$$e^{-jkT} \underset{\sim}{1} = \underset{\sim}{\phi}_p \underset{\sim}{\phi}_L \tag{4-7}$$

Solution of this gives an equation for the wave number k once the structure of $\underset{\sim}{\phi}_p$ is determined. One then looks for frequencies (bands) for which k is real (propagation or pass bands) and for which k is imaginary (attenuation or stop bands). Lam showed, for an infinite, two-conductor line, that for increasing frequency of excitation, the stop bands widen and the pass bands narrow. This expected result shows that less of the energy in the higher frequencies is transmitted down the line.

The difficulty in using Lam's result in a practical situation is that he considered an infinite line. His results cannot be used for a finite length line. Tesche and Liu, however, have investigated the effects of periodic perturbations on the terminal voltage of a two-conductor line in [34]. They essentially formed the overall chain parameter matrix for the finite line as in (4-4), incorporated the terminal conditions and solved for the frequency response of the line. They also looked at the time-domain response via the fast fourier transform of the corresponding frequency response. Several examples of a two-conductor line with $R_C = 120\ \Omega$ with various numbers of cable clamps periodically spaced on the line were investigated. The input to the line was a unit impulse whose frequency spectrum was constant for all frequencies. The frequency response for various numbers of cable clamps matched the infinite line results of Lam as the number of cable clamps in-

creased. However for the line considered, the total line length was .4 meters which was one wavelength at 750 MHz. The lowest edge of the first stop band occurred around 200 MHz and matched Lam's infinite line result (211 MHz). At this frequency the unperturbed line was approximately 1/4 wavelength long. Thus the cable clamps did not significantly affect the frequency response until the unperturbed line became electrically long. An 8 meter line (R_C = 120 Ω) was also considered. Again, the cable clamps did not affect the frequency response until the line length approached a significant portion of a wavelength (37.5 MHz).

Thus the results of Tesche and Lin for periodically spaced cable clamps did not seem to show any effects of those cable clamps until the line became electrically long. The presently employed wire-to-wire and field-to-wire models in IEMCAP as well as those suggested in this report are only valid for frequencies such that the line is electrically short. Thus incorporating models for cable clamps into those models would not be wise since, even though the cable clamps may affect the line response, the coupling models would not show this correctly since they are invalid in this frequency range.

Tesche and Lin also investigated the effects of ribs in [34]. These were modeled as described previously by a lumped capacitance. Their results showed similar results as with cable clamps.

Thus periodic line discontinuities such as cable clamps, ribs, etc. do not affect the low frequency line behavior significantly. Even though they markedly affect the frequency response when the line is electrically long, the present and proposed models in IEMCAP are not valid for this range. Therefore, incorporating models of these perturbations would not add signifi-

cantly to the predictive capabilities of IEMCAP.

4.8 Inclusion of Bulkhead/J-Box Pigtails in the WTWTFR and FTWTFR Subroutines in IEMCAP

As pointed out in previous sections, it appears that the only additional modeling effort that needs to be included in the wire-to-wire and field-to-wire coupling subroutines lies in the need to model pigtails on shielded wires which occur at (1) pressure bulkhead disconnects and (2) junction boxes.

IEMCAP presently places a pigtail on a shielded wire at a bundle point which is at a port to which the wire is attached. The length of that pigtail is specified in the wire table for the wire type used. An obvious first try to put pigtails at other bundle points where a disconnect/J-box and not a port is located is to define a "dummy port" there. This suffers from many problems. The total number of ports allowed in the system is limited to 400; placing ports at all disconnect/J-box points can take up a substantial portion of this number. Furthermore, integrated and point margins will be calculated for these "ports" and this increases run time and output.

A simpler alternative seems to be to define a bundle point at this disconnect/J-box location and assign a variable to this bundle point indicating that it is not a port but that pigtails must be placed on all shielded wires passing through that bundle point. Functionally this can be handled by passing this variable (associated with each bundle point index) to the WTWTFR and FTWTFR subroutines to cause IEENDS and IRENDS to be set properly to cause pigtail coupling to be calculated at these bundle points. So as far as calculating pigtail coupling is concerned, if IRENDS and IEENDS are set as though a "port" is located at these bundle points, then pigtail coupling will

be calculated, but no other effect outside these subroutines (calculating margins for this "port", etc.) will be felt.

One suggestion would be to add as input data a card, the J-box card, to the bundle map input data:

```
BUNDLE = ID
BPTS = PT1, X1, Y1, Z1, PT2, X2, Y2, Z2, ----
JBOX = PTi, PTj, ---
BSEG = ----
  |
  |
  |
WIRE = ---
  |
  |
  |
WIRE = ---
```

The J-box card indicates at which bundle points in this bundle, a disconnect/J-box is to be placed; in other words, pigtails are to be placed. Pass this information only to the WTWTFR and FTWTFR subroutines to set IEENDS and IRENDS for each bundle segment and we will have accomplished our objective of modeling these perturbations in their major effect - pigtail coupling.

There are some restrictions in this simple method:

1) Shield connections cannot be broken at these points; that is, shield continuity is implicit and a shield cannot be, for example, grounded.
2) Lengths of all pigtails at these points are specified in the wire table for the shielded wire and cannot be changed.

3) All shielded wires in the bundle passing through this point will have pigtails placed at the bundle point.

These restrictions are probably quite reasonable but are necessary to prevent a major rewrite of the entire IEMCAP code. The revision can simply be handled by passing the JBOX card indices to the WTWTFR and FTWTFR subroutines to set the two variables IEENDS and IRENDS for this bundle segment. They are needed nowhere else in IEMCAP.

V. Summary and Conclusions

This report has been primarily concerned with the wire-to-wire and field-to-wire coupling models in IEMCAP. Those models along with the antenna-to-antenna and box-to-box coupling models form the heart of this prediction program. Without adequate coupling prediction models, one cannot expect to obtain useful design and analysis information from the program.

On the other hand, modern avionics systems are extraordinarily complex both in function and in structural characteristics. One cannot expect accurate predictions particularly for the extreme frequency range encompassed by IEMCAP (30 Hz to 18 GHz). One can only expect to obtain estimates and/or bounds on the coupling. To obtain very accurate predictions would require not only an extremely sophisticated (and complex) modeling effort but would also require the user to gather and input an enormous amount of data (much of which would not be obtainable).

In this report we have attempted to suggest revisions of the wire-to-wire and field-to-wire coupling models which (1) are theoretically sound (with known limitations), (2) require realistic input data and (3) provide reasonable estimates of the coupling in the low frequency range and bounds in the high frequency range.

We have taken the view that it makes little sense to piecemeal "tack on" various correction factors to the models to adjust for various second-order effects or to postulate equations that may "work sometimes" or satisfy ones intuition. It is better to start with a theoretically sound model of the ideal case and simplify that model to various desired stages. Then we will have some basis for determining its limits as well as deciding what the ap-

propriate input data are.

Appendices A, B, C detail the suggested revisions of the WTWTFR and FTWTFR subroutines to place those models on a sound, theoretical basis. The revisions are also intended to modularize those subroutines so that future revisions and/or maintenance of those subroutines can be easily accomplished. Presently it is extraordinarily difficult to modify the models of those subroutines much less track the effects of those modifications.

The last objective of this report was the investigation of the need for including models of system perturbations. In appreciating these recommendations it is necessary to keep in mind the objective and intended use of the IEMCAP code. The primary objectives are to maintain a system baseline file so that the effects of any proposed modifications to the system or changes in its environment or mission can be assessed and to cull from the enormous number of all possible interactions those that merit further, detailed investigation. The IEMCAP code is not intended to provide a "fine-grained" analysis capability. Numerous other codes are available for this purpose. If the IEMCAP code narrows down the enormous number of possible problem areas to a manageable set for further, detailed analysis it will have been of considerable value.

In this regard, the only system perturbations which we found to merit inclusion into the IEMCAP models was that of pigtails on shielded wires which, in addition to occurring at port terminations, occur at bulkhead disconnects and junction boxes. The code already handles pigtails at port terminations in the wire-to-wire subroutine and, with the incorporation of the revision suggested in Appendix C, will handle pigtails at port terminations in the

field-to-wire subroutine. The incorporation of pigtail effects at bulkhead/disconnect junction boxes can be taken care of without any additional modeling effort as suggested in Chapter 4. Only a simple addition to the input wire bundle data which is passed to the WTWTFR and FTWTFR subroutines will take care of pigtails at any bundle segment point. Thus the models are already included; only an input data change (with associated variable passing) needs to be incorporated to use the present models to accomplish this task.

The incorporation of the suggested revisions in this report should bring the prediction capability of the IEMCAP code up to the highest level that can be reasonably expected of it. The antenna-to-antenna coupling models are and have been adequate and consistent with the level of sophistication of the code. The wire-to-wire models suggested here (along with the bulkhead disconnect/J-box modification) should bring those models in line with the antenna-to-antenna models. The field-to-wire models have been deficient in a number of areas detailed in Chapter 3. The suggested revisions should bring that predictive capability up to that expected of the code.

Care must still be exercised by the user in selecting and specifying the input data and in adapting the code models to situations which they were not specifically designed to address. No set of models, no matter how sophisticated or complex, will be able to remedy this problem. However the simplicity of the suggested models should enhance the ability of the user to correctly adapt these ideal models to a nonideal situation and to adequately assess the resulting IEMCAP output. In this important sense, simplicity of the modeling is a very important asset.

REFERENCES

[1] J. L. Bogdanor, et. al., Intrasystem Electromagnetic Compatibility Analysis Program, Technical Report, RADC-TR-74-342, Vol. I, II, III, Rome Air Development Center, Griffiss AFB, NY, May 1972.

[2] C. R. Paul, "EMC Analysis at the Equipment Level", AGARD Lecture Series No. 116, NATO, August 1981.

[3] C. R. Paul, Applications of Multiconductor Transmission Line Theory to the Prediction of Cable Coupling, Vol. I, Multiconductor Transmission Line Theory, Technical Report, RADC-TR-76-101, Rome Air Development Center, Griffiss AFB, NY, April 1976.

[4] Y. Leviatan and A. T. Adams, The Response of a Two-Wire Transmission Line to Incident Field and Voltage Excitation, Including the Effects of Higher Order Modes, Technical Report, RADC-TR-81-214, Rome Air Development Center, Griffiss AFB, NY, August 1981.

[5] C. R. Paul, "Coupling to Transmission Lines: An Overview", 1983 International Symposium and Technical Exhibition on Electromagnetic Compatibility, Zurich, Switzerland, March 1983.

[6] C. R. Paul, "Solution of the Transmission Line Equations for Three-Conductor Lines in Homogeneous Media," IEEE Trans. on Electromagnetic Compatibility, Vol. EMC-20, No. 1, pp. 216-222, February 1978.

[7] C. R. Paul, "On the Superposition of Inductive and Capacitive Coupling in Crosstalk Prediction Models," IEEE Trans. on Electromagnetic Compatibility, Vol. EMC-24, No. 3, pp. 335-343, August 1982.

[8] C. R. Paul, "A Simple Technique for Estimating Crosstalk," 1983 International Symposium on Electromagnetic Compatibility, Washington, DC, August 1983.

[9] C. R. Paul, "Computation of Crosstalk in a Multiconductor Transmission Line," IEEE Trans. on Electromagnetic Compatibility, Vol. EMC-23, No. 4, pp. 352-358, November 1981.

[10] C. R. Paul, "Effects of Pigtails on Crosstalk to Braided-Shield Cables," IEEE Trans. on Electromagnetic Compatibility, Vol. EMC-22, No. 3, pp. 161-172, August 1980.

[11] C. R. Paul, Applications of Multiconductor Transmission Line Theory to the Prediction of Cable Coupling, Vol. VIII, Prediction of Crosstalk Involving Braided-Shield Cables, Technical Report, RADC-TR-76-101, Rome Air Development Center, Griffiss AFB, NY, August 1980.

[12] C. R. Paul, "Transmission Line Modeling of Shielded Wires for Crosstalk Prediction," IEEE Transactions on Electromagnetic Compatibility, Vol. EMC-23, No. 4, pp. 345-351, November 1981.

[13] C. R. Paul and J. A. McKnight, "Prediction of Crosstalk Involving Twisted Pairs of Wires," Part I and Part II, IEEE Transactions on Electromagnetic Compatibility, Vol. EMC-21, No. 2, pp. 92-114, May 1979.

[14] J. A. McKnight and C. R. Paul, Applications of Multiconductor Transmission Line Theory to the Prediction of Cable Coupling, Vol. V, Prediction of Crosstalk Involving Twisted Wire Pairs, Technical Report, RADC-TR-76-101, Rome Air Development Center, Griffiss AFB, NY, February, 1978.

[15] C. R. Paul and M. B. Jolly, "Sensitivity of Crosstalk in Twisted-Pair Circuits to Line Twist," IEEE Transactions on Electromagnetic Compatibility, Vol. EMC-24, No. 3, pp. 359-364, August 1982.

[16] M. B. Jolly and C. R. Paul, Crosstalk in Twisted-Wire Circuits, Technical Report, RADC-TR-82-286, Vol. IV C, Rome Air Development Center, Griffiss AFB, NY, November 1982.

[17] C. R. Paul and D. Koopman, "Sensitivity of Coupling to Balanced, Twisted Pair Lines to Line Twist," 1983 International Symposium and Technical Exhibition on Electromagnetic Compatibility, Zurich, Switzerland, March 1983.

[18] D. Koopman and C. R. Paul, Crosstalk in Balanced Twisted Pair Lines, Technical Report, to appear, Rome Air Development Center, Griffiss AFB, NY.

[19] C. R. Paul and L. D. Thompson, Revision of the Wire-to-Wire Coupling Subroutine in IEMCAP, Technical Memorandum, submitted to Rome Air Development Center, Griffiss AFB, NY.

[20] W. R. Johnson, A. K. Thomas, et. al., Development of a Space Vehicle Electromagnetic Interference/Compatibility Specification, NASA contract 9-7305, The TRW Company 03900-6001-T000, June 1968.

[21] SVC #79-132, SPR #13, TID #13, User-Specified Pigtail Length Regarding Shielded Wire Calculations (IEMCAP), The IAP Support Center, RADC/RBCTI, Griffiss AFB, NY, July 14, 1980.

[22] G. T. Capraro and C. R. Paul, "A Probabilistic Approach to Wire Coupling Interference Prediction", 4th Symposium and Technical Exhibition on Electromagnetic Compatibility, Zurich, Switzerland, March, 1981.

[23] C. D. Taylor, R. S. Satterwhite and C. W. Harrison, "The Response of a Terminated Two-Wire Transmission Line Excited by a Nonuniform Electromagnetic Field", IEEE Trans. on Antennas and Propagation, Vol. AP-13, pp. 987-989, November 1965.

[24] A. A. Smith, "A More Convenient Form of the Equations for the Response of a Transmission Line Excited by Nonuniform Fields," IEEE Trans. on Electromagnetic Compatibility, Vol. EMC-15, pp. 151-152, August 1973.

[25] C. R. Paul, "Frequency Response of Multiconductor Transmission Lines Illuminated by an Electromagnetic Field", IEEE Trans, on Electromagnetic Compatibility, Vol. EMC-18, pp. 183-190, November 1976.

[26] C. R. Paul, Applications of Multiconductor Transmission Line Theory to the Prediction of Cable Coupling, Vol. VI, A Digital Computer Program for Determining Terminal Current Induced in a Multiconductor Transmission Line by an Incident Electromagnetic Field, Technical Report, RADC-TR-76-101, Rome Air Development Center, Griffiss AFB, NY, February 1978.

[27] C. R. Paul and R. Abraham, "Coupling of Electromagnetic Fields to Transmission Lines", 1981 IEEE International Symposium on Electromagnetic Compatibility, Boulder, CO, August 1981.

[28] C. R. Paul and D. F. Herrick, "Coupling of Electromagnetic Fields to Transmission Lines", 1982 IEEE International Symposium on Electromagnetic Compatibility, Santa Clara, CA, September 1982.

[29] R. T. Abraham and C. R. Paul, Coupling of Electromagnetic Fields onto Transmission Lines: A Comparison of the Transmission Line Model and the Method of Moments, Technical Report, RADC-TR-82-286, Vol. IV A, Rome Air Development Center, Griffiss AFB, NY, November 1982.

[30] J. B. Bogdanor, M. D. Siegel, G. L. Weinstock, Intra-Vehicle Electromagnetic Compatibility Analysis, Technical Report, AFAL-TR-71-155, Part I, Air Force Avionics Laboratory, Wright-Patterson AFB, OH, July 1971.

[31] S. Coen, T. K. Lin, F. M. Tesche, Calculation of the Equivalent Capacitance of a Rib Near a Single-Wire Transmission Line, Technical Report, AFWL-TR-77-60, Air Force Weapons Lab, Kirtland AFB, NM, June 1977.

[32] F. M. Tesche and T. K. Lin, An Electric Model for a Cable Clamp on a Single Wire Transmission Line, Technical Report, AFWL-TR-76-325, Air Force Weapons Lab, Kirtland AFB, NM, June 1977.

[33] J. Lam, Propagation Characteristics of a Periodically Loaded Transmission Line, Technical Report, AFWT-TR-76-324, Air Force Weapons Lab, Kirtland, NM, May 1977.

[34] F. M. Tesche and T. K. Lin, Selected Topics in Transmission-Line Theory for EMP Internal Interaction Problems, Technical Report, AFWT-TR-77-73, Air Force Weapons Lab, Kirtland AFB, NM, August 1977.

[35] L. Brillouin, Wave Propagation in Periodic Structures, New York, Dover Publications, 1953.

[36] E. A. Coddington and N. Levinson, Theory of Ordinary Differential Equations. New York: McGraw-Hill, 1955.

[37] H. M. Fowles, L. D. Scott, A. K. Agrawal and K. M. Lee, Aircraft Cable Parameter Study, Technical Report, AFWL-TR-77-107, Air Force Weapons Lab, Albuquerque, NM, October 1977.

APPENDIX A

DETAILED MODELS FOR THE WIRE-TO-WIRE COUPLING SUBROUTINE (WTWTFR)

This appendix sets forth the detailed models for use in a revision of the wire-to-wire coupling subroutine (WTWTFR) in IEMCAP. The basic philosophy of the models was discussed in Chapter II. The basic flowchart is presented in Fig. 2-13. The circuit types are illustrated in Fig. 2-14 and Fig. 2-15.

A.1 Emitter Models

Two variables will be computed for the emitter circuit. These are the effective emitter current, I_E, for inductive coupling and the effective emitter voltage, V_E, for capacitive coupling.

For a single emitter wire, a shield affects I_E only if it is double-end grounded and affects V_E only if it is grounded at least at one end. For single wire emitters I_E is a common mode current (returning through the ground) and V_E is a common mode voltage between the wire and ground. If a shield is grounded at least at one end, V_E is taken to be zero.

For twisted pair emitters no common mode current or voltage is computed. I_E is a differential mode current proceeding down one wire and returning in the other wire. The presence of a shield, regardless of its grounding configuration is assumed to have no effect on this differential mode current (which is contained within the shield). If a shield is grounded at least at one end, V_E is taken to be zero.

The exact configurations are illustrated in Fig. 2-14 and should be referred to for definitions of the following terms. In the course of the following development we will need the following two "shielding factors":

$$S_i = \frac{Z_{S_i}}{Z_{S_i} + j\omega L_{S_i}}$$

$$S_o = \frac{Z_{S_o}}{Z_{S_o} + j\omega L_{S_o}}$$

Here $S_i(S_o)$ is the shielding factor for the inner (outer) shield, Z_{S_i} (Z_{S_o}) is the per-unit-length impedance of the inner (outer) shield and L_{S_i} (L_{S_o}) is the per-unit-length self-inductance of the inner (outer) shield above the ground plane:

$$L_{S_i} = 2 \times 10^{-7} \ln\left(\frac{2H}{r_{S_i} + t_{S_i}}\right)$$

$$L_{S_o} = 2 \times 10^{-7} \ln\left(\frac{2H}{r_{S_o} + t_{S_o}}\right)$$

where H is the bundle height above ground, r_{S_i} (r_{S_o}) is the inner radius of the inner (outer) shield and t_{S_i} (t_{S_o}) is the thickness of the inner (outer) shield. These terms were discussed in Chapter II and come into play only by multiplying I_E when the appropriate shield is double-end grounded and the emitter is a single wire.

The following is a sequence of results for the emitter models suitable for recoding of WTWTFR. The necessary variables are passed to WTWTFR either through the argument list of the subroutine call statement or via common blocks. A description of those variables sufficient for modifying WTWTFR to incorporate the following modular models is given in [19].

The models (I_E and V_E) are listed in Table A-1. The code used in that table is:

Emitter Wire Type - S = single wire

B = balanced twisted pair

U = unbalanced twisted pair

Emitter Shield Type -	U = Unshielded
	S = Single Shielded
	D = Double Shielded
Emitter Shield Grounding (inner or outer shield) -	U = Ungrounded
	S = Single-end Grounded
	D = Double-end Grounded

A.2 Receptor Models

The coupling from an emitter circuit to a receptor circuit is assumed to be characterized by the "low-frequency" model described in Chapter II. The essential parameters characterizing this coupling are the per-unit-length mutual inductance, ℓ_m, and capacitance, c_m. Computation of these mutual elements is described in the next section.

The receptor circuit configurations are described in Fig. 2-15. The received voltages are separated into inductive coupling components:

$$V_S^{IND} = \frac{Z_{SR}}{Z_{SR} + Z_{LR}} \omega \ell m \mathcal{L}_\ell I_E$$

$$V_L^{IND} = \frac{Z_{LR}}{Z_{SR} + Z_{LR}} \omega \ell_m \mathcal{L}_\ell I_E$$

and capacitive coupling components:

$$V_S^{CAP} = V_L^{CAP}$$

$$= \frac{Z_{SR}Z_{LR}}{Z_{SR} + Z_{LR}} \omega c_m \mathcal{L}_c V_E$$

The total voltages are

$$V_S = \left|V_S^{IND}\right| + \left|V_S^{CAP}\right|$$

Table A-1

Emitter Models

Wire Type	Shield Type	Shield Grounding		Z_{LG} I_E	V_E
		Inner	Outer		
S	U			1	1
S	S		U	1	1
S	S		S	1	0
S	S		D	S	0
S	D	U	U	1	1
S	D	U	S	1	0
S	D	U	D	S_o	0
S	D	S	U	1	0
S	D	S	S	1	0
S	D	S	D	S_o	0
S	D	D	U	S_i	0
S	D	D	D	$S_o S_i$	0
B	U			1	2
B	S		U	1	2
B	S		S	1	0
B	S		D	1	0
B	D	U	U	1	2
B	D	U	S	1	0
B	D	U	D	1	0
B	D	S	U	1	0
B	D	S	S	1	0
S	D	D	S	S_i	0

Table A-1 (continued)

Wire Type	Shield Type	Shield Grounding		Z_{LG} I_E	V_E
		Inner	Outer		
B	D	S	D	1	0
B	D	D	U	1	0
B	D	D	S	1	0
B	D	D	D	1	0
U	U			1	1
U	S		U	1	1
U	S		S	1	0
U	S		D	1	0
U	D	U	U	1	1
U	D	U	S	1	0
U	D	U	D	1	0
U	D	S	U	1	0
U	D	S	S	1	0
U	D	S	D	1	0
U	D	D	U	1	0
U	D	D	S	1	0
U	D	D	D	1	0

$$V_L = \left|V_L^{IND}\right| + \left|V_L^{CAP}\right|$$

where $|\cdot|$ denotes the magnitude of the enclosed complex number.

The models differ only in ℓ_m, c_m, $\mathcal{L}_\ell$, and $\mathcal{L}_c$. The quantities $\mathcal{L}_\ell$ and $\mathcal{L}_c$ are the effective line lengths for inductive and capacitive coupling, respectively. In addition, $\mathcal{L}$ denotes the segment length and PG(PR) denotes the pitch of a generator emitter (receptor) twisted pair in meters/twist. (Note: The segment length is determined as a portion of the bundle segment length via the pigtail calculation detailed in section A.4.)

Once the above received voltages are computed they should be compared to unity received voltage (voltage transfer ratio). If any are larger than unity, set those received voltages to unity.

Table A-2 lists these parameters. The receptor models depend on the emitter circuit type. The following code is used in Table A-2:

Wire Type -	S = Single Wire
(emitter or receptor)	B = Balanced, Twisted Pair
	U = Unbalanced, Twisted Pair
Shield Type -	U = Unshielded
(receptor)	S = Single Shielded
	D = Double Shielded
Shield Grounding -	U = Ungrounded
(receptor)	S = Single-end Grounded
(inner or outer shield)	D = Double-end Grounded
Common Lengths -	M_G = min ($\mathcal{L}$, PG/2)
	M_R = min ($\mathcal{L}$, PR/2)
	M = min ($\mathcal{L}$, PG/2, PR/2)

Table A-2

Receptor Models

Receptor				Emitter	ℓ_m	$\mathcal{L}_\ell$	c_m	$\mathcal{L}_c$
Wire Type	Shield Type	Shield Grounding						
		Inner	Outer					
S	U			S	ℓ_{SWSW}	$\mathcal{L}$	C_{SWSW}	$\mathcal{L}$
S	U			B	ℓ_{BASW}	M_G	C_{BASW}	M_G
S	U			U	ℓ_{UNSW}	M_G	C_{UNSW}	$\mathcal{L}$
S	S		U	S	ℓ_{SWSW}	$\mathcal{L}$	C_{SWSW}	$\mathcal{L}$
S	S		U	B	ℓ_{BASW}	M_G	C_{BASW}	M_G
S	S		U	U	ℓ_{UNSW}	M_G	C_{UNSW}	$\mathcal{L}$
S	S		S	S	ℓ_{SWSW}	$\mathcal{L}$	0	$\mathcal{L}$
S	S		S	B	ℓ_{BASW}	M_G	0	M_G
S	S		S	U	ℓ_{UNSW}	M_G	0	$\mathcal{L}$
S	S		D	S	ℓ_{SWSW} S	$\mathcal{L}$	0	$\mathcal{L}$
S	S		D	B	ℓ_{BASW} S	M_G	0	M_G
S	S		D	U	ℓ_{UNSW} S	M_G	0	$\mathcal{L}$
S	D	U	U	S	ℓ_{SWSW}	$\mathcal{L}$	C_{SWSW}	$\mathcal{L}$
S	D	U	U	B	ℓ_{BASW}	M_G	C_{BASW}	M_G
S	D	U	U	U	ℓ_{UNSW}	M_G	C_{UNSW}	$\mathcal{L}$
S	D	U	S	S	ℓ_{SWSW}	$\mathcal{L}$	0	$\mathcal{L}$
S	D	U	S	B	ℓ_{BASW}	M_G	0	M_G
S	D	U	S	U	ℓ_{UNSW}	M_G	0	$\mathcal{L}$
S	D	U	D	S	ℓ_{SWSW} S_o	$\mathcal{L}$	0	$\mathcal{L}$

Table A-2 (continued)

Receptor				Emitter	ℓ_m	$\mathcal{L}_\ell$	c_m	$\mathcal{L}_c$
Wire Type	Shield Type	Shield Grounding						
		Inner	Outer					
S	D	U	D	B	$\ell_{BASW}{}^{S_o}$	M_G	0	M_G
S	D	U	D	U	$\ell_{UNSW}{}^{S_o}$	M_G	0	$\mathcal{L}$
S	D	S	U	S	ℓ_{SWSW}	$\mathcal{L}$	0	$\mathcal{L}$
S	D	S	U	B	ℓ_{BASW}	M_G	0	M_G
S	D	S	U	U	ℓ_{UNSW}	M_G	0	$\mathcal{L}$
S	D	S	S	S	ℓ_{SWSW}	$\mathcal{L}$	0	$\mathcal{L}$
S	D	S	S	B	ℓ_{BASW}	M_G	0	M_G
S	D	S	S	U	ℓ_{UNSW}	M_G	0	$\mathcal{L}$
S	D	S	D	S	$\ell_{SWSW}{}^{S_o}$	$\mathcal{L}$	0	$\mathcal{L}$
S	D	S	D	B	$\ell_{BASW}{}^{S_o}$	M_G	0	M_G
S	D	S	D	U	$\ell_{UNSW}{}^{S_o}$	M_G	0	$\mathcal{L}$
S	D	D	U	S	$\ell_{SWSW}{}^{S_i}$	$\mathcal{L}$	0	$\mathcal{L}$
S	D	D	U	B	$\ell_{BASW}{}^{S_i}$	M_G	0	M_G
S	D	D	U	U	$\ell_{UNSW}{}^{S_i}$	M_G	0	$\mathcal{L}$
S	D	D	S	S	$\ell_{SWSW}{}^{S_i}$	$\mathcal{L}$	0	$\mathcal{L}$
S	D	D	S	B	$\ell_{BASW}{}^{S_i}$	M_G	0	M_G
S	D	D	S	U	$\ell_{UNSW}{}^{S_i}$	M_G	0	$\mathcal{L}$
S	D	D	D	S	$\ell_{SWSW}{}^{S_i S_o}$	$\mathcal{L}$	0	$\mathcal{L}$
S	D	D	D	B	$\ell_{BASW}{}^{S_i S_o}$	M_G	0	M_G
S	D	D	D	U	$\ell_{UNSW}{}^{S_i S_o}$	M_G	0	$\mathcal{L}$
B	U			S	ℓ_{SWBA}	M_R	C_{SWBA}	M_R

Table A-2 (continued)

Receptor				Emitter	ℓ_m	$\mathcal{L}_\ell$	c_m	$\mathcal{L}_c$
Wire Type	Shield Type	Shield Grounding						
		Inner	Outer					
B	U			B	ℓ_{BABA}	M	C_{BABA}	M
B	U			U	ℓ_{UNBA}	M	C_{UNBA}	M_R
B	S		U	S	ℓ_{SWBA}	M_R	C_{SWBA}	M_R
B	S		U	B	ℓ_{BABA}	M	C_{BABA}	M
B	S		U	U	ℓ_{UNBA}	M	C_{UNBA}	M_R
B	S		S	S	ℓ_{SWBA}	M_R	0	M_R
B	S		S	B	ℓ_{BABA}	M	0	M
B	S		S	U	ℓ_{UNBA}	M	0	M_R
B	S		D	S	ℓ_{SWBA}	M_R	0	M_R
B	S		D	B	ℓ_{BABA}	M	0	M
B	S		D	U	ℓ_{UNBA}	M	0	M_R
B	D	U	U	S	ℓ_{SWBA}	M_R	C_{SWBA}	M_R
B	D	U	U	B	ℓ_{BABA}	M	C_{BABA}	M
B	D	U	U	U	ℓ_{UNBA}	M	C_{UNBA}	M_R
B	D	U	S	S	ℓ_{SWBA}	M_R	0	M_R
B	D	U	S	B	ℓ_{BABA}	M	0	M
B	D	U	S	U	ℓ_{UNBA}	M	0	M_R
B	D	U	D	S	ℓ_{SWBA}	M_R	0	M_R
B	D	U	D	B	ℓ_{BABA}	M	0	M
B	D	U	D	U	ℓ_{UNBA}	M	0	M_R
B	D	S	U	S	ℓ_{SWBA}	M_R	0	M_R
B	D	S	U	B	ℓ_{BABA}	M	0	M

Table A-2 (continued)

Receptor				Emitter	ℓ_m	$\mathcal{L}_\ell$	c_m	$\mathcal{L}_c$
Wire Type	Shield Type	Shield Grounding						
		Inner	Outer					
B	D	S	U	U	ℓ_{UNBA}	M	0	M_R
B	D	S	S	S	ℓ_{SWBA}	M_R	0	M_R
B	D	S	S	B	ℓ_{BABA}	M	0	M
B	D	S	S	U	ℓ_{UNBA}	M	0	M_R
B	D	S	D	S	ℓ_{SWBA}	M_R	0	M_R
B	D	S	D	B	ℓ_{BABA}	M	0	M
B	D	S	D	U	ℓ_{UNBA}	M	0	M_R
B	D	D	U	S	ℓ_{SWBA}	M_R	0	M_R
B	D	D	U	B	ℓ_{BABA}	M	0	M
B	D	D	U	U	ℓ_{UNBA}	M	0	M_R
B	D	D	S	S	ℓ_{SWBA}	M_R	0	M_R
B	D	D	S	B	ℓ_{BABA}	M	0	M
B	D	D	S	U	ℓ_{UNBA}	M	0	M_R
B	D	D	D	S	ℓ_{SWBA}	M_R	0	M_R
B	D	D	D	B	ℓ_{BABA}	M	0	M
B	D	D	D	U	ℓ_{UNBA}	M	0	M_R
U	U			S	ℓ_{SWUN}	M_R	C_{SWUN}	$\mathcal{L}$
U	U			B	ℓ_{BAUN}	M	C_{BAUN}	M_G
U	U			U	ℓ_{UNUN}	M	C_{UNUN}	$\mathcal{L}$
U	S		U	S	ℓ_{SWUN}	M_R	C_{SWUN}	$\mathcal{L}$
U	S		U	B	ℓ_{BAUN}	M	C_{BAUN}	M_G
U	S		U	U	ℓ_{UNUN}	M	C_{UNUN}	$\mathcal{L}$

Table A-2 (continued)

Receptor				Emitter	ℓ_m	$\mathcal{L}_\ell$	c_m	$\mathcal{L}_c$
Wire Type	Shield Type	Shield Grounding						
		Inner	Outer					
U	S		S	S	ℓ_{SWUN}	M_R	0	$\mathcal{L}$
U	S		S	B	ℓ_{BAUN}	M	0	M_G
U	S		S	U	ℓ_{UNUN}	M	0	$\mathcal{L}$
U	S		D	S	ℓ_{SWUN}	M_R	0	$\mathcal{L}$
U	S		D	B	ℓ_{BAUN}	M	0	M_G
U	S		D	U	ℓ_{UNUN}	M	0	$\mathcal{L}$
U	D	U	U	S	ℓ_{SWUN}	M_R	C_{SWUN}	$\mathcal{L}$
U	D	U	U	B	ℓ_{BAUN}	M	C_{BAUN}	M_G
U	D	U	U	U	ℓ_{UNUN}	M	C_{UNUN}	$\mathcal{L}$
U	D	U	S	S	ℓ_{SWUN}	M_R	0	$\mathcal{L}$
U	D	U	S	B	ℓ_{BAUN}	M	0	M_G
U	D	U	S	U	ℓ_{UNUN}	M	0	$\mathcal{L}$
U	D	U	D	S	ℓ_{SWUN}	M_R	0	$\mathcal{L}$
U	D	U	D	B	ℓ_{BAUN}	M	0	M_G
U	D	U	D	U	ℓ_{UNUN}	M	0	$\mathcal{L}$
U	D	S	U	S	ℓ_{SWUN}	M_R	0	$\mathcal{L}$
U	D	S	U	B	ℓ_{BAUN}	M	0	M_G
U	D	S	U	U	ℓ_{UNUN}	M	0	$\mathcal{L}$
U	D	S	S	S	ℓ_{SWUN}	M_R	0	$\mathcal{L}$
U	D	S	S	B	ℓ_{BAUN}	M	0	M_G
U	D	S	S	U	ℓ_{UNUN}	M	0	$\mathcal{L}$
U	D	S	D	S	ℓ_{SWUN}	M_R	0	$\mathcal{L}$

Table A-2 (continued)

Receptor				Emitter	ℓ_m	$\mathcal{L}_\ell$	c_m	$\mathcal{L}_c$
Wire Type	Shield Type	Shield Grounding						
		Inner	Outer					
U	D	S	D	B	ℓ_{BAUN}	M	0	M_G
U	D	S	D	U	ℓ_{UNUN}	M	0	$\mathcal{L}$
U	D	D	U	S	ℓ_{SWUN}	M_R	0	$\mathcal{L}$
U	D	D	U	B	ℓ_{BAUN}	M	0	M_G
U	D	D	U	U	ℓ_{UNUN}	M	0	$\mathcal{L}$
U	D	D	S	S	ℓ_{SWUN}	M_R	0	$\mathcal{L}$
U	D	D	S	B	ℓ_{BAUN}	M	0	M_G
U	D	D	S	U	ℓ_{UNUN}	M	0	$\mathcal{L}$
U	D	D	D	S	ℓ_{SWUN}	M_R	0	$\mathcal{L}$
U	D	D	D	B	ℓ_{BAUN}	M	0	M_G
U	D	D	D	U	ℓ_{UNUN}	M	0	$\mathcal{L}$

Once again the shielding factors S_i and S_o for double shields and S for a single shield defined in the previous section apply to these receptor shields.

A-3 Pigtail Calculations

For a bundle segment containing shielded wires the basic philosophy is to superimpose the coupling over like portions of the segment as shown in Fig. A-1. This was shown to yield acceptable prediction for electrically short segments in [10, 11].

The bundle segment is divided into four subsegment lengths over which the emitter and receptor wire types do not change: $\mathcal{L}_{UEUR}$, $\mathcal{L}_{UESR}$, $\mathcal{L}_{SESR}$, $\mathcal{L}_{SEUR}$ where

$UE \triangleq$ unshielded (pigtail) section emitter

$UR \triangleq$ unshielded (pigtail) section receptor

$SE \triangleq$ shielded section emitter

$SR \triangleq$ shielded section receptor

$\mathcal{L}_B \triangleq$ bundle segment length

The models of the previous two sections are called for each of these four cases. The four results are added to give the total contribution over this bundle segment. In dividing the bundle segment into these four subsections what is important is not the sequence of occurrence of these subsegments but the lengths of these subsegments. These subsegment lengths replace $\mathcal{L}$ in the models of the previous two sections.

In computing these subsegment lengths we use four parameters which are passed to WTWTFR for each bundle segment calculation:

PIGE = Pigtail length for emitter shield

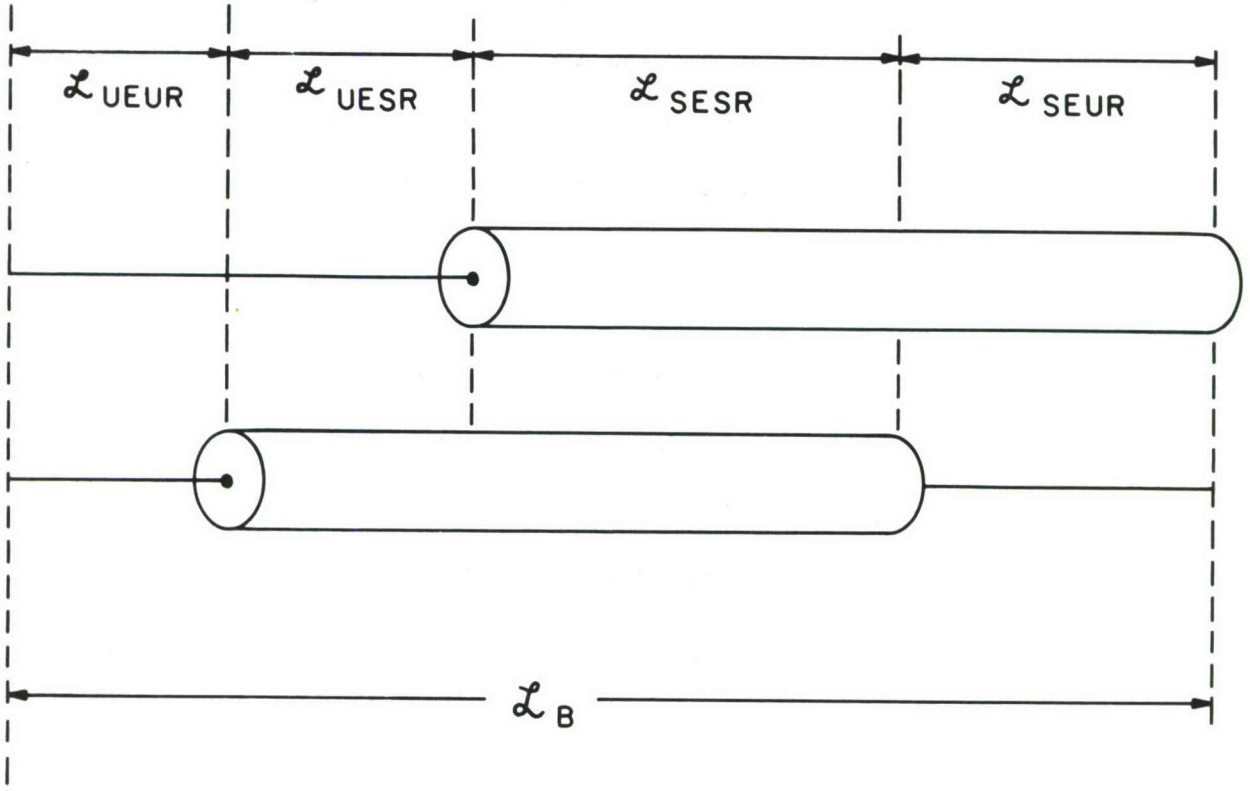

UE $\triangleq$ Unshielded (Pigtail) Section Emitter

UR $\triangleq$ Unshielded (Pigtail) Section Receptor

SE $\triangleq$ Shielded Section Emitter

SR $\triangleq$ Shielded Section Receptor

$\mathcal{L}_B \triangleq$ Bundle Segment Length

Fig. A-1. Determining uniform section lengths in computing pigtail coupling.

IEENDS = number of terminations of emitter shield for this bundle segment (0, 1, 2)

PIGR = pigtail length for receptor shield

IRENDS = number of terminations of receptor shield for this bundle segment (0, 1, 2)

A total of four cases exist for a bundle segment. These are detailed in Fig. A-2, A-3, A-4, A-5. The appropriate subsection lengths are shown in these figures.

A.4 Common Impedance Coupling

Common Impedance Coupling is computed only in the case that both the emitter and receptor have the possibility of common mode currents through the ground plane. Thus ONLY IF the emitter is single wire and the receptor is single wire do we add the following to the above:

$$V_S^{CI} = \frac{Z_{SR}}{Z_{SR} + Z_{LR}} \; Z_{CI} \; I_E$$

$$V_L^{CI} = \frac{Z_{LR}}{Z_{SR} + Z_{LR}} \; Z_{CI} \; I_E$$

If the receptor is shielded and double end grounded, multiple these factors by the shielding factors of the receptor (S, S_i, S_o, or $S_i S_o$). Z_{CI} is the system impedance between the ends of the circuits and is the per-unit-length value (input) multiplied by the bundle segment length, $\mathcal{L}_B$.

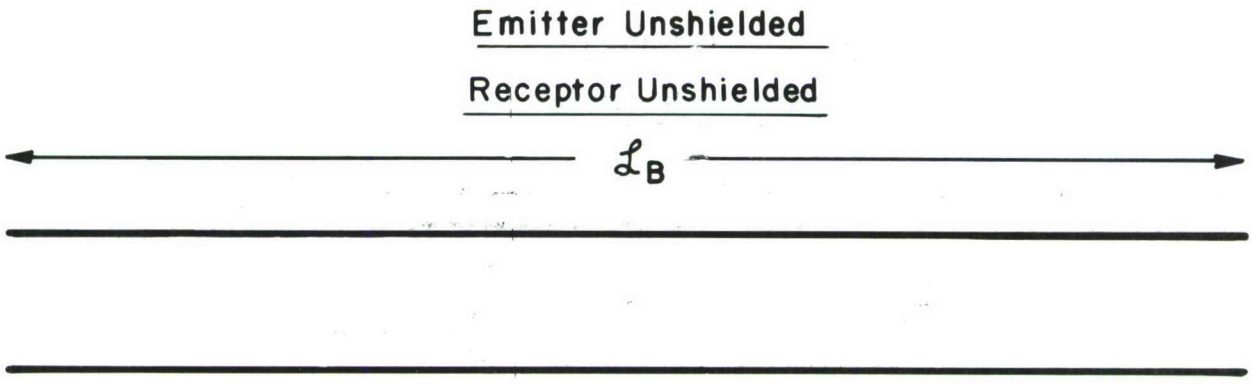

$$\mathcal{L}_{UEUR} = \mathcal{L}_B$$

$$\mathcal{L}_{UESR} = 0$$

$$\mathcal{L}_{SEUR} = 0$$

$$\mathcal{L}_{SESR} = 0$$

Fig. A-2.

Emitter Unshielded

Receptor Shielded

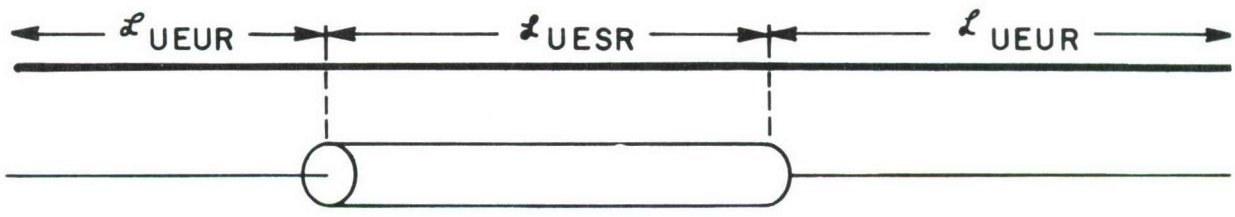

$\ell_{UEUR} = PIGR * IRENDS$

$\ell_{UESR} = \ell_B - PIGR * IRENDS$

$\ell_{SEUR} = 0$

$\ell_{SESR} = 0$

Fig. A-3.

Emitter Shielded
Receptor Unshielded

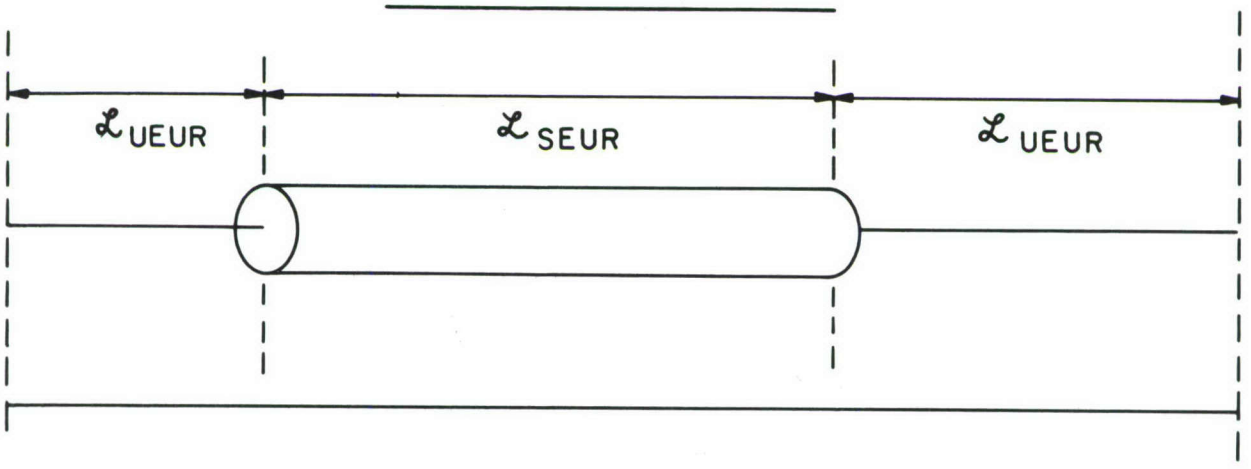

$$\mathcal{L}_{UEUR} = PIGE * IEENDS$$

$$\mathcal{L}_{UESR} = 0$$

$$\mathcal{L}_{SEUR} = \mathcal{L}_{S} - PIGE * IEENDS$$

$$\mathcal{L}_{SESR} = 0$$

Fig. A-4.

Emitter and Receptor Shielded

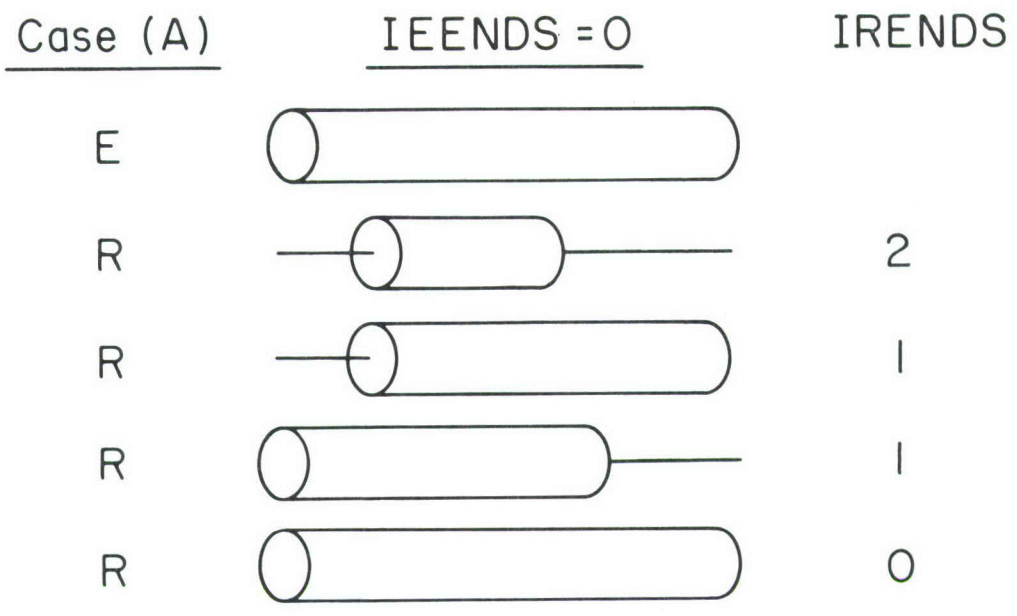

$$\mathcal{L}_{UEUR} = 0$$

$$\mathcal{L}_{UESR} = 0$$

$$\mathcal{L}_{SEUR} = PIGR * IRENDS$$

$$\mathcal{L}_{SESR} = \mathcal{L} - PIGR * IRENDS$$

Fig. A-5.

Emitter and Receptor Shielded

Case (B) IEENDS = 2

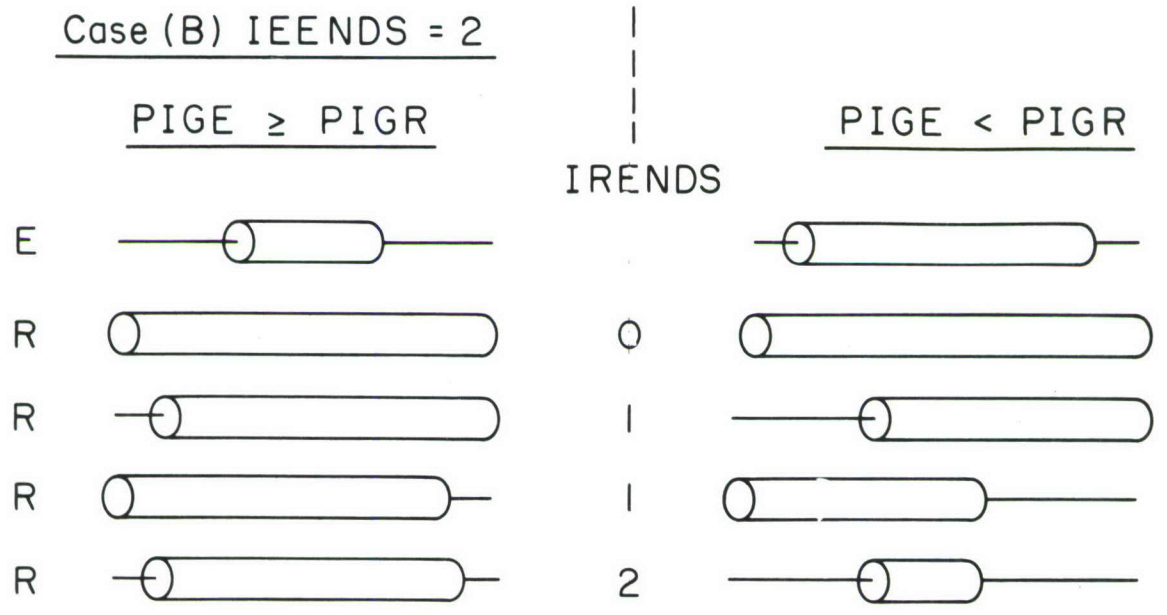

PIGE ≥ PIGR	PIGE < PIGR
$\mathcal{L}_{UEUR} = PIGR * IRENDS$	$\mathcal{L}_{UEUR} = PIGE * IRENDS$
$\mathcal{L}_{UESR} = \mathcal{L}_B - PIGR * IRENDS$ $-\mathcal{L}_B + PIGE * IRENDS$	$\mathcal{L}_{UESR} = PIGE * (IEENDS - IRENDS)$
$\mathcal{L}_{SEUR} = 0$	$\mathcal{L}_{SEUR} = PIGR * IRENDS - PIGE * IRENDS$
$\mathcal{L}_{SESR} = \mathcal{L}_B - PIGE * IEENDS$	$\mathcal{L}_{SESR} = \mathcal{L}_B - PIGE * IEENDS$ $-\mathcal{L}_B + PIGR * IRENDS$ $+ PIGE * IRENDS$

Fig. A-5. (continued)

Emitter and Receptor Shielded

Case(c) IEENDS = 1

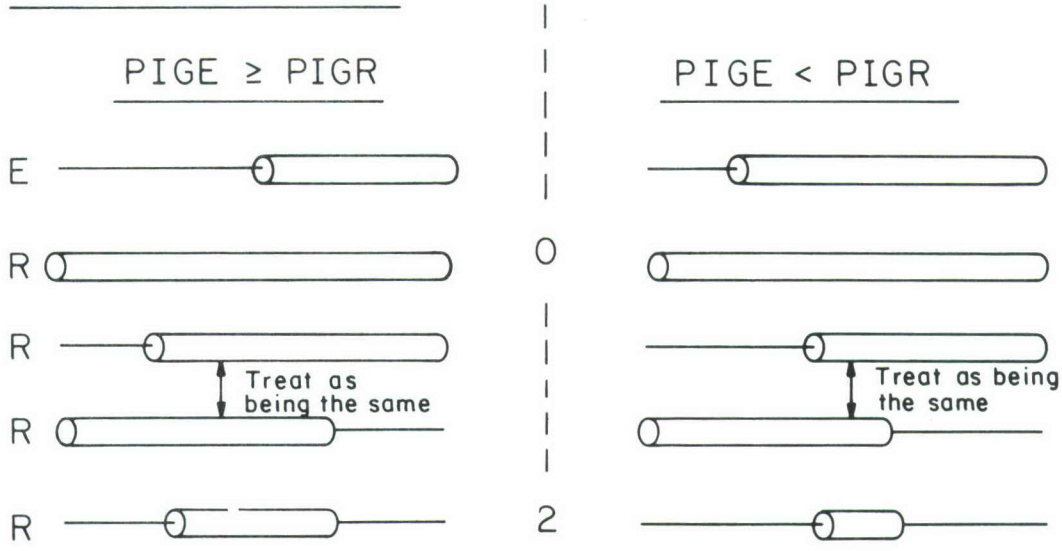

(i) IRENDS = 0

PIGE ≥ PIGR	PIGE < PIGR
$\mathcal{L}_{UEUR} = 0$	$\mathcal{L}_{UEUR} = 0$
$\mathcal{L}_{UESR} = PIGE$	$\mathcal{L}_{UESR} = PIGE$
$\mathcal{L}_{SEUR} = 0$	$\mathcal{L}_{SEUR} = 0$
$\mathcal{L}_{UEUR} = \mathcal{L}_B - PIGE$	$\mathcal{L}_{SESR} = \mathcal{L}_B - PIGE$

(ii) IRENDS = 1

PIGE ≥ PIGR	PIGE < PIGR
$\mathcal{L}_{UEUR} = PIGR$	$\mathcal{L}_{UEUR} = PIGE$
$\mathcal{L}_{UESR} = PIGE - PIGR$	$\mathcal{L}_{UESR} = 0$
$\mathcal{L}_{SEUR} = 0$	$\mathcal{L}_{SEUR} = PIGR - PIGE$
$\mathcal{L}_{SESR} = \mathcal{L}_B - PIGE$	$\mathcal{L}_{SESR} = \mathcal{L}_B - PIGR$

(iii) IRENDS = 2

PIGE ≥ PIGR	PIGE < PIGR
$\mathcal{L}_{UEUR} = PIGR$	$\mathcal{L}_{UEUR} = PIGE$
$\mathcal{L}_{UESR} = PIGE - PIGR$	$\mathcal{L}_{UESR} = 0$
$\mathcal{L}_{SEUR} = PIGR$	$\mathcal{L}_{SEUR} = 2 * PIGR - PIGE$
$\mathcal{L}_{SESR} = \mathcal{L}_B - PIGE - PIGR$	$\mathcal{L}_{SESR} = \mathcal{L}_B - 2 * PIGR$

Fig. A-5. (continued)

APPENDIX B

MUTUAL INDUCTANCE AND CAPACITANCE CALCULATIONS FOR THE WIRE-TO-WIRE COUPLING SUBROUTINE (WTWTFR)

Two of the key parameters in the crosstalk between an emitter and a receptor circuit are the mutual inductance and mutual capacitance between those circuits. There are four combinations - single wire to single wire, single wire to twisted pair, twisted pair to single wire, and twisted pair to twisted pair. The cross-sectional configurations (above a ground plane) are shown in Fig. B-1. In those figures, H denotes the bundle height above ground, and D denotes the wire separation (computed in IEMCAP as the maximum of the minimum wire separation and one-quarter of the bundle diameter). Symbols G and R denote, as usual, emitter and receptor, respectively. In addition, for a twisted pair, U and L denote the upper and lower wires of the pair, respectively. Also ΔG and ΔR denote one-half the separation between the two wires of a twisted pair in a generator or receptor pair.

The technique is to compute the per-unit-length inductance matrix and from its inverse the per-unit-length capacitance matrix [3]. From these two matrices, the appropriate mutual elements are extracted.

B-1 Single Wire Emitter to Single Wire Receptor

The cross-sectional configuration is shown in Fig. B-1 (a). From this we may form the per-unit-length inductance matrix as

$$\underset{\sim}{L} = \begin{bmatrix} \ell_{GG} & \ell_{GR} \\ \ell_{GR} & \ell_{RR} \end{bmatrix}$$

where [3]

$$\ell_{GG} = 2 \times 10^{-7} \ln\left(\frac{2H}{r_G}\right)$$

$$\ell_{RR} = 2 \times 10^{-7} \ln\left(\frac{2H}{r_R}\right)$$

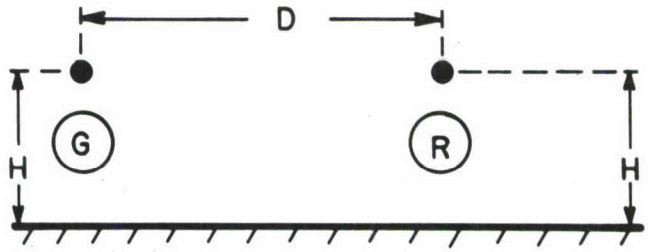

(a) Single wire emitter-single wire receptor.

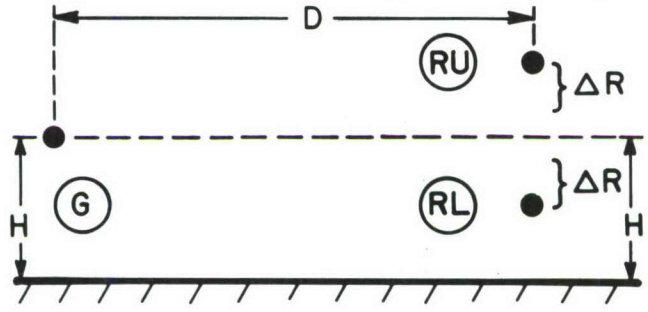

(b) Single wire emitter - twisted pair receptor.

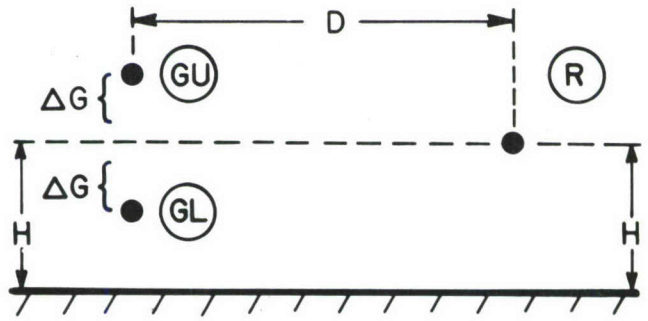

(c) Twisted pair emitter - single wire receptor.

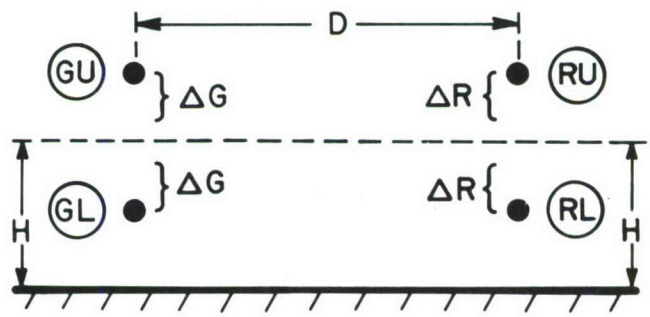

(d) Twisted pair emitter - twisted pair receptor.

Fig. B-1. The cross-sectional configurations.

$$\ell_{GR} = 10^{-7} \ln \left[1 + \frac{4H^2}{D^2}\right]$$

where r_G and r_R are the appropriate wire radii.† The per-unit-length capacitance matrix, $\underset{\sim}{C}$, and $\underset{\sim}{L}$ are related as (ignoring the wire insulation) [3]

$$\underset{\sim\sim}{LC} = \frac{1}{v^2}\,\underset{\sim 2}{1}$$

where $\underset{\sim 2}{1}$ is the 2 x 2 identity matrix. Thus

$$\underset{\sim}{C} = \begin{bmatrix} C_{GG} & -C_{GR} \\ -C_{GR} & C_{RR} \end{bmatrix}$$

$$= \frac{1}{v^2}\,\underset{\sim}{L}^{-1}$$

and $v = 3 \times 10^8$, the velocity of light in free space. From this we obtain

$$\ell_{SWSW} = \ell_{GR}$$

$$C_{SWSW} = C_{GR}$$

$$= \frac{1}{9 \times 10^{16}} \quad \frac{\ell_{GR}}{[\ell_{GG}\ell_{RR} - \ell_{GR}^2]}$$

B-2 Single Wire Emitter to Twisted Pair Receptor

The cross-sectional configuration is shown in Fig. B-1 (b). From that

$$\underset{\sim}{L} = \begin{bmatrix} \ell_{GG} & \ell_{GRU} & \ell_{GRL} \\ \ell_{GRU} & \ell_{RURU} & \ell_{RURL} \\ \ell_{GRL} & \ell_{RURL} & \ell_{RLRL} \end{bmatrix}$$

where [3]

$$\ell_{GG} = 2 \times 10^{-7} \ln \left(\frac{2H}{r_G}\right)$$

† Note that reciprocity implies equality of mutual inductances, i.e., $\ell_{GR} = \ell_{RG}$.

$$\ell_{RURU} = 2 \times 10^{-7} \ln \left(\frac{2(H+\Delta R)}{r_R} \right)$$

$$\ell_{RLRL} = 2 \times 10^{-7} \ln \left(\frac{2(H-\Delta R)}{r_R} \right)$$

$$\ell_{GRU} = 10^{-7} \ln \left[1 + \frac{4H(H+\Delta R)}{(D^2+\Delta R^2)} \right]$$

$$\ell_{GRL} = 10^{-7} \ln \left[1 + \frac{4H(H-\Delta R)}{(D^2+\Delta R^2)} \right]$$

$$\ell_{RURL} = 10^{-7} \ln \left[1 + \frac{4(H+\Delta R)(H-\Delta R)}{4\Delta R^2} \right]$$

Similarly

$$\underset{\sim}{C} = \frac{1}{v^2} \underset{\sim}{L}^{-1}$$

$$= \begin{bmatrix} C_{GG} & -C_{GRU} & -C_{GRL} \\ -C_{GRU} & C_{RURU} & -C_{RURL} \\ -C_{GRL} & -C_{RURL} & C_{RLRL} \end{bmatrix}$$

Thus

$$\ell_{SWBA} = \ell_{GRU} - \ell_{GRL}$$

$$\ell_{SWUN} = \ell_{SWBA}$$

$$C_{SWBA} = C_{GRU} - C_{GRL}$$

$$C_{SWUN} = C_{GRU}$$

B-3 Twisted Pair Emitter to Single Wire Receptor

The cross-sectional configuration is shown in Fig. B-1 (c). From this we obtain

$$\underset{\sim}{L} = \begin{bmatrix} \ell_{GUGU} & \ell_{GUGL} & \ell_{GUR} \\ \ell_{GUGL} & \ell_{GLGL} & \ell_{GLR} \\ \ell_{GUR} & \ell_{GLR} & \ell_{RR} \end{bmatrix}$$

where [3]

$$\ell_{GUGU} = 2 \times 10^{-7} \ \ell n \left(\frac{2(H+\Delta G)}{r_G} \right)$$

$$\ell_{GLGL} = 2 \times 10^{-7} \ \ell n \left(\frac{2(H-\Delta G)}{r_G} \right)$$

$$\ell_{RR} = 2 \times 10^{-7} \ \ell n \left(\frac{2H}{r_R} \right)$$

$$\ell_{GUGL} = 10^{-7} \ \ell n \left[1 + \frac{4(H+\Delta G)(H-\Delta G)}{4\Delta G^2} \right]$$

$$\ell_{GUR} = 10^{-7} \ \ell n \left[1 + \frac{4(H+\Delta G)H}{(D^2+\Delta G^2)} \right]$$

$$\ell_{GLR} = 10^{-7} \ \ell n \left[1 + \frac{4(H-\Delta G)H}{(D^2+\Delta G^2)} \right]$$

Similarly

$$\underset{\sim}{C} = \frac{1}{v^2} \ \underset{\sim}{L}^{-1}$$

$$= \begin{bmatrix} C_{GUGU} & -C_{GUGL} & -C_{GUR} \\ -C_{GUGL} & C_{GLGL} & -C_{GLR} \\ -C_{GUR} & -C_{GLR} & C_{RR} \end{bmatrix}$$

Thus

$$\ell_{BASW} = \ell_{GUR} - \ell_{GLR}$$

$$\ell_{UNSW} = \ell_{BASW}$$

$$C_{BASW} = C_{GUR} - C_{GLR}$$

$$C_{UNSW} = C_{GUR}$$

B-4 Twisted Pair Emitter to Twisted Pair Receptor

The cross-sectional configuration is shown in Fig. B-1 (d). From this we obtain

$$\underset{\sim}{L} = \begin{bmatrix} \ell_{GUGU} & \ell_{GUGL} & \ell_{GURU} & \ell_{GURL} \\ \ell_{GUGL} & \ell_{GLGL} & \ell_{GLRU} & \ell_{GLRL} \\ \ell_{GURU} & \ell_{GLRU} & \ell_{RURU} & \ell_{RURL} \\ \ell_{GURL} & \ell_{GLRL} & \ell_{RURL} & \ell_{RLRL} \end{bmatrix}$$

where [3]

$$\ell_{GUGU} = 2 \times 10^{-7} \ln \left(\frac{2(H+\Delta G)}{r_G} \right)$$

$$\ell_{GLGL} = 2 \times 10^{-7} \ln \left(\frac{2(H-\Delta G)}{r_G} \right)$$

$$\ell_{RURU} = 2 \times 10^{-7} \ln \left(\frac{2(H+\Delta R)}{r_R} \right)$$

$$\ell_{RLRL} = 2 \times 10^{-7} \ln \left(\frac{2(H-\Delta R)}{r_R} \right)$$

$$\ell_{GUGL} = 10^{-7} \ln \left[1 + \frac{4(H+\Delta G)(H-\Delta G)}{4\Delta G^2} \right]$$

$$\ell_{GURU} = 10^{-7} \ln \left[1 + \frac{4(H+\Delta G)(H+\Delta R)}{D^2+(\Delta R-\Delta G)^2} \right]$$

$$\ell_{GURL} = 10^{-7} \ln \left[1 + \frac{4(H+\Delta G)(H-\Delta R)}{D^2+(\Delta R+\Delta G)^2} \right]$$

$$\ell_{GLRU} = 10^{-7} \ln \left[1 + \frac{4(H-\Delta G)(H+\Delta R)}{D^2+(\Delta R+\Delta G)^2} \right]$$

$$\ell_{GLRL} = 10^{-7} \ln \left[1 + \frac{4(H-\Delta G)(H-\Delta R)}{D^2+(\Delta R-\Delta G)^2} \right]$$

$$\ell_{RURL} = 10^{-7} \ln \left[1 + \frac{4(H+\Delta R)(H-\Delta R)}{4\Delta R^2} \right]$$

Similarly,

$$\underset{\sim}{C} = \frac{1}{v^2} \underset{\sim}{L}^{-1}$$

$$= \begin{bmatrix} C_{GUGU} & -C_{GUGL} & -C_{GURU} & -C_{GURL} \\ -C_{GUGL} & C_{GLGL} & -C_{GLRU} & -C_{GLRL} \\ -C_{GURU} & -C_{GLRU} & C_{RURU} & -C_{RURL} \\ -C_{GURL} & -C_{GLRL} & -C_{RURL} & C_{RLRL} \end{bmatrix}$$

Thus

$$\ell_{BABA} = \ell_{GURU} - \ell_{GURL} - \ell_{GLRU} + \ell_{GLRL}$$

$$\ell_{BAUN} = \ell_{BABA}$$

$$\ell_{UNBA} = \ell_{BABA}$$

$$\ell_{UNUN} = \ell_{BABA}$$

$$C_{UNUN} = C_{GURU}$$

$$C_{UNBA} = C_{GURU} - C_{GURL}$$

$$C_{BABA} = C_{GURU} - C_{GLRU} + C_{GURL} - C_{GLRL}$$

$$C_{BAUN} = C_{GURU} - C_{GLRU}$$

APPENDIX C

DETAILED MODELS FOR THE FIELD-TO-WIRE COUPLING SUBROUTINE (FTWTFR)

This appendix provides the detailed models for use in a revision of the field-to-wire coupling subroutine. The basic philosophy of the models was discussed in Chapter III. The circuit types are shown in Fig. 3-11 and consist of a single wire with ground return, an unbalanced, twisted pair above ground or a balanced, twisted pair above ground. Each of these configurations may be surrounded by a single or double shield and each shield may be ungrounded, single-end grounded or double-end grounded. The shields modify the unshielded pickup in the following fashion. An ungrounded shield is assumed to have no effect. If a shield is grounded at least at one end, the induced current source representing electric field or "capacitive" coupling in the unshielded model is eliminated. The induced voltage source representing magnetic field or "inductive" coupling is modified for a double-end grounded shield and a single wire by multiplying that contribution for the unshielded case by the shielding factor

$$S = \frac{Z_{SH}}{Z_{SH} + j\omega L_S}$$

where Z_{SH} is the shield self impedance and L_S is the self inductance of the shield above ground.

$$L_S = 2 \times 10^{-7} \ln \left(\frac{2h}{r_s + t_s} \right)$$

and h is the bundle height, r_s is the shield inner radius and t_s is the shield thickness. For double shields the shielding factors of the appropriate shields must be used, S_i and S_o, and the overall shielding factor is

$$S = S_i S_o$$

For unbalanced or balanced twisted pairs, the shield (regardless of its grounding configuration) has no effect as discussed in Chapter III.

The induced source end and load end currents are separated into inductive (magnetic field) and capacitive (electric field) components:

$$I_S^{IND} = \frac{E^i}{Z_S+Z_L} \frac{\omega}{v} A^{IND}$$

$$I_L^{IND} = \frac{E^i}{Z_S+Z_L} \frac{\omega}{v} A^{IND}$$

$$I_S^{CAP} = \frac{Z_L}{Z_S+Z_L} \frac{E^i}{R_C} \frac{\omega}{v} A^{CAP}$$

$$I_L^{CAP} = \frac{Z_S}{Z_S+Z_L} \frac{E^i}{R_C} \frac{\omega}{v} A^{CAP}$$

where $\omega=2\pi f$, $v=3x10^8$, A is the appropriate loop area and E^i is the magnitude of the incident electric field in the vicinity of the bundle. The appropriate inductive and capacitive components are added to yield the total induced currents. In all cases, the only change among the models is in the areas, A^{IND}, A^{CAP}. In all cases, the characteristic resistance, R_C, is given by

$$R_C = 60 \ln \left(\frac{2H}{r_w} \right)$$

The areas depend on whether inductive or capacitive coupling is being considered. The areas are

Single Wire:

$$A^{IND} = A^{CAP}$$
$$= h\ell$$

Unbalanced Twisted Pair:

$$A^{IND} = \frac{dp}{2} , \quad A^{CAP} = h \frac{P}{2}$$

Balanced Twisted Pair:

$$A^{IND} = \frac{dp}{2} \quad , \quad A^{CAP} = h \frac{P}{2} \left[1 - \frac{(h-d/2)}{(h+d/2)} \frac{R_{C1}}{R_{C2}} \right]$$

where

h = bundle height

$\mathcal{L}$ = bundle segment length (or aperture length)

p = twisted pair pitch

d = twisted pair wire separation

$$R_{C1} = 60 \ \ell n \left[\frac{2(h+\Delta)}{r_w} \right]$$

$$R_{C2} = 60 \ \ell n \left[\frac{2(h-\Delta)}{r_w} \right]$$

In all cases where a segment is exposed to an aperture, one must use the smaller of the above length and the length of the aperture.

When the segment is shielded, we multiply the above inductive coupling components by the appropriate shielding factor(s) if the shield(s) is double-end grounded. Otherwise, the shield has no effect on the unshielded inductive coupling. The capacitive coupling terms are set equal to zero if the shield(s) is grounded at least at one end. Otherwise, for an ungrounded shield, the capacitive coupling contributions are unchanged.

Pigtails are treated in the same way as for wire-to-wire coupling. The unshielded models are used to give the contributions via coupling over the unshielded pigtails. The lengths of the pigtails are determined by

$$\mathcal{L}_p = 2 * \text{IRENDS} * \text{PIGR}$$

where IRENDS = 0, 1, 2 depending on whether this wire has port terminations at none, one or both ends of this bundle segment. PIGR is the pigtail length (user input) for this shield. Of course one must use the smaller of $\mathcal{L}_p$ and

the aperture length if this segment is exposed to an aperture.

Each total induced current contribution (over the pigtails and over the shielded section) is compared to a bound and the minimum selected. For a single wire and an unbalanced twisted pair.

$$|I_S|_{bound} = E^i \sqrt{\frac{Z_L}{Z_S(Z_S+Z_L)} \quad \frac{h\ell}{377}}$$

$$|I_L|_{bound} = E^i \sqrt{\frac{Z_S}{Z_L(Z_S+Z_L)} \quad \frac{h\ell}{377}}$$

For a balanced twisted pair

$$|I_S|_{bound} = E^i \sqrt{\frac{Z_L}{Z_S(Z_S+Z_L)} \quad \frac{(h+\frac{d}{2})\frac{P}{2}}{377}} - E^i \sqrt{\frac{Z_S}{Z_L(Z_S+Z_L)} \quad \frac{(h-d/2)P/2}{377}}$$

$$|I_L|_{bound} = E^i \sqrt{\frac{Z_S}{Z_L(Z_S+Z_L)} \quad \frac{(h+d/2)P/2}{377}} - E^i \sqrt{\frac{Z_S}{Z_L(Z_S+Z_L)} \quad \frac{(h-d/2)P/2}{377}}$$

Table C-1 categorizes the models. The areas for each model consist of the product of a wire separation, SEP, and a wire length, LEN, as

$$A = SEP \cdot LEN$$

Table C-1 details these. In addition there is a factor

$$BAL = \left[1 - \frac{(h-d/2)}{(h+d/2)} \quad \frac{R_{C1}}{R_{C2}}\right]$$

in the A^{CAP} term. Also the various shielding factors are

$$S = \frac{Z_{SH}}{Z_{SH}+j\omega L_S}$$

for a single, double-end grounded shield and S_i and S_o for double shields which are double-end grounded.

The following code is used in Table C-1:

Wire Type - S = single wire

B = balanced, twisted pair

U = unbalanced, twisted pair

Shield Type - U = unshielded

S = single shielded

D = double shielded

Shield Grounding - U = ungrounded

S = single-end grounded

D = double-end grounded

Table C-1

Wire Type	Shield Type	Shield Grounding		IND		CAP	
		Inner	Outer	SEP	LEN	SEP	LEN
S	U			h	$\mathcal{L}$	h	$\mathcal{L}$
S	S		U	h	$\mathcal{L}$	h	$\mathcal{L}$
S	S		S	h	$\mathcal{L}$	0	0
S	S		D	h•S	$\mathcal{L}$	0	0
S	D	U	U	h	$\mathcal{L}$	h	$\mathcal{L}$
S	D	U	S	h	$\mathcal{L}$	0	0
S	D	U	D	$h \cdot S_o$	$\mathcal{L}$	0	0
S	D	S	U	h	$\mathcal{L}$	0	0
S	D	S	S	h	$\mathcal{L}$	0	0
S	D	S	D	$h \cdot S_o$	$\mathcal{L}$	0	0
S	D	D	U	$h \cdot S_i$	$\mathcal{L}$	0	0
S	D	D	S	$h \cdot S_i$	$\mathcal{L}$	0	0
S	D	D	D	$h \cdot S_i \cdot S_o$	$\mathcal{L}$	0	0
B	U			d	P/2	h•BAL	P/2
B	S		U	d	P/2	h•BAL	P/2
B	S		S	d	P/2	0	0
B	S		D	d	P/2	0	0
B	D	U	U	d	P/2	h•BAL	P/2
B	D	U	S	d	P/2	0	0
B	D	U	D	d	P/2	0	0
B	D	S	U	d	P/2	0	0

Table C-1 (continued)

Wire Type	Shield Type	Shield Grounding		IND		CAP	
		Inner	Outer	SEP	LEN	SEP	LEN
B	D	S	S	d	P/2	0	0
B	D	S	D	d	P/2	0	0
B	D	D	U	d	P/2	0	0
B	D	D	S	d	P/2	0	0
B	D	D	D	d	P/2	0	0
U	U			d	P/2	h	P/2
U	S		U	d	P/2	h	P/2
U	S		S	d	P/2	0	0
U	S		D	d	P/2	0	0
U	D	U	U	d	P/2	h	P/2
U	D	U	S	d	P/2	0	0
U	D	U	D	d	P/2	0	0
U	D	S	U	d	P/2	0	0
U	D	S	S	d	P/2	0	0
U	D	S	D	d	P/2	0	0
U	D	D	U	d	P/2	0	0
U	D	D	S	d	P/2	0	0
U	D	D	D	d	P/2	0	0

MISSION
of
Rome Air Development Center

RADC plans and executes research, development, test and selected acquisition programs in support of Command, Control Communications and Intelligence (C^3I) activities. Technical and engineering support within areas of technical competence is provided to ESD Program Offices (POs) and other ESD elements. The principal technical mission areas are communications, electromagnetic guidance and control, surveillance of ground and aerospace objects, intelligence data collection and handling, information system technology, ionospheric propagation, solid state sciences, microwave physics and electronic reliability, maintainability and compatibility.